5-2016

Creation of a Pioneer-Neuron Axonal Pathfinding Model for Future Applications in Developmental Neurotoxicity Testing

Nicholas Robert Erdman
Clemson University, nickerdman@gmail.com

CREATION OF A PIONEER-NEURON AXONAL PATHFINDING MODEL FOR FUTURE USE IN DEVELOPMENTAL NEUROTOXICITY TESTING APPLICATIONS

A Dissertation
Presented to
the Graduate School of
Clemson University

In Partial Fulfillment
of the Requirements for the Degree
Doctor of Philosophy
Bioengineering

---

by
Nicholas Robert Erdman
May 2016

Accepted by:
Dr. Bruce Gao, Committee Chair
Dr. Ken Web
Dr. Delphine Dean
Dr. Mark Kindy

ABSTRACT

The developing central nervous system is a unique target for environmental toxicants both pre- and postnatal. Exposure to industrial chemical toxicants at various stages throughout development are known to contribute to injuries that result in autism, attention-deficit hyperactivity disorder (ADHD), dyslexia, and other cognitive impairments [81]. The damage caused by these exposures is often untreatable and frequently permanent, resulting in reduced intelligence (expressed in terms of lost IQ points) or behavioral abnormalities. It is now reported that 10-15% of all births are associated with disorders of neurobehavioral development [81], where 1 in 68 children in the United States is diagnosed with some form of an autism spectrum disorder (ASD) [7, 93, 188] and 14% of the roughly 4 million children born each year suffer from ADHD [124]. It is estimated that 3% of developmental disabilities are the direct result of environmental exposure, and that another 25% stem from interactions between environmental factors and genetic susceptibility [80, 146]. With more diagnosed cases and rising costs, the identification of the chemicals responsible for the deleterious effects on the developing nervous system has become significant topic of research.

Current developmental neurotoxicity (DNT) testing relies heavily on whole animal approaches for hazard identification and dose-response evaluations. These methods are not practical for screening the over 82,000 chemicals already used in commerce with an additional 700 new chemicals introduced annually [24]. Following the first workshop on "Incorporating *In Vitro* Alternative Methods for Developmental Neurotoxicity (DNT) Testing into International Hazard and Risk Assessment Strategies" in 2005, it was determined that *in vitro* DNT testing methods should be included as part of a tiered approach to help create a reference list of potential developmentally neurotoxic

chemicals and catalog the effects they have on various developmental mechanistic endpoints [40, 127].

Using directionality of pioneer-neuron axonal pathfinding as the mechanism for evaluation, we developed a biochip-based single-neuron axonal pathfinding assay to subjugate extending axons to simultaneous geometric and chemical guidance. To achieve this we devised a laser cell-micropatterning system to facilitate the placement of individual-neurons to exact locations on a PDMS substrate. The cell-culture conditions were optimized to promote single-neuron axonal extension through and beyond the confinements of a geometric guidance microchannel. Evaluation of the pathfinding direction in response to geometric guidance was compared to that of geometric and chemical stimuli. We found using our system that the addition of a chemical guidance component 1) increased the number of individual-neurons extending an axon at least 20 μm beyond the end of a guidance microchannel structure and 2) showed the potential to elicit a growth cone turning event by abruptly changing the initial pathfinding trajectory of an axon. Based on our previous study that single-neuron axonal pathfinding under geometric guidance is one order of magnitude more sensitive to a chemical toxicant, our research data demonstrate that we have created a platform that can be used to test the possible effects that low dose (nM concentrations) chemical exposures may have on pioneer-neuron axonal pathfinding.

DEDICATION

This work is dedicated to my parents. To my dad, for encouraging me to take the road less traveled and to pursue further knowledge in engineering and science, and to my mom, for her unconditional love and support. Words cannot express how much you both mean to me.

ACKNOWLEDGEMENTS

I would first like to thank Dr. Bruce Gao for allowing me to study under his guidance. Coming to Clemson I didn't know exactly what area of bioengineering I wanted to pursue and because of Dr. Gao's energy and enthusiasm I immediately knew that I wanted to work with him. Together, we were able to produce this work and for that I will be forever grateful.

Next I would like to thank all my lab group members. In particular, I would especially like to thank Lucas Schmidt. Lucas is an invaluable colleague and more importantly, a great friend. Having someone I could rely on for consultation about any topic, work or non-work related, really helped to alleviate the many stresses that accompany graduate school. Without him, I can honestly say that I may have never finished this work.

Finally, I would like to thank my future wife, April Holland. The many sacrifices that you have had to make while I have pursued this achievement have not been forgotten. Your constant support and cooking were what fueled me to complete this dream of mine. I look forward to spending the rest of my life with you!

TABLE OF CONTENTS

Page

Table of Contents (Continued)

Page

LIST OF TABLES

Table Page

LIST OF FIGURES

Figure Page

List of Figures (Continued)

Figure Page

List of Figures (Continued)

Figure Page

List of Figures (Continued)

Figure Page

List of Figures (Continued)

Figure Page

List of Figures (Continued)

Figure Page

List of Figures (Continued)

List of Figures (Continued)

Figure Page

CHAPTER I
INTRODUCTION

1.1 Scope of the research

The scope and approach of the project described herein was to develop a biochip-based single-neuron axonal pathfinding assay to model *in vivo* pioneer-neuron axonal pathfinding events and evaluate its potential use for future applications of chemical-developmental neurotoxicity (DNT) assessment. Current DNT testing relies heavily on whole animal approaches for hazard identification and dose-response evaluations. These methods are not practical for screening the over 82,000 chemicals already used in commerce with an additional 700 new chemicals introduced into commerce annually [24]. Following the first workshop on "Incorporating *In Vitro* Alternative Methods for Developmental Neurotoxicity (DNT) Testing into International Hazard and Risk Assessment Strategies" in 2005, it was determined that *in vitro* DNT testing methods should be included as part of a tiered approach to help create a reference list of potential developmentally neurotoxic chemicals and catalog the effects they have on various developmental mechanistic endpoints [40, 127]. Since these recommendations, great effort has gone into creating high-throughput and highly sensitive *in vitro* models to study the chemical effects on key developmental processes such as: proliferation, migration, differentiation, formation of axons and dendrites, synaptogenesis, and apoptosis [9, 44].

1.2 Background knowledge

Our nervous system allows us to sense, interpret, and respond to our surrounding environment through sight, smell, hearing, taste, and touch. Using these senses as inputs, information in the form of an electrical signal is transmitted through what is undoubtedly the most complex information-processing network known to man,

including its central processing system — the brain. In the brain, decisions about the proper course of action in response to environmental stimuli are made. On the macroscopic scale, researchers have been working for centuries to decipher the functions of the nervous system; a very complex network formed by connected nerve cells — neurons. More recently, efforts on the microscopic scale have been geared towards understanding how the nervous system circuitry and networks are initially established.

The brain is the most complex organ in our body. In adult humans, over a trillion neurons make connections with over a thousand target cells to create this elaborate information-processing network [35, 211]. Neuronal connections form during embryonic development when each differentiating neuron extends an axon (a long and thin projection that extends from the body of a neuron for the purpose of transmitting information to target cells) that migrates through the embryonic environment. In later developmental stages, axonal extension is largely influenced by pre-established axonal tracts that help to guide the growth cone (a protean environmental-sensing structure at the distal tip of the axon) to the proper target. However, the earliest axons that appear in the developing brain do not have this luxury. This axon-free environment consists mainly of undifferentiated neuroepithelial cells. Therefore, axons associated with these neurons are termed “pioneers,” and are thought to lay down the initial path that will help guide subsequent “follower” axons [55]. Without a predetermined path to follow, pioneer axons must rely on growth-cone-detection of molecular guidance cues presented by cells in the surrounding extracellular environment to reach the appropriate target regions [77]. Segmentation of specific brain regions suggests that the first axons recognize guidance cues distributed in a regionalized manner in the neuroepithelium [35]. The specific

mechanisms responsible for guiding the pioneer axon growth cone are not well understood; however, various works demonstrate that contact attraction, chemoattraction, contact repulsion, and chemorepulsion act simultaneously in a coordinated manner to direct axonal pathfinding (Figure 1.1) [202, 211].

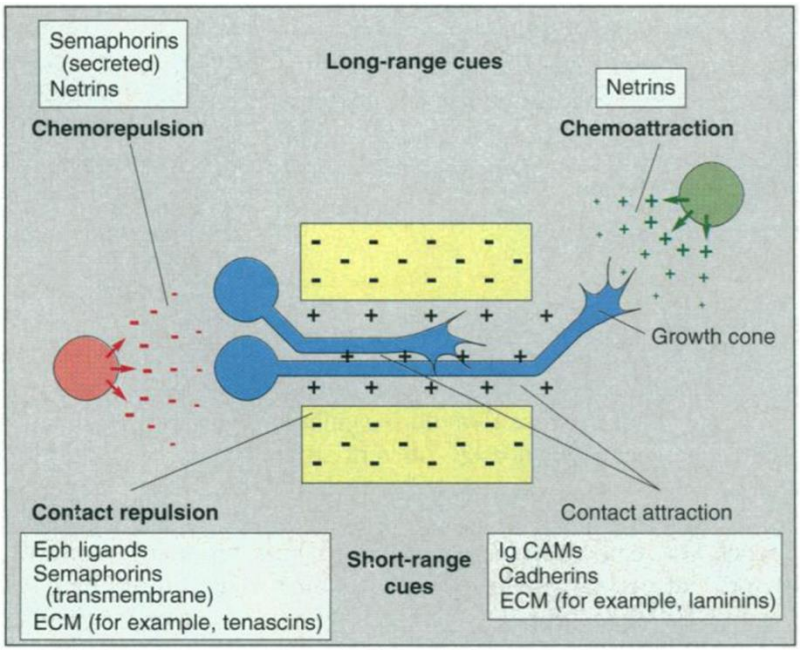

Figure 1.1: Diagram of the mechanisms and molecules involved in guiding growth cones. The different mechanisms involve chemorepulsion and chemoattraction from diffusible molecules and contact repulsion and contact attraction from membrane bound factors. Reproduced with permission from AAAS from Science, [211], Copyright 1996.

Formation of an axon

To understand how extracellular guidance molecules influence axonal pathfinding, it would first be beneficial to discuss how axons are initially formed. Similar to an axon, another morphological characteristic associated with a neuronal cell is formation of dendrites, short and usually arborized projections that extend from the body

of a neuron (referred to as the soma) for receiving information. In the beginning stages of development, axons and dendrites cannot be clearly distinguished and any projections from the cell body are referred to as neurites (Figure 1.2(A), stage 2). Neurite initiation from the soma occurs via a combination of events where increased expression of microtubule associated proteins (MAPs) along with substrate adhesion allows for polymerization of actin filaments. Myosin II motor proteins pull microtubules and organelles towards the adhesion site to overcome the retrograde flow of untethered actin filaments. When a specific neurite has differentiated from the other neurites (which will develop into dendrites) to form an axon, the asymmetric distribution of neuronal components allows the neuron to be classified as being polarized. For rapid growth of an axon there must be a continual addition of cytoplasm and membrane. Initially, it was thought that cytoplasmic protein production occurred only in the cell body followed by transport to the terminal end of the neurite. Now, however, it is evident that local protein synthesis within the axon itself plays an important role in axon growth and directionality [72]. Establishment of neuronal polarity *in* vitro follows a sequence of five stages of morphological changes (Figure 1.2) [53, 207]. Depending on the specific neuronal cell type the morphological changes will be different for each stage. As an example, dissociated mammalian hippocampal neurons begin development as round spheres that spread a lamellipodium around the cell body to facilitate attachment to the substrate, initiating stage 1. Stage 2 is characterized by the extension of several short neurites (usually 15-25 μm) from the cell body. Stage 3 is marked by the rapid growth of one of the short neurites to establish the axon. This typically occurs within 24-48 hours after plating cells. Further morphological events include the development of the remaining

shorter neurites into dendrites and the functional polarization of axons and dendrites (stage 4), which will ultimately result in the formation of synapses (stage 5) [43, 207].

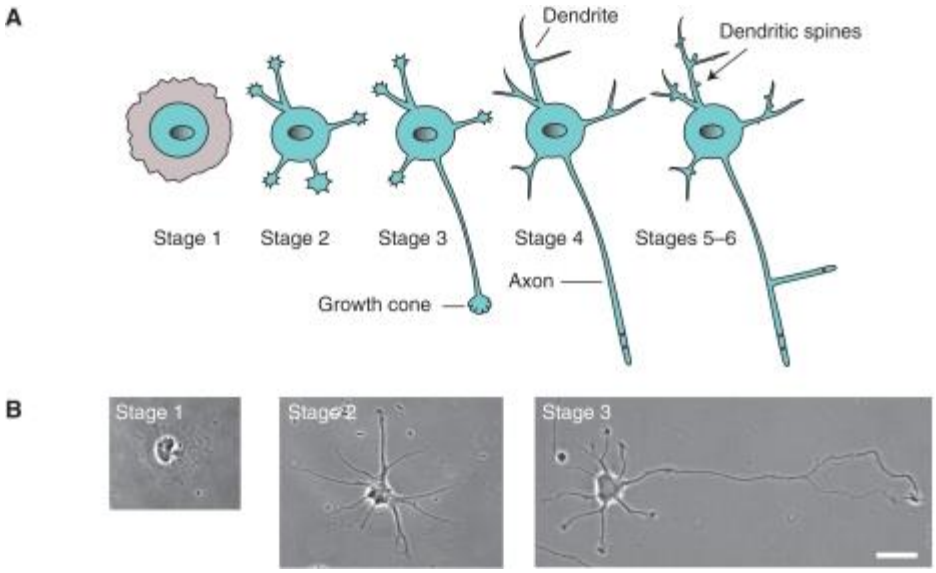

Figure 1.2: The different stages of neuronal development *in vitro.* A) Schematic drawings showing the five different stages of neuronal maturation. B) Phase contrast images of a rat hippocampal neuron progressing from stage 1 to stage 3. Scale bar = 20 µm. Reproduced with permission from Cold Spring Harbor Perspectives in Biology [207], Copyright 2009.

The growth cone

The idea that axon motility and target innervation was driven by growth cone-detection of the extracellular environment is attributed to Santiago Ramón y Cajal [176]. Over half a century later his foresight about the dynamic structure at the distal tip of axons helped pave the way for Roger Sperry to investigate how growth cones are guided *in vivo*. In his work, Sperry demonstrated through histological slices that fibers arising from different parts of the retina preferentially select separate pathways as they grow into the brain and connect with predetermined target zones within the midbrain

[203]. He postulated that growth cones had membrane receptors that detected gradients of guidance molecules and responded by directing growth up an attractive one or down a repulsive one. This came to be known as the chemoaffinity hypothesis and has served as the basis for many models of axonal guidance [37, 203]. The specific mechanistic aspect for the chemotropic behavior of growth cones to soluble molecular gradients is the fundamental basis of this work.

At this point an important question to ask is, “How does the growth cone implement extracellular guidance cue information to influence the trajectory of the elongating axon?” The growth cone can be divided into three regions: the central, transitional, and peripheral domains (Figure 1.3(B)). The central domain is closest to the axon and is abundant with microtubules, which provide structural rigidity. The peripheral domain is at the leading edge of the growth cone and is primarily made up of fibrillar actin, giving rise to lamellar sheets and long protrusions, called filopodia. The transitional domain, lies between the microtubule-dominated central domain and the actin-rich peripheral domain [131]. Growth cone motility results from cycles of actin polymerization at the leading edge, myosin-driven retrograde flow of actin polymers through the peripheral domain, depolymerization of actin near the transitional domain, diffusion of released actin monomers to the leading edge, and repolymerization in the lamellae and filopodia [178]. Each type of neuron differentially expresses specific membrane receptors for guidance molecules. Guidance cue information received by the neuron is transduced by cytoplasmic second messenger pathways that govern cytoskeletal rearrangements of tubulin and actin filaments (Figure 1.4) [35, 37, 119, 147, 211].

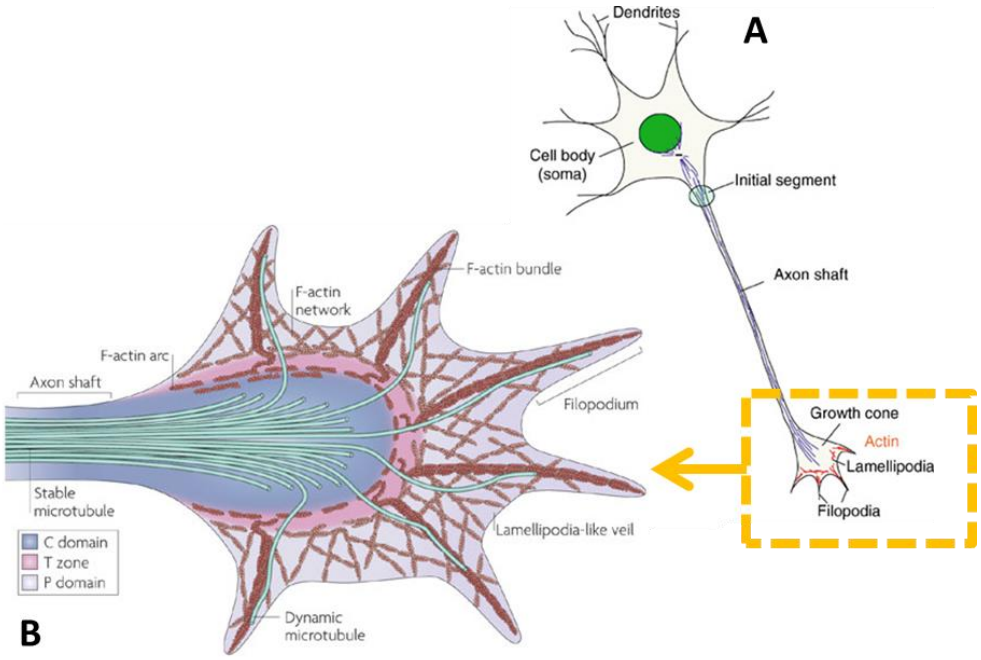

Figure 1.3: Diagram of the morphological characteristics of a developing neuron. A) Morphology of a typical developing neuron, with dendrites, soma, axon, and growth cone. The highlighted region is the growth cone of the developing axon. Reproduced with permission of Springer, Encyclopedia of Neuroscience [95], Copyright 2009. B) Exploded view of the growth cone structural components comprised of microtubules and actin filaments. Reproduced by permission from Macmillan Publishers Ltd: Nature Reviews Molecular Cell Biology [131], Copyright 2009.

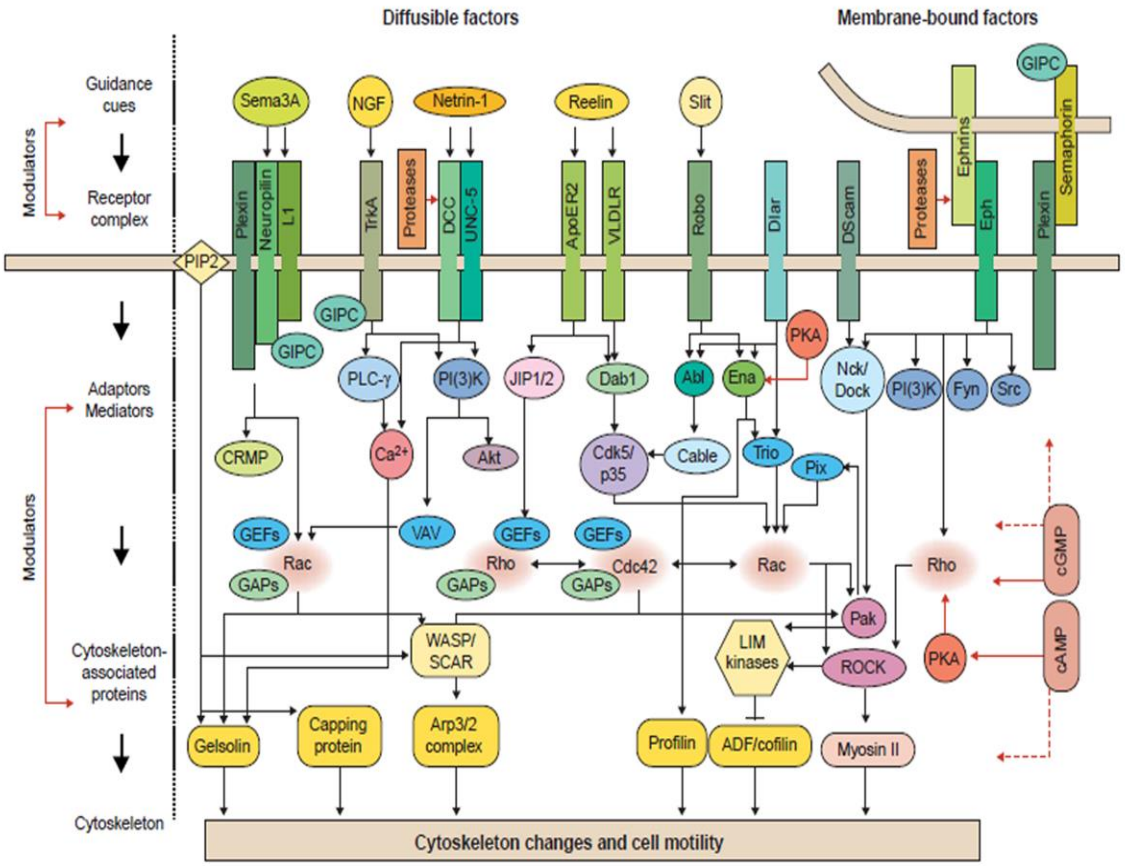

Figure 1.4: Simplified diagram of the signaling molecules that link guidance receptors to cytoskeletal rearrangements which direct growth cone motility. Reproduced by permission from Macmillan Publishers Ltd: Nature Cell Biology [202], Copyright 2001.

Axonal guidance molecules

There exist many known and most likely many more unknown substances that are responsible for inducing axonal growth and guiding axonal pathfinding (a process by which neurons extend axons to reach the correct targets) *in vivo*. Axonal pathfinding is further complicated because of restricted concentration ranges and the dual roles some molecules play in promoting growth (extension only) as well as having the potential to act as a guidance cue (something that causes extending axons to turn or branch so as

to navigate to the proper target). Examples of this have been demonstrated by Gunderson and Barrett (1979) and Ming et al. (2002) where members of a family of peptide neurotrophic factors, called neurotrophins, play widespread roles in regulating the developing and adult nervous system. In the first case, localized diffusible gradients (gradients of soluble molecules that serve as long-range chemoattractive or chemorepulsive agents) of nerve growth factor (NGF)-B were shown to elicit a positive redirection (extension and turning towards) of the axonal trajectory of chick dorsal root ganglia (DRG) neurons towards the source [85]. In the second case, a similar technique for creating localized molecular gradients was used to show that brain-derived neurotrophic factor (BDNF) elicited a similar extension-promoting and turning response for *Xenopus* spinal neurons [145]. It should be noted that different neurons are frequently responsive to different trophic factors and in most cases combinations of multiple neurotrophic factors are necessary to promote axonal growth, although the full importance of growth factors related to axonal guidance is poorly understood. Additionally, there are extracellular matrix molecules (e.g. laminin) and cell adhesion molecules (e.g. L1) that play pivotal roles in promoting axon growth *in vitro* and *in vivo* [72]. As with the diffusible guidance molecules, differential gradients of these molecules bound to the extracellular substrate environment can modulate the growth rate and trajectory of an extending axon [87, 220, 228].

In vivo diffusible axonal guidance molecules

The first identified diffusible axon-guidance molecules were from the netrin family [195]. They comprise a phylogenetically conserved family of long-range guidance cues related to the laminin family of glycoproteins. In the chick, netrin-1 and netrin-2 were identified via purification of the embryonic brain based on their ability to mimic

outgrowth-promoting effects of floorplate cells on commissural axons in collagen matrices [195]. Netrins are bifunctional in that they can attract some axons and repel others. The attractive effects of netrins are mediated by the receptors of the DCC (Deleted in Colorectal Carcinomas) family, while the repulsive effects are mediated by the UNC5 family [35]. Netrins are secreted by non-neuronal cells at the floor plate at the ventral midline to guide commissural axons [128]. Floor plate signaling occurs in both the spinal cord and in the brain. Using immunohistochemical techniques, MacLennan et al. (1997) were able to determine the spatial and temporal relationships between netrin-1 localization and growth of pioneer axons in the embryonic chick nervous system. This work suggests that the primary function of netrin-1 *in vivo* is almost exclusively haptotactic for spinal cord commissural neurons. In the brain relatively high levels of netrin-1 expression can be found in the metencephalon and caudal mesencephalon. The more rostral portions of the ventral midline in the diencephalon indicate little or no netrin-1 expression; however, it was detected in the more dorsal regions of the prosencephalon, implicating the ventral growth of axons from early differentiating neurons [135]. Thus, it is possible that local shallow gradients of netrin-1 chemotropically influence commissural and longitudinal axonal pathways of pioneer-neurons in the developing brain.

Many other diffusible molecules have been identified as having guidance effects on the growth cone of extending axons. Among them are semaphorins, slits, and fibroblast growth factors (FGFs) [202]. Semaphorins are a large family of cell-surface and secreted proteins that typically act as chemorepellents and axonal extension inhibitors. They can influence trajectories of axons by inhibiting branching or the formation of synaptic arbors and by causing growth cone collapse [34, 37, 142, 211].

Much like semaphorins, slits mainly act as chemorepellents. Slits are produced by midline glia and are responsible for expelling axons from the midline. In the absence of slit secretion, axons will coalesce into a single longitudinal bundle [116]. It has been demonstrated that virtually all of the molecules involved in axonal guidance effect cytosolic Ca^{2+} levels in the growth cone. Transient levels of Ca^{2+} on the side of the growth cone proximal to the gradient source result in selective activation of intracellular signaling pathways that ultimately determine growth cone guidance [72, 191]. Tight regulation of the intracellular and extracellular environment is essential for proper axonal guidance.

In vivo geometrical and topological axonal guidance

The geometric environment that surrounds an extending axon *in vivo* plays an important role in directing its navigation to the proper destination. Delineation of neuroepithelial domains in the developing nervous system results in regionalized expression of distinct combinations of transcription factors, cell adhesion molecules, and morphogens [35]. These different domains can give rise to specific structures, such as interstitial spaces and channels created by ependymal cells, which serve as roadmaps for axonal extension. In other instances, growth cones navigate by traversing through the extracellular matrix environment, making specific interactions with adjoining cells. In almost all cases, axonal extension is directly related to the presence of glial cells. For example, just prior to the formation of the corpus callosum, glial cells migrate medially laying down a transient pathway known as the “glial sling” [177]. Immediately following this glial action, pioneer axons of callosal fibers extend on the sling.

Growth cone morphology *in vivo* can be categorized based on the behaviors expressed when in contact with various substrata and extracellular environments.

Typically observed during extension on axon bundles in tracts, elongated growth cones display convex and concave lamellar protrusions extending from the central shaft [178]. Expansion of growth cones is a regular occurrence at choice points where axon directions tend to change in response to the localized environment. This could be the result of direct contact with a guidepost cells or interpretation of a graded expression of cell adhesion molecules. Growth cone collapse or retraction occurs when aversive cues are encountered. This prevents undesirable pathfinding and prompts the axon to momentarily stop and probe the environment before continuing on in the proper direction.

1.3 Pioneer-neuron axonal pathfinding and neurotoxicity-induced neurodevelopmental disorders

A major part of the development of the human central nervous system consists of a series of systematically orchestrated axonal pathfinding events that initiate the formation of a complex information-processing and -responding neuronal network. Disturbance of these pathfinding events may cause miswiring of the network that will result in various dysfunctions of the nervous system [149]. There is an expanding body of evidence that points to an increase in the prevalence of neurodevelopmental disorders (e.g., autism spectrum disorders, ASDs; attention deficit disorder, ADD; mental retardation; cerebral palsy; and sensory deficits) being directly linked to unintentional low-dose exposure to environmental chemicals [108, 235]. Exposure at various stages of development may disturb the delicate sequence of events associated with forming a fully-functional nervous system, including pioneer-neuron axonal pathfinding — a select group of neurons that extend the first axon to a target to establish a route for subsequent

axons to follow [35]. The establishment of an initial tract provides a scaffold for follower axons to fasciculate with, creating a common pathway. The follower axons respond to some or all of the same molecular cues used by the pioneer axon to navigate and cues provided by the pioneer-neuron axons themselves. The importance of pioneer-neurons is reflected by the fact that ablation their axons (pioneer axons) can disturb the guidance of follower axons by delaying or misrouting them from target destinations. In certain developmental pathways pioneer axons are absolutely essential for follower axons to make proper connections [167].

Pioneer-neuron axonal pathfinding is highly stereotyped and dependent on the transduction of molecular navigational cues supplied by the surrounding environment [68, 211]. Represented in Figure 1.1, the pioneer axon is guided by diffusible molecules secreted from target cells and by direct physical interaction with cell adhesion molecules and the extracellular matrix [37]. Because there is no existing tract for the axon to follow, pioneer-neuron axons have to rely heavily on transient spatiotemporal molecular guidance cues. In some instances, the sensitivity of the axon's growth cone to soluble chemical gradient-based guidance may be on the order of 0.2% across the spatial extent of the growth cone [147, 170]; thus, there is the possibility that toxic chemical insults may disrupt growth cone-detection of molecular gradients. As a result, minute quantities of toxicants may have a profound effect on the normal mechanisms governing precise neural connection [167, 180]. Recent insights indicate the possibility that low-dose subclinical neurotoxic exposures, which initially present no measurable symptoms, may play a substantial role in the manifestation of neurodegenerative diseases in adults [31]. Therefore, pioneer-neuron axonal pathfinding was chosen for this study due to its developmental importance and potential for low-dose neurotoxicant detection.

In vitro axonal guidance methods

In 1979, Gunderson and Barrett showed for the first time that axonal pathfinding could be directly manipulated by soluble chemical guidance molecules. They used a micropipette filled with various concentrations of NGF to locally establish a chemical gradient that elicited a positive response from the growth cones of chick dorsal-root ganglion (DRG) neurons [85]. This paved the way for subsequent experiments that tested the chemical guidance properties of various soluble biological molecules [37, 130, 238].

Other methods to influence axonal pathfinding have also been contrived *in vitro*. They range from patterns of chemical immobilization on substrate surfaces [88, 111], to secretion of diffusible guidance molecules from target sources [17, 85, 130], to engineered substrates with geometric confines and constraints [54, 136, 230], or combinations of these techniques [73, 106, 153, 196]. The advancements in neurobiology have elucidated many of the spatiotemporal molecular signaling events necessary for axonal pathfinding. In-depth reviews of the biological molecules and mechanisms involved in axonal guidance can be found in the work done by Mark Tessier-Lavigne [211] and Alain Chédotal [35]. Taking advantage of this knowledge, in this dissertation a single-neuron axonal pathfinding system was devised to reproducibly subject individual neurons to identical microenvironments conditions for evaluating developmental and pathfinding capabilities.

1.4 Project goals and applications

Creating a single-neuron axonal pathfinding biochip that utilizes geometric and chemical guidance of axons will provide a statistically relevant method to evaluate the

response of multiple individual axons simultaneously. This has the potential to replace the existing method of the micropipette experiment used for diffusible axonal guidance in favor of a more spatially defined system. We anticipate the future use of this system could be instrumental as a preliminary screen for developmental neurotoxicity testing of various chemical compounds. As an example, it could be used to test the *hypothesis* that *axonal turning and extension is more sensitive to sub-lethal doses of chemical toxicants than axonal extension along the initial trajectory during chemically-guided single-neuron axonal pathfinding*. This idea is based on our preliminary data showing geometrically constrained axonal pathfinding is sensitive to methylmercury (MeHg) at concentrations as low as 5-10 nM [225]. Therefore, the necessary objectives to create the single-neuron axonal pathfinding system are to 1) increase the throughput of the laser cell-micropatterning process, 2) identify the proper cell-culture conditions to promote individual axonal extension on a polydimethylsiloxane (PDMS) substrate, and 3) create a microfluidic biochip system capable of generating a localized spatial gradient of chemical guidance molecules. The specific aims of this work are:

Aim 1: Design and fabricate a microfluidic cell-delivery biochip to increase the efficiency laser cell-micropatterning. A removable microfluidic cell-delivery biochip will be incorporated into the laser cell-micropatterning chamber for single-cell placement onto a cell-culture substrate. This will allow the user to identify a cell from a gentle flowing cell suspension in an effort increase throughput and to select a viable cell to be patterned.

Aim 2: Determine the cell-culture conditions necessary to promote individual axonal elongation within and beyond the confines of a geometric microstructure. PDMS biochips will be designed to geometrically limit extension directionality of

developing axons. Individual-neurons will be placed into the confines of these microstructures and the extension of individual axons thru and beyond the geometric guidance microchannels will be evaluated. Various substrate-bound axon-growth promoting molecules will be tested to determine the most desirable conditions for promoting axonal extension.

Aim 3: Design and fabricate a single-neuron axonal pathfinding biochip system with the capability to reproducibly generate localized spatial gradients of chemical guidance molecules.

Using the cell-culture conditions and geometric microstructure designs outlined in Aim 2, a biochip system will be designed with the capability to create localized spatial gradients of diffusible chemical guidance molecules. Once established, application of chemical guidance molecules from the localized source will be tested to identify a substance or combination of substances capable of positively attracting an extending axon (turn and/or extend towards) beyond the confines of the geometric guidance microchannel.

Chemical guidance of an individual axon can be achieved by creating a localized spatial gradient of a chemoattractant molecule. Therefore, creating a system where individual cells can be placed at a specified distance from the source will allow multiple neurons to be simultaneously exposed to the effects of the gradient due to radial diffusion of the guidance molecule.

To make full use of the exceptionally high sensitivity of pioneer-neurons to soluble chemical guidance, we will construct a biochip-based single-neuron axonal pathfinding assay using microfluidics to reproduce the classical micropipette experiment with a higher spatial resolution. The importance of using individual-neurons for this

assay is the creation of a pioneer-neuron axonal pathfinding model, which for future applications, will be the most sensitive to the administration of a neurotoxic substance while being subjected to a chemical guidance gradient, because there is no trophic support from other cells. Unlike the micropipette experiments, we will be able to systematically evaluate the simultaneous chemical guidance of multiple individual axons to a localized chemical gradient. To achieve this, microfabricated geometric guidance microchannels will be used to orient a single extending axon to a choice point (an intermediate destination where the growth cone turns or changes direction as it enters the next segment of its journey) and a thru-hole connecting two layers of PDMS will serve as microfluidic source for the release of soluble chemical guidance molecules [64, 136, 217, 230]. First we will establish the cell-culture conditions necessary to promote single-neuron axonal extension and then test the ability of individual axons to be guided in the direction of an increasing chemical gradient. This will serve as our soluble guidance molecule model for pioneer-neuron axonal pathfinding.

To initiate an axonal pathfinding event, individual-neurons from a neuronal cell suspension will be laser cell-micropatterned into a biochip equipped with a matrix of microwells, each connected to a geometric guidance microchannel open at the end. Based on gathered data, we will statistically evaluate axonal pathfinding 20 μm beyond the choice point (the end of the geometric guidance microchannel). After the extending axon is geometrically guided by the microchannel, at the choice point, its pathfinding direction will be influenced solely by the establishment of a localized chemical gradient of soluble chemical guidance molecules released from a microfluidic source. Although determination of a single molecular compound to influence axonal pathfinding of a specific type of neuron is a complicated endeavor, evidence obtained from random cell-

cultures indicate that more than 50% of isolated individual chick forebrain neurons (CFNs) will extend an axon to contribute to the formation of a neuronal network. This suggests that many CFNs can be induced by unknown signals that may be secreted from other neurons from the same cellular population to become part of the network. Therefore, we will make full use of a biochip system that contains many identical single-cell axonal pathfinding units and choose those units, without sorting the cell type in advance, as the investigation subjects in which pathfinding events occur. In addition, we will use media that has been “conditioned” by established networks in random cultures of the same cell population as our chemical guidance source.

CHAPTER II
BACKGROUND AND LITERATURE REVIEW ON DEVELOPMENTAL NEUROTOXICITY TESTING

2.1 Importance of developmental neurotoxicity (DNT) testing

There is great concern about a children's health pandemic with regards to the neurodevelopmental disorders that afflict them. The developing central nervous system (CNS) is a unique target for environmental toxicants both pre- and postnatal. Exposure to industrial chemical toxicants at various stages throughout development are known to contribute to injuries that result in autism, attention-deficit hyperactivity disorder (ADHD), dyslexia, and other cognitive impairments [81]. The damage caused by these exposures is often untreatable and frequently permanent; resulting in reduced intelligence (expressed in terms of lost IQ points) or behavioral abnormalities. Reports indicate a rise in the incidence of learning and neurodevelopmental disorders in children over the past three decades; now approximately 10-15% of all births are associated with disorders of neurobehavioral development [81], with 1 in 68 children in the United States being diagnosed with some form of an autism spectrum disorder (ASD) [7, 93, 188]. Additionally, ADHD affects 14% of the ~4 million children born each year [124]. Scientific evidence is showing support that the increases in diagnoses are due to actual illnesses and not merely attributed to greater recognition of the conditions. It is estimated that 3% of developmental disabilities are the direct result of an environmental exposure, and that another 25% stem from interactions between environmental factors and genetic susceptibility [80, 146]. As an example of the burden posed by neurodevelopmental disorders, in 2007 it was estimated that the lifetime per capita incremental societal cost for a person with autism would be $3.2 million, due to lost productivity and the need for adult care [69]. With more diagnosed cases of developmental disabilities and rising costs

associated with them, the search for the causes of these diseases and finding cures has become a significant topic in neurological research.

Chemical susceptibility of developing brain

The brains of infants and children are uniquely sensitive to chemical neurotoxicants at levels far below those known for adults [41, 80, 180]. This high sensitivity is attributed to an immature blood-brain barrier, increased adsorption versus low body weight, and diminished capability to metabolically remove exogenous chemicals [200]. The developing brain is not completely unprotected from chemical toxicants due to the placental barrier protecting the fetus and blood-milk barrier protecting infants. Unfortunately, many chemicals and substances are fully capable of crossing these barriers [97]. Metals and low-molecular weight lipophilic compounds are of particular concern due to the relative ease at which they cross these protective barriers; with the latter having the capability to accumulate in maternal adipose tissue and then transferred to the infant via breast milk. The blood-brain barrier does not fully develop until about 6 months after birth and during this time, as well as after, synaptic pruning activity increases, reaching a maximum level around the age of two [183]. Thus, there exists a large window of opportunity for chemical toxicity to influence the developing CNS. Therefore, exposure to environmental chemical toxicants at various stages of development may disturb the delicate sequence of events associated with forming a fully-functional nervous system.

2.2 Industrial and environmental chemicals contributing to DNT

According to the Environmental Protection Agency (EPA), over 3,000 high production volume chemicals (in excess of 1 million pounds) are either produced or

imported each year in the United States. In addition to this there are over 80,000 existing industrial chemicals registered for commercial use with the EPA in accordance with the Toxic Substances Control Act of 1977, which at the time of the passage there were approximately 62,000 chemicals already in use [22, 80, 215]. Despite the large database of chemicals, most are never tested for DNT because there are no general requirements for DNT testing of chemicals or pesticides. Testing is only required for chemicals that are thought to have neurotoxic effects prior to their registration [200]. The paucity of information related to chemical DNT is largely due to the current testing guidelines; specifically, the explicit use of *in vivo* models [137]. While informative, to test one chemical under these guidelines it typically takes three months, requiring the sacrifice of approximately 1000 rat pups, with a total associated cost upwards of $1.4 million. It should come as no surprise that absent mandatory regulatory requirement, chemical evaluations for DNT will remain elusive. Furthermore, because there is such a small database of chemicals that have been evaluated for DNT, any DNT study that is performed will have a difficult time interpreting the results and drawing comparisons between other chemicals in a meaningful way to contribute to regulation and risk assessment.

In 2006, Grandjean and Landrigan published a report specifically related to the developmental neurotoxicity of industrial chemicals [80, 221]. Because causal relationships are difficult to prove unless the effects are pronounced, epidemiological studies for DNT resulted in only a few chemicals classified as being definitive developmental neurotoxicants in man; methyl mercury, lead, arsenic, polychlorinated biphenyls (PCBs), toluene, and ethanol. These industrial chemicals have been studied extensively and all of them have been shown to have debilitating effects on the

developing nervous system [29, 42, 102, 146, 168, 192]. Additionally, at that time another ~200 metals, solvents, and pesticides were identified for their clinical neurotoxic effects in adults. Of these ~200 chemicals, almost half of them are high production volume chemicals. In 2014 Grandjean and Landrigan augmented the DNT toxicant list to include fluoride, manganese, tetrachloroethylene, chlorpyrifos, dichlorodiphenyltrichloroethane, and brominated diphenyl ethers [81]. Thus, on average two new chemicals were added to the DNT toxicant list each year. Despite the increase in identification, there remains a gap between the number of substances known to be toxic to the adult brain (214) and those known to cause DNT (12). This is primarily attributed to the nature of toxicity of the adult brain as being a result of acute poisoning events that can be systematically identified with cause and effect relationships. Whereas, identification of DNT is subject to exposure data being collected during pregnancy and neurobehavioral evaluation of the child 5-10 years later [81]. Because the brain develops through a series of strict sequential events any disruption has the potential to cause permanent damage that may not present until later in life, contributing to diseases such as, Parkinsonism-dementia, Alzheimer's disease, and amyotrophic lateral sclerosis [71, 146, 182].

Toxic potential of lead exposure

As an example of the far reaching affects that a developmental neurotoxicant can have, a brief overview of lead toxicity will be highlighted. Lead is arguably the most well-known and studied neurotoxic substance. The effects of lead exposure have been dated as far back as ancient Rome. At that time there were many sources of exposure: from the water supply due to lead plumbing; contamination of food from the use of lead plates; and contamination of containers used for storing wine [224]. Lead poisoning has

been known to cause brain damage, mental retardation, and various behavioral abnormalities. Despite the long-known adverse effects of lead, there was continual use of organic lead in products up until the late 20th century. Lead was a popular additive to paints as well as to gasoline as an anti-knocking agent, spurring the sale of leaded fuels from the 1920s through 1980s [71].

The first reported case of the developmental neurotoxic effects of lead in children occurred in Queensland, Australia in 1904. It was discovered that the ingestion of peeling lead-based paint was causing neurological dysfunction in children [70]. Not long after articles about childhood lead poisoning began showing up in the United States [174]. It wasn't until the 1970s that serious clinical evaluations of the subtle, yet powerful, effects of lead neurotoxicity in children began to surface [121, 123, 151]. This work demonstrated that deficits in academic performance and the attention spans of children could be attributed to lead exposure. At that time, the acceptable level of lead in blood for children was 60 µg/dL; the same level at which clinical signs of neurotoxicity could be seen in adults [146]. Throughout the years from the 1970s up until 1991 the acceptable blood-lead concentration level was lowered to 25 µg/dL. In 1991, this level was readjusted in accordance with clinical findings to 10 µg/dL, and that remains the current tolerable amount to this day [71]. Although the current acceptable level is one-sixth of its initial value, there is evidence showing that concentrations lower than 10 µg/dL can cause IQ deficits and behavioral abnormalities [30, 125]. Furthermore, some researchers believe that there is no safe threshold for the adverse effects of blood lead on neurobehavioral function [109].

Developmentally, lead has shown to be toxic at various stages: including but not limited to cell proliferation, cell differentiation and synaptogenesis [27, 102]. At the

molecular level, lead is known to disrupt neural cell adhesion molecules and calcium ion (Ca^{2+})-mediated enzymatic function; with significant regard to synaptic activity [25, 101]. Research has shown that lead neurotoxicity has its greatest adverse effects during the later stages of brain development, where it disrupts natural cell apoptosis and the synaptic trimming/pruning process [155, 183]. Irregularities in cell apoptosis and the pruning process can lead to deficits in memory, learning, and motor function associated with the hippocampus, cerebral cortex, and cerebellum [61]. In newborns and young children, lead toxicity has been shown to cause learning and IQ deficits as well as abnormal social behavior [14, 125, 151].

Toxic potential of methyl mercury (MeHg) exposure

Organic mercury compounds have a long history associated with neurological dysfunction. It was first reported in 1865 by George Edwards after laboratory accidents produced clinical symptoms that did not resemble those caused by any known disease at that time [82]. Despite this alarming report, organic mercury compounds were continually applied in various areas including as a cure for syphilis and as a fungicide. Some of the mechanisms by which MeHg causes neurotoxicity have been deciphered. Transport of MeHg from the blood to the CNS across the blood brain barrier (BBB) is aided by the L-type neutral amino acid carrier transport (LAT) system. This occurs when MeHg binds to sulfhydrul groups of the amino acid cysteine, creating a MeHg-L-cysteine conjugate that is a substrate for the LAT system. Once across the BBB, MeHg can dissociate from cysteine compounds and bind with the thiol groups of small molecules and peptides. Of particular concern is MeHg binding to sulfhydrl-containing enzymes, such as plasma cholinesterase, inhibiting the enzymatic activity. Another critical pathway susceptible to MeHg disruption is the antioxidant γ –glutamyl-cysteinyl-glycine (GSH)

system. GSH is the most abundant intracellular low molecular weight thiol-containing molecule in the CNS. The mercury atom directly interacts with the thiol group of GSH creating a compound (GS-$HgCH_3$) that is marked for excretion, thus reducing the overall levels of GSH. Decreased levels of GSH cause an increase in reactive oxygen species (ROS) that result in oxidative stress that can affect nucleic acids, lipids and proteins. Lastly, MeHg has been shown in many studies to cause glutamate dyshomeostasis by inhibiting glutamate uptake into synaptic vesicles and increasing the spontaneous release of glutamate; however, the mechanisms associated with mediating glutamate increased glutamate release and decreased glutamate uptake in MeHg toxicity are not completely understood [59].

2.3 Neurodevelopmental disorders greatly impacting society

The definition of DNT can be summarized as the adverse effects of pre- and postnatal chemical exposure on the developmental function of the nervous system. These adverse effects may be expressed at any time during the life span of the individual and are typically evaluated by neurochemical changes, structural/morphological changes, or by behavioral abnormalities [40]. Examples of neurodevelopmental disorders in children include mental retardation, ADHD, autism, and associated learning disabilities. Children with neurodevelopmental disorders experience difficulties with language and speech, motor skills, behavior, memory, learning, or other neurological functions. While the symptoms and behaviors of neurodevelopmental disabilities often change as a person ages, some individuals with childhood neurodevelopmental disabilities in end up with disabilities that persist throughout adulthood. Diagnosis and treatment of these disorders can be difficult; treatment often

involves a combination of professional therapy, pharmaceuticals, and home- and school-based programs [216].

Autism spectrum disorder (ASD)

Autism spectrum disorders (ASDs) are disorders of the brain where genetic mutations, deletions and copy number variants cause abnormalities in behavior, communication, learning, and social interactions with others. The term “spectrum” refers to the wide range of symptoms, skills, and varying levels of impairment that children with ASD can have. It has been estimated that the prevalence of autism in children has increased by a factor of four in one decade from 7.5 per 10,000 for children born in the 1980s to 31.2 per 10,000 for children born in the 1990s [236]. According to California Health and Human Services Agency, from 1987 to 2002 there was an increase in the rate of autism by 634%. Direct causes for the disease remain elusive because there are no broad genetic ties to which all diagnoses can be related. There are no specific biomarkers or anatomical anomalies that define autism, rather diagnosis is based on clinical and behavioral assessment [122]. Thus, popular theory has shifted to the idea that early environmental exposure working synergistically with genetic susceptibility could be the underlying cause of the disease [15, 81, 122, 124, 221].

Further investigations into the environmental contributions associated with ASDs have shown supporting evidence that early exposure during critical periods of development results in manifestation of the disease. Medications given during the first trimester of pregnancy such as, thalidomide, misoprostol, and valproic acid have all been determined to induce autism-like disease [122, 124] as well as a growing number of industrial chemicals being linked to neurological deficits [15, 80, 160]. More recently, the topic of vaccine-related causal relationship of thimerosal and autism has garnered

much attention. Thimerosal is a mercury-containing compound that has been used to extend the shelf life of vaccines and was once thought to cause autism. Substantial effort was conducted to validate this claim; however, there appears to be no known association between autism and childhood immunization [52, 122].

Attention deficit hyperactivity disorders (ADHDs)

ADHD is a heterogeneous syndrome of persistent, inappropriate levels of inattention and/or hyperactivity and impulsivity that result in pervasive impairments across multiple life domains [139]. Symptoms of this disease include difficulty staying focused and paying attention, difficulty controlling behavior, and hyperactivity. Population studies indicate that five percent of children worldwide have impaired levels of attention, as well as hyperactivity [33]. In the United States, this number rises dramatically to 14% of children born each year; with boys being 4-5 times more likely to be diagnosed than girls [124]. ADHD has three categorical classifications: predominantly hyperactive-impulsive, predominantly inattentive, and combined hyperactive-impulsive and inattentive. The continual increase in diagnosis is leading the scientific community to investigate low level chemical exposures as a potential cause [118, 190]. There is evidence showing that children with mothers who smoked, or are exposed to lead or mercury are more likely to develop ADHD [97]. Diagnosis of ADHD is based on observed behavioral responses such as duration of looking, head turning, reaction time and speech performance. Onset of symptoms is typically noticeable between the ages of 3 to 6 years and with the right diagnosis and treatment they can effectively disappear; however, a small number of individuals will be afflicted with the disease throughout their entire life.

Fetal alcohol syndrome (FAS)

Fetal alcohol syndrome (FAS) is a disease that is characterized by birth defects due to the consumption of alcohol by the mother during pregnancy. Alcohol passes easily from a mother's bloodstream into the developing baby's blood and can disrupt fetal development at any stage of pregnancy. Children with FAS may grow less quickly than other children, have facial malformations, and typically have abnormalities of the CNS contributing to mental retardation and ADHD. FAS is the leading cause of mental retardation and birth defects in the world [229]. The name was first coined in 1973 by Ken Jones and David Smith when they resurrected the notion of the adverse effects prenatal exposure to alcohol can have on children [107]. Since then, great effort has been expended to provide the necessary information on the dangers of prenatal alcohol exposure to expecting mothers, as well as increased detection methods to begin treatment for the disease. The societal impact of FAS is quite alarming when you consider that a preventable disease afflicts between 1,000 to 6,000 children of the approximately 4 million born each year in the United States [51]. Added to that is the estimated $3 million lifetime expenditure for care for someone with FAS. According to the National Institutes of Health, binge drinking puts a fetus at the greatest risk; however, even lesser amounts can still cause damage with researchers concluding that there is no safe level of alcohol consumption during pregnancy.

2.4 *In vitro* DNT testing methods

Traditional neurotoxicity testing methods involve the use of large numbers of sacrificial animals to test various chemical, morphological, and behavioral endpoints related to toxic chemical exposures. In 1998, the United States Environmental Protection

Agency (USEPA) reissued testing guidelines for neurotoxicity testing, including a section devoted to developmental neurotoxicity (DNT) assessment [22]. In 2007, the Organization of Economic Co-operation and Development (OECD) drafted DNT test guideline 426 (TG 426) to provide information on the effects of repeated exposure to substance during *in utero* and early postnatal development [137]. Both of these testing methods were explicitly focused on the use of rodent models. Despite the wealth of information that can be gained by using these models, they consume large quantities of money, time, and animals and are thus, not suitable for screening large numbers of chemicals. In an effort to expedite assessment of the developmental neurotoxic potential of various substances, non-mammalian animal models and *in vitro* cell-based methods have been devised to mimic critical developmental events of the human nervous system [40].

Background neurodevelopmental biology

Development of the CNS initially begins upon the complete formation of the neural tube. At this time, anterior-posterior and dorsal-ventral positioning is established and the stem cells of the neural plate and tube undergo induction into neural precursor cells. Bone morphogenetic proteins (BMPs) and FGFs are key endogenous signaling molecules that influence the fate of neural stem cells. In the neural tube, the dorsal region is known as the roof plate. This structure is responsible for establishing gradients of a variety of signaling molecules including BMPs, dorsalin, retinoic acid and noggin. Retinoic acid acts as a transmembrane signaling molecule that activates nuclear retinoid receptors which modulate transcription. Roof plate signaling is predominantly responsible for establishing the precursors for sensory, relay, and interneuron cells. In contrast to the roof plate, the ventral portion of the neural tube is known as the floor

plate. This structure secretes and establishes gradients of Sonic hedgehog, retinoic acid, noggin, and chordin. Sonic hedgehog is a peptide hormone that binds to two surface receptors, Patched and Smoothened, which disinhibit a protein complex that modulates the functionality of the transcription factors Gli1, Gli2, and Gli3. The floor plate is responsible for organizing the position of the precursor cells that form the hindbrain, spinal cord and the motor neurons associated with them. The cells at the dorsalmost midline position are known as neural crest cells. These are transient, multipotent, migratory cells that will give rise to neurons, glia, neurosecretory cells, enteric system neurons, pigment cells, cartilage, and bone. From the direct influence of these specific neural tube structures, much of the neural tissue foundation is coded and from which the entire nervous system is generated.

In the developing nervous system neuronal and glial cells arise from the proliferation of neural precursors found in the ventricular zone of the developing brain; the innermost cell layer surrounding the lumen of the neural tube. At the peak of gestational cell proliferation, it is estimated that a developing human generates about 250,000 neurons each minute [172]. Dividing cells in the ventricular zone undergo stereotyped patterns of cell movements through the cell cycle that will influence whether they will become new stem cells or postmitotic neuroblasts (immature nerve cells). Different neuronal populations of the CNS materialize from the distinct times that the component neurons are generated and by local differences in signaling molecules and transcription factors that contribute to their fate. Differentiation of neuronal precursors into neurons and glia is heavily based on local cell-cell interactions and the associated transcriptional regulatory mechanisms that are inherent to contact-mediated and diffusible signaling molecules.

Developmental mechanisms used for DNT assessment

Many neural developmental processes are well understood at the cellular and molecular level making them suitable for *in vitro* methods. Evolutionarily conserved mechanistic neurodevelopmental processes such as, cell migration [244], stem cell differentiation [23, 243], and neurite outgrowth [91, 225] are just a few of the many key events that can be simplified and used to evaluate the toxic potential of environmental contaminants. These toxicity testing models utilize neural cells and tissues available at various stages of development, including cultures of primary neuronal or glial cells, neuron-glia co-cultures and organotypic slice cultures [10]. Most of the primary cell-cultures utilize avian and rodent sources due to the low scientific costs (ethics, time and money) and relative ease of cell extraction [11, 92, 110, 194].

Cell migration

To study the developmental toxic effects of chemicals on cell migration, Zimmer et al. created a functional test based on the migration of human neural crest (NC) cells [244]. In this work they generated NC cells from human embryonic stem cells (ESCs) and incorporated them into what they called a “migration assay of NC cells (MINC

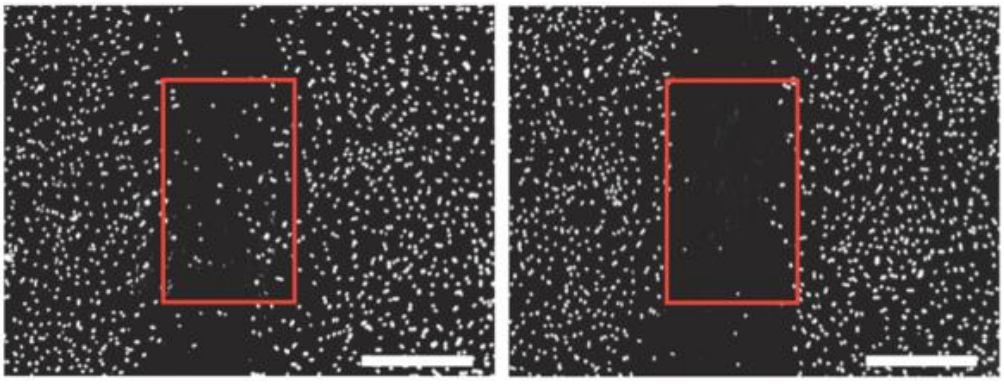

Figure 2.1: Representative image of the scratch assay showing cell migration into the “scratch zone.” Scale bar = 500 µm. Reproduced from Environmental Health Perspectives [244], Copyright 2012.

assay).” This assay was created by first establishing a confluent layer of cells and then mechanically scratching away a certain area to establish a cell-free zone. Migration of cells into this “scratch zone” was monitored in the presence of various toxic compounds (Figure 2.1). They found that methylmercury, valproic acid, and lead-acetate negatively affected the migration of NC cells at concentrations of 50 nM, > 10 μM, and 1 μM respectively. With this assay, they concluded that human NC cell migration can be impaired by developmental toxicants at remarkably low levels.

Cell differentiation

The genetic programming associated with cellular differentiation involves precise expression of transcription and other related factors to determine the cell’s fate. Due to the complex sequences of events, it should come as no surprise that cellular differentiation is susceptible to neurotoxicant disruption. To illustrate this, Hill et al. exposed three-dimensional neurospheres of human tetracarcinoma NT2/D1 cells to various teratogens. NT2/D1 cells have similarities to ESCs in that when exposed to retinoic acid they differentiate into neurons, astrocytes and oligodendrocytes [94]. The results of this work showed that valproic acid, a common anticonvulsant and mood-stabilizing drug, severely affected neurogenesis by decreasing cell viability and expression of specific neural gene markers. In another study, Zimmer et al. investigated the temporal sensitivity of CNS development by analyzing the orchestrated waves of gene expression associated with neuronal differentiation [243]. In this work, differentiation of the murine ESC line (CGR8) was found to be non-cytotoxically disturbed by retinoic acid and cyclopamine. A more in-depth analysis of transcription profile expression revealed that there are coordinated waves of gene expression during neuronal differentiation of ESCs that are susceptible to toxic disruption. As an example,

they were able to show that a short exposure (~7 days) to lead (1 µM) during the final phase of differentiation caused a disturbance in neuronal maturation and the expression of markers consistent with neuronal disease.

Electrophysiological approaches

Neurons have the unique ability to recognize and transmit electrical signals in the form of action potentials. Using the giant squid axon, Hodgkin and Huxley established the principles that electrical signaling via action potentials arise from ion fluxes brought about by the selective permeability of nerve cell membranes to different ions, due to the non-uniform distribution of ions across the cell membrane. Ion concentration gradients inside the cell relative to the outside of the cell are established by ion-channels and active transporters [96]. They were able to show that action potential initiation corresponded to voltage-gated Na^+ ion-channels opening allowing a massive influx of Na^+ ions into the cell, depolarizing the cell membrane. This caused the resting membrane potential to sharply increase until the voltage-gated Na^+ ion-channels closed and the voltage-gated K^+ ion-channels opened. The outflow of K^+ ions into the extracellular medium drastically reduces the membrane potential and slightly overshoots it below the resting membrane potential. Due to the higher permeability of the nerve membrane to K^+ ions, they diffuse back into the cell and the original resting potential is reestablished. Along with Na^+ and K^+ ions, Ca^{2+} and Cl^- ions are present in nontrivial concentrations inside and outside the cell, and contribute to the overall membrane potential. The Goldman Equation (2.1) can be used to estimate the resting membrane potential (E_m) by accounting for the individual concentrations of various charged species and their permeability through the membrane:

$$E_m = \frac{RT}{F}\left(\frac{\sum_i^N P_{M_i^+}[M_i^+]_{out} + \sum_j^Q P_{A_j^-}[A_j^-]_{in}}{\sum_i^N P_{M_i^+}[M_i^+]_{in} + \sum_j^Q P_{A_j^-}[A_j^-]_{out}}\right) \quad (2.1)$$

M_i is a monovalent positive ionic species, A_j is a monovalent negative species, and P_x is the respective membrane permeability for each species. For a typical neuron the resting membrane potential is approximately -60 mV.

For an action potential to be initiated the presynaptic neurotransmitters released into the synaptic cleft must result in the opening of voltage-gated and ligand-gated ion-channels, enabling ion flux. If the presynaptic neurotransmitter causes depolarization of the membrane potential it is considered to be an excitatory postsynaptic potential (EPSP). Opposite of this would be a neurotransmitter signal that causes hyperpolarization of the membrane, known as an inhibitory postsynaptic potential (IPSP). When the overall summation of synaptic inputs to a cell raises the membrane potential above a certain threshold (approximately -50 mV), an all or nothing self-propagating action potential is initiated via a positive feedback mechanism from the voltage-gated ion-channels in the membrane (Figure 2.2). The axon hillock is a specialized region of the soma, adjacent to the axon; where there is an increased density of voltage-gated ion-channels and is the site of action potential origination. When the axon is myelinated, the action potential propagates along the axon from one node of Ranvier to the next in what is known as salutatory conduction. This method of signal transduction prevents charge leakage through the membrane and drastically increases the conduction velocity of the signal. Once the depolarizing signal reaches the axon terminal, Ca^{2+} ions enter the presynaptic terminal causing the synaptic vesicles to fuse with the membrane and neurotransmitters are released into the synaptic cleft.

The conventional tool for studying electrophysiology has been the patch clamp. A typical patch clamp system is comprised of a fire polished micropipette that has been created by pulling a capillary tube and placing within it an electrode and intracellular-like fluid. Under a microscope the tip of the micropipette is carefully positioned using a micromanipulator to make contact with a cell. Due to the small size of the micropipette tip (1-2 μm opening) only a small portion of the cell membrane surface area, “patch,” comes into contact with the micropipette. Most commonly, suction is applied allowing for a high resistance (gigaohms) seal to be created between the pipette and cell membrane, known as a “cell-attached patch.” The patch clamp can also be operated in a manner where the applied suction ruptures the cell membrane enabling measurements of the intracellular components; called a “whole-cell” patch. In this configuration the patch clamp can act in voltage or current clamp modes, enabling detailed measurements of currents and membrane potentials, membrane resistance, and membrane capacitance. Due to the ability to analyze the electrical activity of an individual cell, patch clamp has been routinely used to assess neuronal health and functionality when exposed to chemical toxicants. An example of this was recently demonstrated by patch clamp recordings of striatal medium spiny neurons from neonatal rats exposed to antiepileptic drugs with proapoptotic action [62]. The patch clamp recordings revealed augmented inhibitory post synaptic currents leading to disruptions in functional synaptic maturation. Thus, they were able to show that exposure to antiepileptic drugs during sensitive postnatal periods can impair physiological maturation of synapses for the neurons that survive the initial drug insult.

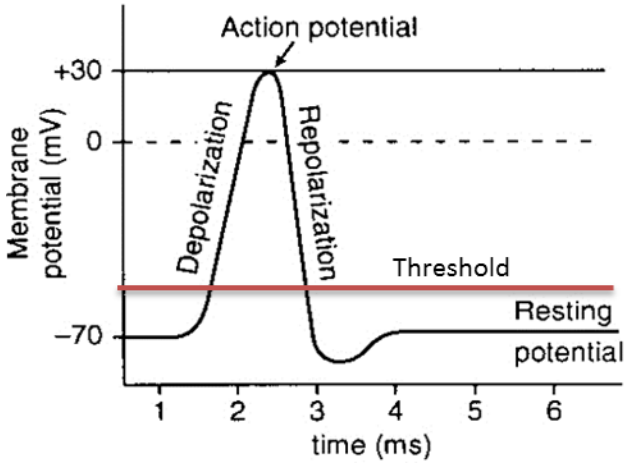

Figure 2.2: Representative image of the change in cell-membrane potential associated with an action potential.

Microelectrode arrays (MEAs) can be used to record the electrophysiological activity of cell-cultures and tissue slices (Figure 2.3). During recording sessions, the electrodes on an MEA will transduce the voltage change from the environment carried by ions into currents carried by electrons. This allows the spontaneous electrical activity of the cellular environment to be monitored. MEAs can also stimulate the culture environment by transducing electronic currents into ionic currents through the media triggering the voltage-gated ion-channels of the cell membranes, causing the neuronal membrane to depolarize. In one study, MEAs were used to determine if chemical-induced changes in function could be detected via monitoring the development of spontaneous network activity of primary cultures of rat cortical neurons [181]. To assess the effects of chemicals, individual action potential spikes and groups of spikes (bursts) were recorded over a period of days. It was determined that 5 µM bisindolymaleamide-1 (Bis-1) negatively affected culture development by decreasing the number of active channels on each MEA and the number of bursts; while not affecting burst duration or

the number of spikes in a burst. Thus, it was shown that MEAs can be used to assess toxic chemically-induced electrophysiological dysfunction.

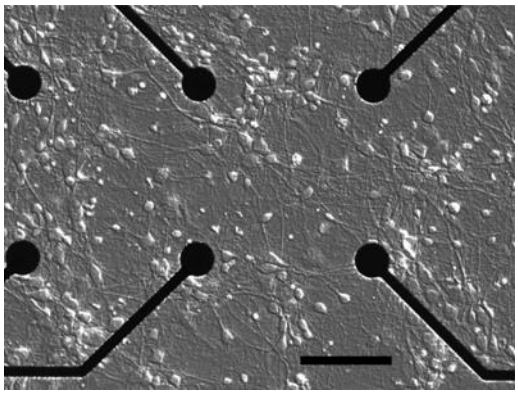

Figure 2.3: Representative image of rat cortical neuron cell-culture on a commercial MEA. Scale bar = 100 µm. Reproduced from Frontiers in Neuroengineering [181], Copyright 2011.

Neurite outgrowth

Neurite outgrowth is an essential developmental process of the nervous system. Many models associated with neurite outgrowth characteristics have been extensively investigated for applications of *in vitro* chemical DNT testing. High content screening analysis of PC12 cells plated at a cell density of 2,000 cells/well in a 96-well format has been used to assess the toxic effects of various chemicals on neurite growth [175]. For the chemicals tested in that particular study, neurite outgrowth was inhibited as a function of total neurite length and in some instances there was reduced cell viability. Heidemann et al. (2001) conducted a low cell-culture density study using primary chick forebrain neurons (CFNs) and monitored the effect that methyl mercury (MeHg) has on neurite outgrowth [91]. They found that after a 2 hour exposure to MeHg at concentrations between 0.25 and 0.5 µM, there was a significant reduction in the

number of neurons that developed an axon without a decrease in cell viability. A more in-depth review of developmental *in vitro* models used to assess chemical effects on neurite outgrowth was prepared by Radio and Mundy [175]. Briefly, in this work they describe semi-quantitative, quantitative, and biochemical methods of neurite outgrowth assessment, as well as, cell-culture models using cell lines, primary cultures, and neural stem cells. Using these techniques they concluded that neurite outgrowth models have the potential to rapidly evaluate a large number of potentially neurotoxic chemicals.

Each of the aforementioned techniques for *in vitro* chemical DNT assessment provides an important evaluation of the mechanisms of action associated with critical developmental endpoints. The greatest drawbacks to using these assays are the lack of spatial reproducibility of the culture environment and the inability to test for low-dose toxicity. All of these techniques are based on a random cell-culture environment where the trophic interactions provided by cell-cell interactions cannot be accurately determined. While the use of cell lines produces a homogeneous population for which observations can be made, the inherent genetic deviations may not make them the suitable for DNT testing. On the other hand, primary cell-cultures preserve the native cell genotype and phenotype, but the heterogeneous cell populations that result make it difficult to properly evaluate cell-specific effects. Therefore, new and emerging toxicity testing paradigms need to be developed to rapidly screen large numbers of chemicals by integrating high-throughput *in silico* and *in vitro* techniques with an emphasis on spatial reproducibility and low-dose testing limits.

CHAPTER III
DEVELOPMENT OF BIOCHIP-BASED SINGLE-NEURON AXONAL PATHFINDING MODELS

3.1 Introduction

Polydimethylsiloxane (PDMS) was selected as the material used to fabricate biochips. PDMS has been used extensively to create membranes for biological uses due to its optical transparency (transmission spectra from infrared down to ~230 nm), biocompatibility (impermeable to water, nontoxic to cells, and permeable to gases), and low cost. Using soft lithography replica relief molding, three-dimensional impression structures can be generated into the membranes to create endless biochip geometries. For this work, PDMS was used to create multi-layer cell-culture substrates with thru-holes, microchannels, microwells, and microwalls to isolate single-neurons to observe axonal development and growth cone response to a localized gradient of chemotropic guidance molecules. PDMS was also used to create a removable microfluidic cell-delivery biochip to enhance the performance of the laser cell-micropatterning system.

3.2 Creating a master mold

The first step in creating a PDMS membrane involves the generation of a microscale two-dimensional layout of the desired geometric structures that will be created through replica relief molding. SolidWorks® and AutoCAD™ were used to design both cell-culture substrates and microfluidic channel networks. Once a design was completed it was laser-photoplotted (CAD/Art Services, Inc.) onto a photomask. The masks selectively block UV radiation from the Karl-Suss MJB3 mask aligner. The advantages of using the photomasks are that they are relatively inexpensive and easy to use. The disadvantages are that they have a limited resolution of 10μm and they scratch

easily, allowing unwanted UV light to pass through. In the case where a multi-layer mold was desired, it was necessary to incorporate alignment marks into the design (Figure 3.1). When using the photomask the emulsion side was placed downward so that the mask was in direct contact with the photoresist-coated wafer in order to obtain the best results. To do this, the masks were first were cut from the photomask sheet and then attached to 4”x4”x1/4” soda-lime glass by taping all four corners with transparent Scotch™ tape. Before attaching the mask, it is essential that the glass be thoroughly cleaned and wiped (70% isopropanol) to remove any surface debris and to enable the mask to sit flat, which will allow the maximum amount of light to pass through the transparent areas.

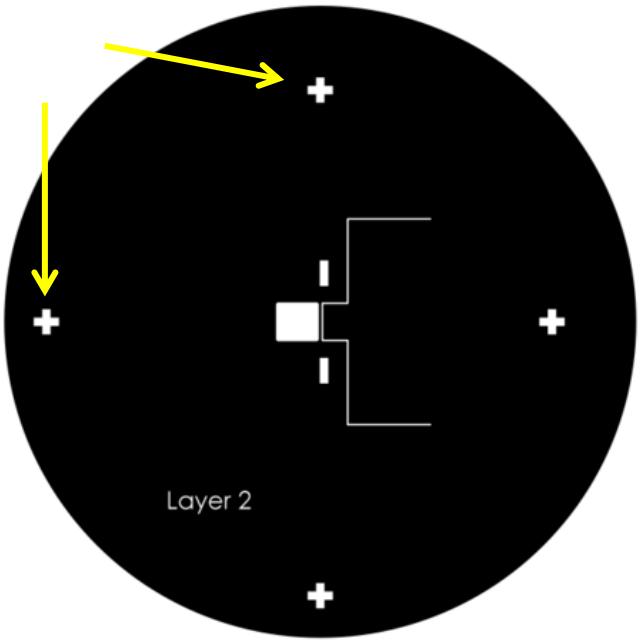

Figure 3.1: Example of a photomask design where the black areas block the UV light and the white areas allow light to pass through. The yellow arrows point to alignment marks necessary for making a multi-layer master mold.

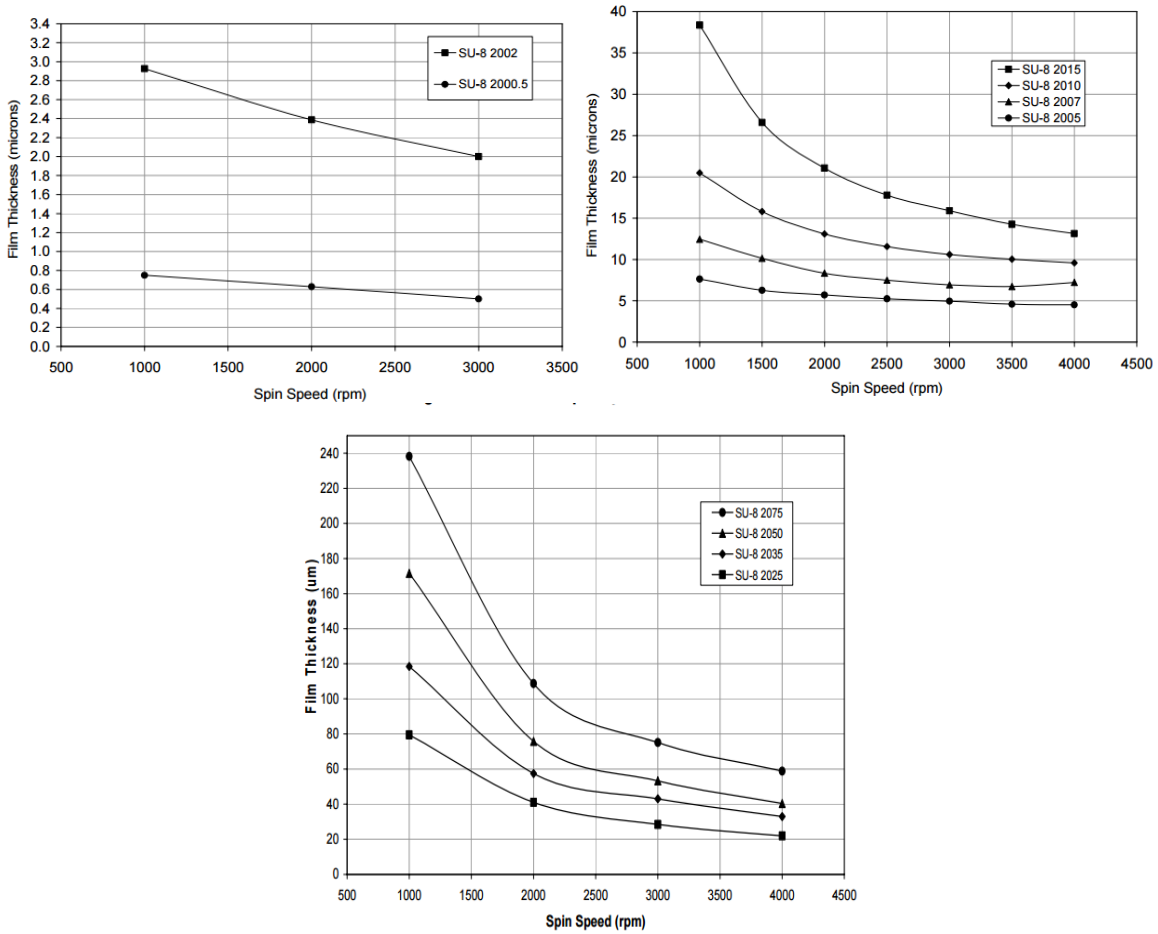

Figure 3.2: Manufacturer's (Microchem) spin speed charts for SU-8 formulations to create films of desired thicknesses.

Spin coating and soft bake

Silicon wafers (University Wafer) were used as the foundation for creating the master molds that are ultimately used to fabricate PDMS membranes. To create microstructures, SU-8 photoresist (MicroChem Corp.) was spin-coated (Laurell WS-400B) onto the silicon wafer. Based on the design of the photomask, the proper wafer size (2", 3" and 4" diameter) was selected. For one spin coating, there are a variety of formulations of SU-8, based on viscosity, that can be used to create layers < 1 µm and as thick as 250 µm. Figure 3.2 shows the spin speed charts for the various SU-8 2000

series formulations. To create the highest quality photoresist layer, it is imperative that the wafer be clear of any debris. Before spinning, compressed nitrogen was blown across the surface to displace any dust particles. Next the wafer was mounted to the spinner chuck. For wafers greater than 2”, specialty tools manufactured out of acrylic were used to aid in alignment (Figure 3.3). This was a necessary step because spinning an off-centered wafer can create an uneven coat. Moreover, at high spin speeds an off-centered wafer can lose vacuum suction to the chuck sending the wafer flying off of the chuck and destroying it. Adhering to the manufacturer’s guidelines, spinning the SU-8 involved at least a two-step process of ramping up the spin speed to 500 RPM with an acceleration of 100 RPM/s and holding for 5 seconds followed by another increase in spin acceleration at 300 RPM/s until the final spin speed is reached, and held for at least 30 seconds to evenly coat the wafer at the desired thickness. Following the spin, the wafer was placed onto a hotplate to remove the SU-8 solvent and solidify the photoresist; this was known as a “soft bake.” Longer bake times typically resulted in a better final product so the recommended guidelines were adjusted by a factor of 1.5, shown in Table 3.1. Thicker layers required a two-step baking process beginning at 65°C and finishing at 95°C to allow the solvent to evolve at a more controlled rate; increasing photoresist adhesion to the wafer. After the soft bake, the coated wafer was allowed to cool to room temperature before being mounted onto the MJB3 mask aligner for UV exposure.

UV exposure and hard bake

The SU-8 photoresist becomes cross-linked and hard when exposed to UV radiation immediately followed by a thermal input (hard bake). This is the result of a two-step process where (1) a strong acid is formed during UV exposure which leads to (2) an

acid-catalyzed thermally driven epoxy cross-linking reaction when exposed to a heat source. The amount of input energy (mJ/cm^2) required to fully cross-link the SU-8 is dependent on the thickness of the layer. The optical energy controller (Mimir, Model 505) regulates the power output (mW/cm^2) of the UV lamp on the MJB3 mask aligner to keep it at a constant intensity. Thus, the total energy necessary to crosslink the photoresist is simply the output intensity multiplied by the duration of the exposure. Overexposure can result in a phenomenon called T-topping, where excessive absorption the top part of the photoresist below 350 nm creates exaggerated negative sidewall profiles. Underexposure of the photoresist renders it incompletely cross-linked reducing the binding capabilities to the silicon substrate and consequently, the microstructures are removed during the development step. Therefore, for all manufacturing applications a 5-10% overexposure was employed to ensure the photoresist was completely cross-linked.

The hard bake, sometimes referred to as the post exposure bake (PEB), is necessary to facilitate the selective cross-linking of the exposed photoresist areas. Just as the case with the soft bake, the hard bake times were increased by a factor of 1.5 over the manufacturer's baseline recommendations to provide the best results. For

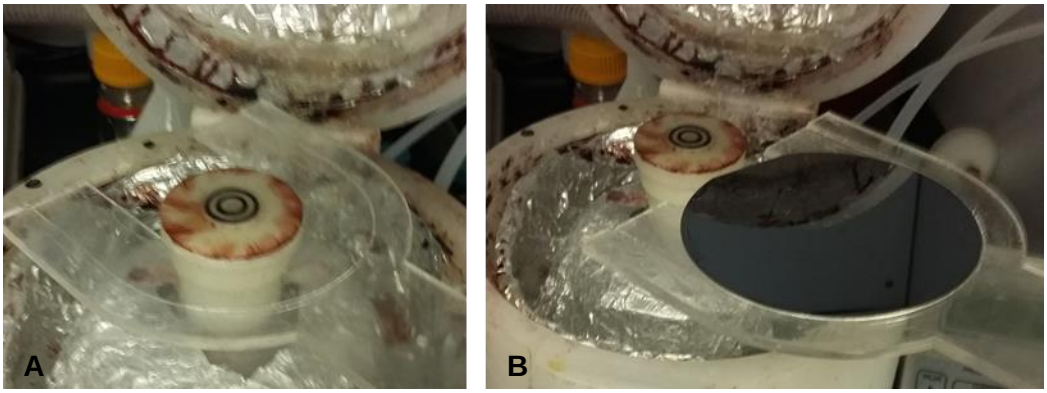

Figure 3.3: Demonstration for using a 4" acrylic wafer alignment tool. A) The bottom layer of the wafer tool aligned with the 2" chuck of the spinner. B) A loaded wafer ready to be placed onto the spinner chuck.

thicker layers of photoresist, the wafer/photoresist would be heated on a hotplate at 65°C followed by a longer period of time at 95°C. After the designated amount of time at the higher temperature had elapsed, the heat was ramped down to cool the wafer/photoresist to room temperature before development.

Development and final bake

The exposed cross-linked portions of the SU-8 are insoluble to liquid developers. Therefore, the nonessential areas of the wafer coated with uncross-linked SU-8 can be removed by covering the surface with SU-8 developer (1-methoxy-2-propyl acetate, Microchem). Based on the photoresist thickness the amount of time for development should be adjusted. The best results were obtained by covering the entire surface with developer and letting it sit for half of the total amount of time required for development. The wafer was agitated briefly to help the developer interact with hard to reach areas and then carefully removed and disposed; followed by re-immersion of the surface with developer for the remainder of the recommended time. Once the full development time had elapsed all of the developer was removed. Then, a slow stream of compressed nitrogen was blown across the surface of the wafer to help drive off any remaining developer solution. If there remains any residual uncross-linked photoresist after the nitrogen stream, the wafer should be covered and agitated with developer followed by drying with nitrogen until there is no presence of uncross-linked photoresist on the surface. Finally, the last step was to place the fully-developed wafer into a vacuum oven at 150°C and 25 mmHg for 2 hours to help further cross-link the photoresist and remove any remaining liquid developer solution.

Table 3.1: SU-8 processing parameters used to create different film thicknesses.

	Soft Bake			Hard Bake		
Thickness (Microns)	Pre Bake (Minutes @ 65°C)	Adjusted Soft Bake Time (Minutes @ 95°C)	Exposure Energy (mJ/cm^2)	Pre Bake (Minutes @ 65°C)	Adjusted Post Exposure Bake Time (Minutes @ 95°C)	Development Time (Minutes)
0.5 - 2	N/A	1.5	60 - 80	N/A	1.5 - 3	1
3 - 5	N/A	3	90 - 105	N/A	3 - 4.5	1
6 - 15	1	3 - 4.5	110 - 140	1	4.5 - 6	2 - 3
16 - 25	2 - 3	4.5 - 6	140 - 150	1	6 - 7.5	3 - 4
26 - 40	3 - 5	6 - 7.5	150 - 160	1	7.5 - 9	4 - 5
45 - 80	5	9 - 13.5	150 - 215	1 - 2	9 - 10.5	5 - 7
85 - 110	5	15 - 30	215 - 240	2 - 5	12 - 15	7 - 10
115 - 150	5	30 - 45	240 - 260	5	15 - 18	10 - 15
160 - 225	7	45 - 67.5	260 - 350	5	18 - 22.5	15 - 17

3.3 Creating PDMS biochips using the master mold

PDMS membrane preparation

PDMS (Sylgard® 184, Dow Corning) was obtained as two-part base-curing agent elastomer kit and mixed in a 10:1 w/w ratio. Typically, the two solutions were added to a 50 mL centrifuge tube and hand stirred for 10 minutes to ensure thorough mixing between the base and cross-linker. The mixing results in the formation of air bubbles that must be removed before spinning or casting membranes. Bubbles in the membrane distort the optics as well as reduce the mechanical integrity. To remove the air bubbles two different methods can be used. The first involves a time-intensive constant-monitoring process of placing the mixture in a vacuum desiccator. Reducing the pressure allows the air bubbles to rise to the surface and ultimately pop. However, the cohesion between the PDMS bubbles pulls a significant amount of mixture with them, and if left unattended, will spill out of the 50 mL centrifuge tube. Therefore, constant application and removal of the vacuum will enable the bubbles to be removed without losing any material due to spills. Depending on the volume of PDMS mixture, this process can take upwards of 1 hour to remove all the visible bubbles. The second

method I discovered when I was searching for a better way to mix the PDMS that involved inverting the centrifuge tube many times. This proved to be a less efficient way to mix the base and curing agent over hand stirring. To prevent a large mess when removing the cap of the centrifuge tube I decided to spin down the mixture. The high forces placed bubbles during the centrifugation caused them all to pop, leaving a bubble-free mixture. Thus, from that point forward all PDMS was “degassed” by spinning the mixture at 1000 RPM for 4 minutes.

Once a bubble-free mixture is obtained the PDMS becomes a versatile material to work with. To create a membrane with replica relief structures, PDMS solution is first poured onto the surface of the SU-8 master mold. To ensure proper deposition into the small crevices of the mold structures, the master mold with PDMS on top placed under

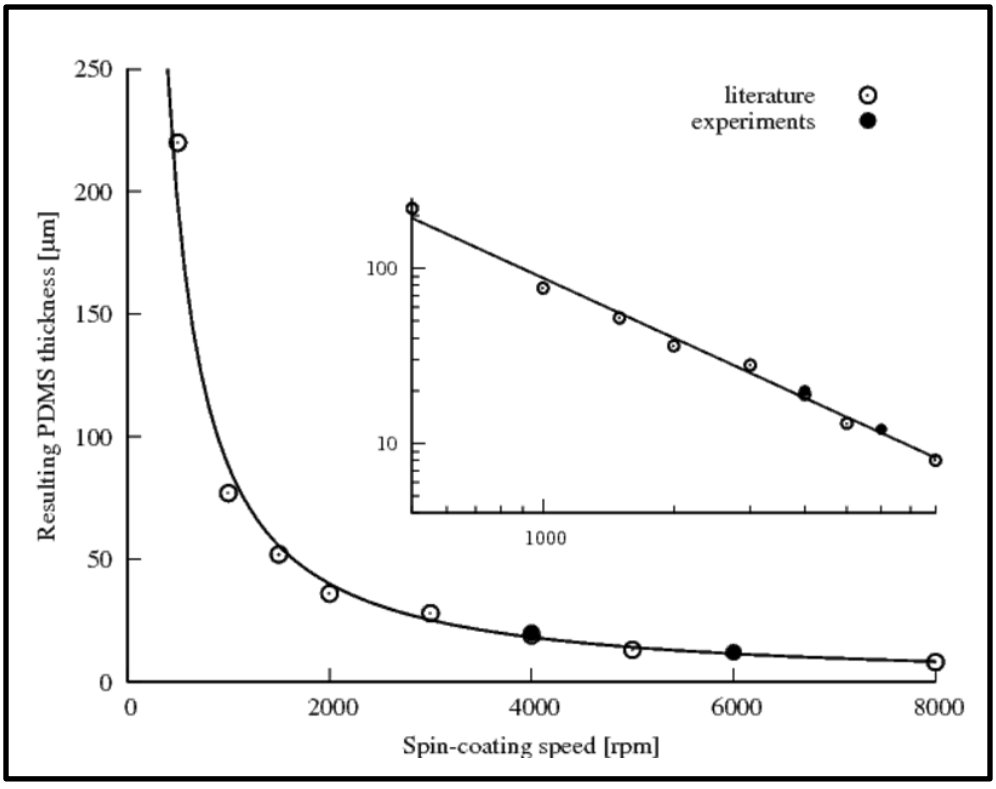

Figure 3.4: PDMS chart of spin speed vs. thickness for a 30 second spin time. Reproduced from IEEE [237], Copyright 2004.

vacuum. The vacuum allows for the elution of any air bubbles that may have been trapped or created due to pouring the PDMS and increases the structural integrity of the final membrane. PDMS can be spun at different speeds to create membranes of varying thicknesses [237] (Figure 3.4). To spin a membrane, the master mold with degassed PDMS solution was mounted to the spinner chuck and spun for a duration of 30 or 60 seconds at the proper spin speed to generate the desired thickness. For instance, if the spin speed resulted in an overall PDMS membrane thickness that was less than that of the height of the master mold structures, it would result in a complete thru-hole of the membrane for a particular mold structure. Typically, for most applications spun PDMS layers were baked at 125°C for 3 minutes and 20 seconds. This created a very flexible membrane that could be peeled off of the master mold with the negative impression of the mold structures being transferred to the membrane (Figure 3.5), giving rise to geometric microstructures. These membranes were then baked for an additional amount of time to fully cure. According to the manufacturer, the PDMS becomes fully cured when heated for 10 minutes at 150°C, 20 minutes at 125°C, or 35 minutes at 100°C. To create thicker membranes (> 1 mm) or blocks, PDMS can be poured into forms to create cast parts. This was routinely done by designing acrylic forms. PDMS does not form a strong bond to acrylic, unlike glass and other silicon-based materials, making it a suitable material for many PDMS applications. The only drawback to using acrylic as the material for creating forms is its low glass transition temperature (105°C). Therefore, when curing PDMS in an acrylic form, it was placed in a vacuum oven set to 80°C and baked for one hour at atmospheric pressure. It was found that at temperatures above 80°C the acrylic forms began to lose integrity and the form would warp.

Binding PDMS to PDMS

Many of the devices outlined in this work were made by combining multiple layers of PDMS membranes. PDMS has repeating units of $–OSi(CH_3)_2–$ groups. A weak seal can be made between two fully cured layers of PDMS when brought into contact. However, to increase the bond strength between two layers, surface modification techniques are usually employed. Exposing the surface to air or oxygen plasma generates silanol (Si-OH) groups and destroys the methyl groups ($Si-CH_3$) to make the surface hydrophilic [126]. When these hydrophilic surfaces come into contact with one another a covalent siloxane (Si-O-Si) bond is formed, and upon heating, an irreversible bond is created [138]. The effective timeframe for this method requires contact between the two layers within 1 minute after plasma treatment [141]. After 1 minute surface rearrangements occur that bring new hydrophobic methyl groups to the surface to lower the surface free energy [126]. To extend the “shelf life” of the silanol surface, PDMS extraction processes have been devised to remove un-cross-linked PDMS contaminants from the bulk polymer using organic solvents that decrease the rate of regeneration of the hydrophobic surface [126, 144, 219]. It was demonstrated by Vickers that following an extraction process, the surface of PDMS remained hydrophilic in air for up to 7 days while non-extracted PDMS reverted back to its hydrophobic state in less than 3 hours [219]. Therefore, as a practical means for working with PDMS, all membranes were subjected to a triple solvent extraction process (triethylamine, ethyl acetate, and acetone) to improve the overall biocompatibility and functionality of PDMS devices [166, 219].

Other methods for binding PDMS membranes involve the use of uncured PDMS to act as “glue.” At room temperature, a 10:1 mixture of PDMS will fully cure in 48 hours.

To extend the functional time range, mixtures can be placed in a refrigerator or freezer. The reduction in the thermal energy slows the curing process prolonging the utility of the mixture. Typically, the best results for using PDMS as glue occurred when leftover PDMS was used after being stored in a freezer (-20°C) for a period of 24-48 hours. The increased viscosity of the solution made it easier to apply to surfaces intended to be bonded together. Subsequent heating of the partially cured mixture creates a permanent bond between the two surfaces. Another way to bind two layers of PDMS was developed by the Beebe group using corona discharge [89]. A hand-held corona device uses high voltage to locally ionize the air around the electrode to create corona discharge. This modifies the PDMS surface much in the same way the oxygen plasma treatment does by making it hydrophilic. Because of the versatility of this technique, we adopted it in our fabrication procedures to bind fully cured PDMS layers together. We used an Electro-Technic model BD-20AC corona wand with a 3 inch wire electrode tip to treat the surfaces of PDMS before irreversibly binding them together. Each time two layers of PDMS were bonded together using corona treatment; the resulting newly-joined material was immediately placed on a hotplate at 125°C for 20 minutes to accelerate the bonding process. Altogether, using the methods and techniques outlined in this section we were able to fabricate the numerous PDMS biochips and devices that are described in later chapters.

3.4 Culture substrate design and surface modifications

Culture substrate design

Li and Folch determined that murine embryonic cortical neurons extend axons that actively search for the straightest permissive path while simultaneously taking into

account biochemical and topographical information during navigation in a three-dimensional environment of a PDMS substrate [153]. They found that there was a threshold height of ~22 µm where a step (change in topography) in the path of the extending axon caused it to redirect in a minimal angle of turning. Axons on plateaus would continue and extend along the top edge of the vertical wall while axons in grooves would continue extension along the bottom edge of the wall. The height of walls less than ~22 µm resulted in axons that disregarded the geometric topography and extended in a less-restricted manner. At wall heights of 10-11 µm it was determined that half of the axons would turn as result of the topography and half would not.

Similar work by Francisco et al. showed that a 15 µm high wall was sufficient to topographically regulate ~90% of chick DRG axons [64]. In their system of cell compartments connected to each other by gates/doors, they observed that confinement of a cell had no significant effect on the initial growth of axons when at least two directions were available for extension without spatial constraints; however, significant reduction in growth of axons occurred when there was confinement in all directions. When an axon extended through a gate to another compartment they found that an overall gate length less than 15 µm resulted in approximately 30% shorter axons compared to control neurons in the periphery unencumbered by any geometric constraints. The width of the gate did not seem to have any effect on axonal extension. Additionally, they observed that growth cones that interacted with the walls responded to contact with the three-dimensional constraint by decreasing surface area which coincided with an inhibition of axonal extension. These observations are consistent with the work of Mahoney et al. where they also reported that physical contact with the walls

of a three-dimensional microenvironment reduced the overall length of PC12 neurites [136].

Incorporating the results of Li and Francisco, the PDMS cell-culture substrate design presented here resulted in a three-dimensional structure where a microwell is attached to an axonal extension guidance microchannel. The microwell is 50 μm in diameter and is used to isolate the cell body of the neuron from the surrounding environment. Previous studies [166, 225] indicated that a 50 μm diameter microwell is suitable for the culture of an individual-neuron by allowing cell attachment and neurite extension without effecting cell viability. The 20 μm long and 15 μm wide microchannel connects to the microwell and provides the only path for which axonal extension can occur unobstructed. The width of the microchannel is wide enough that physical inhibition of growth cone advancement should not be a concern, while providing a guidance effect. The length of the microchannel is long enough to ensure that if neurite extension through and beyond the channel occurs, it is most likely attributed to the neurite being the axon of the cell. The height of the walls of for the microwell and microchannel is 25 μm. At this height, neurite extension up and over the walls is greatly diminished while being shallow enough to ensure proper nutrient exchange with the surrounding cell-culture media [153]. With these dimensions, the single-cell isolation units can be used to statistically reproduce the initial polarized axonal pathfinding of an individual-neuron in conjunction with a three-dimensional microenvironment. Upon reaching the end of the geometric guidance microchannel the growth cone of the axon reaches a “choice point” where further extension is no longer impeded by the walls of the microchannel. The angle of extension at 20 μm beyond the end of the geometric guidance microchannel is found by measuring the deflection of axonal pathfinding from

the centerline of the microchannel. Figure 3.5 shows the design and finished product of the cell-culture substrate. The actual dimensions of the microstructures closely follow those of the design, indicating the fabrication process outlined in this chapter is well suited to create identical geometric microenvironments with micrometer resolution.

Substrate surface modification for cell-culture

To implement the membranes into a cell-culture experiment, the surface properties must be augmented to promote cell attachment. Cell adhesion to a culture substrate is influenced by several factors including topography, surface charge, surface hydrophobicity, surface chemistry, and protein interactions. Neuronal cell membranes are negatively charged and in order for neurons to survive they must attach to the culture substrate. The most common substrate materials used for cell-culture are plastic and glass, and in this work PDMS was widely used. Manipulations in the manufacturing of plastic culture vessels allow the surfaces to be more hydrophilic, promoting even cell attachment and increasing cell growth. Cured PDMS has a slightly negative charge, and natively it is not suitable as a substrate material. Therefore, surface modification is necessary to make it more cytophilic. As previously mentioned, oxidation of a PDMS surface can be achieved through O_2 plasma treatment; where the replacement of $–CH_3$ groups with –OH groups creates a hydrophilic surface. Hydrophilic surfaces can also be achieved by exposing the surface to acidic and basic chemicals that covalently bind functional groups [19, 219, 239]. Thus, due to the widespread use of plasma oxidation and relative ease at which this can be done, we used a Harrick Plasma PDC-32G Basic Plasma Cleaner to clean and oxidize both PDMS and glass surfaces.

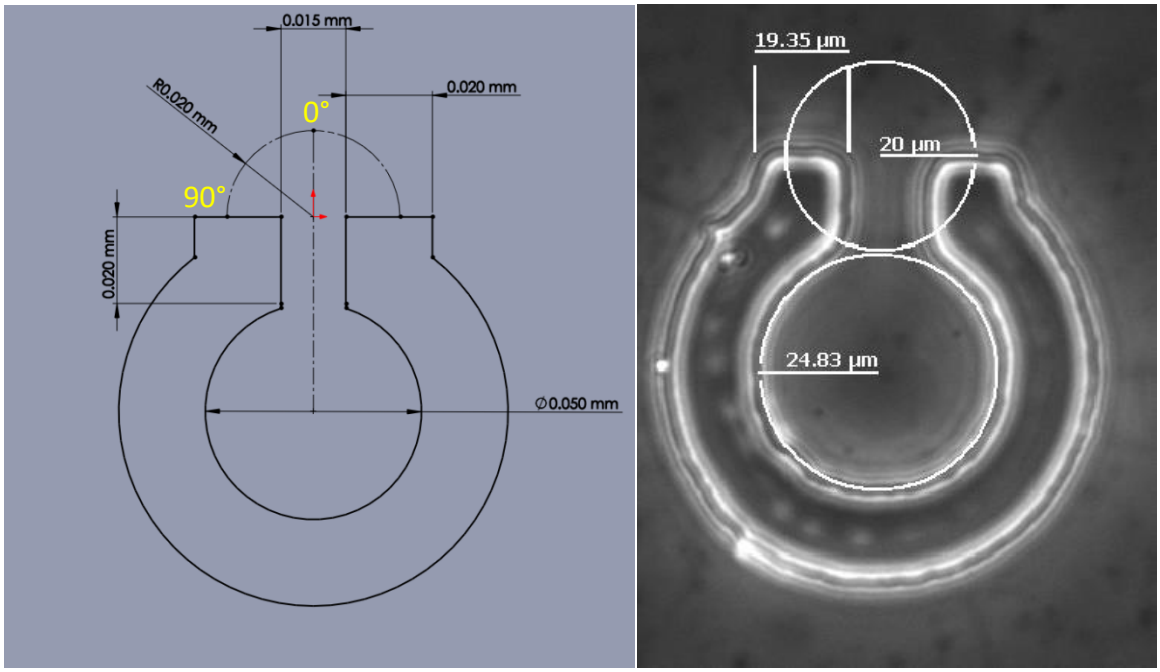

Figure 3.5: Geometric dimensions of the single neuron cell-culture substrate. A SolidWorks schematic of the design and dimensions (left) and a 20x phase contrast image of the actual substrate made out of PDMS (right).

Once a surface has been cleaned and activated further modification is necessary to support cell attachment. Physiosorption of cationic biological and synthetic polymers is a common practice to overcome the negative charge of the surface to promote electrostatic attraction and membrane receptor binding to the substrate. Some of the substances used for neuron culture are poly-l-lysine (PLL), poly-d-lysine (PDL), polyethylenimine (PEI), laminin, and fibronectin.

PLL and PDL are two synthetic poly-amino acids where the “L” and “D” refer to the chirality of lysine’s central carbon. At physiological pH of 7.4, the amino group is positively charged making the molecule hydrophilic. The precursor amino acid for PLL occurs naturally while the PDL precursor is an artificially produced amino acid that naturally occurs in plants. Due to the differences in structure and origin of the molecule,

it is thought that PDL is more resistant to animal-protease enzymatic breakdown, prolonging the duration of cell-culture [140]. PLL and PDL are typically applied to a cell-culture surface in concentrations ranging from 0.01-1.0 mg/mL. According to Brewer, for a PLL concentration of 5 µg/mL, low molecular weight solutions (MW ~27-30 kDa) are more effective at promoting neurite generation than high molecular weight solutions (MW ~130 kDa) [26].

PEI $(CH_2CH_2NH)_n$ is an organic polymer that has a high density of amino groups that can be protonated. As with PLL and PDL, at physiological pH, PEI is positively charged and promotes the cell attachment of primary cells and cell lines, which normally do not produce enough extracellular matrix factors to strongly adhere to the culture surface. At a concentration of 25 µg/mL PEI was shown to be as effective and more economical for the attachment and culture of PC-12 cells when compared to surfaces coated with PDL or collagen [217]. Although the use of PEI solutions is not as robust as more traditional substrate coating materials, it has been shown to be effective at concentrations as low as 0.001% w/v [186] and as high as 0.1% w/v [158].

Laminin is a heterotrimeric, cross-shaped glycoprotein (MW ~850 kDa) that is a major component of the basal lamina and is responsible for influencing the biological functions of cell differentiation, migration, and adhesion [132]. As a component of the extracellular matrix, laminin has been shown to be influential in guiding and promoting the differentiation and growth of neurons. Specific adhesion of the growth cone to the laminin substrate helps to expedite microtubule and organelle transfer increasing the rate of neurite outgrowth [208]. Laminin also influences the mechanisms by which diffusible guidance molecule signaling regulates axonal pathfinding. In one study, *Xenopus* retinal growth cones were shown to be guided by diffusible gradients of netrin-

1, but in the presence of soluble peptide fragment of laminin-1 (YIGSR), there was a conversion of netrin-induced attraction to repulsion [98]. Accompanying the repulsive-guidance was a reduction in cytosolic cyclic AMP levels in the growth cone, suggesting a possible mechanism for laminin's effect. Typically, to improve the efficacy of neuronal cell-culture, laminin is applied to a culture surface in a layer-by-layer technique with the first layer being PLL [111], PDL [153], or PEI [90]. The range of concentrations at which laminin is applied spans 1 µg/mL to 100 µg/mL, with the most common concentrations for use being 25 and 50 µg/mL, respectively.

Neural cell adhesion molecule (NCAM) L1 is a membrane protein that is expressed on most developing axons and is responsible for promoting growth and guidance [112]. The L1 protein consists of six immunoglobulin domains, five fibronectin type 3 domains, a single transmembrane region, and an intracellular domain [28]. In neurons, L1 interactions activate neuronal FGF receptors that trigger a second messenger cascade that will result in activation of Ca^{2+} channels, inducing neurite outgrowth [99]. As with laminin, L1 is applied to substrate surfaces in a layer-by-layer fashion, with the base layer typically being PLL. However, in stark contrast to laminin, L1 does not promote fasciculation between axons, while laminin does. The growth cone morphology is also affected by the substrate conditions with L1 having a spreading effect on the lamellipodium with short filopodia, while laminin promotes long filopodia with a reduced lamellipodium in chick DRG cells [28].

CHAPTER IV
MICROFLUIDICS-BASED LASER CELL-MICROPATTERNING

4.1 History and utility of laser cell-micropatterning

Background

In 1970 while working at Bell Labs Arthur Ashkin first described the principles associated with optical manipulations of small particles using laser light [3]. In this work he described the mathematical and physical applications for radiation pressure forces of a laser light and the effects it can have on micron-sized particles suspended in liquid or gas. When the laser encountered a particle of higher refractive index (n_H) suspended in a medium with a lower refractive index (n_L), the subsequent reflection and refraction of the light rays resulted in a net positive force in the axial direction of the propagating beam and a net negative radial force pulling the particle into the center of the beam. Figure 4.1 is from Ashkin's work [3] representing a dielectric particle located at a position off the beam axis and the resultant forces imparted on it by the incident light from a single mode (TEM_{00}) laser beam with Gaussian intensity profile. This demonstrated the utility of radiation pressure forces for laser light and established the foundation for modern optical manipulations in biology.

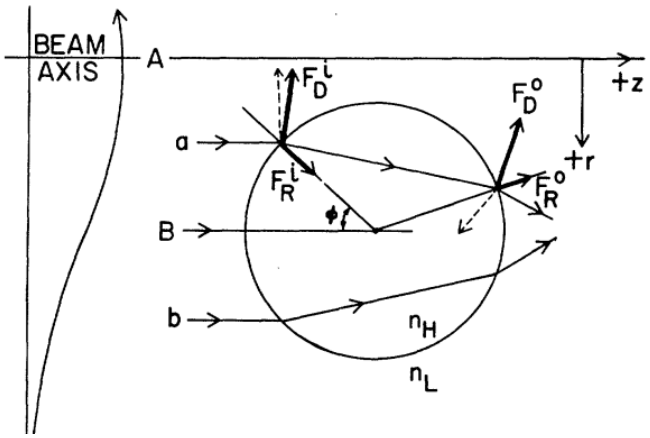

Figure 4.1: Free body diagram of a dielectric particle off-axis of a TEM_{00}-mode beam and the resultant forces due to symmetrical rays a and b. Reproduced figure with permission from American Physical Society [3], Copyright 1970.

There are currently two prominent techniques utilizing optical force to manipulate cells in biological experiments: optical trapping (laser tweezer) and laser guided direct writing (laser guidance). The development of these methods was again pioneered by Ashkin in 1986 [6, 38]. It was during an experiment trying to optically trap atoms that bacteria were accidentally trapped instead. Soon after, experiments demonstrated damage-free trapping of cells using infrared lasers. To create a single beam optical trap, light was focused through a microscope lens with a high enough numerical aperture (NA) such that the forces due to refraction and radiation pressure are greater than the axial forces from scattering and reflection. The existence of the negative radiation pressure (backward force) is due to an axial intensity gradient [6]. This phenomena is shown in Figure 4.2, where the position of the focal spot of the light (f) and the resulting forces (F) from incident light rays (a and b) causes the particle to move into the center of the beam in three dimensions. To perform optical guidance, laser light is weakly focused with a microscope lens of lower NA such that there is a radial trap (two dimensions) with a net force in the axial direction of laser propagation. In addition to NA considerations,

working distance (the distance between the lens and the focal point) must also be taken into consideration. Typically, high NA lenses have short working distances that may limit the applications of use.

Utility of laser cell-micropatterning

The ability to pattern cells at the single-cell level is essential in understanding the fundamental molecular mechanisms that regulate cell-cell and cell-extracellular matrix interactions. These interactions, which play a significant role in cellular heterogeneity, occur via direct contact or by exchange of soluble factors at distinct spatial and temporal points. To study these spatiotemporally specific interactions, cell-micropatterning techniques have been developed to create cell-culture models with a defined spatial cell arrangement [1, 46, 47, 84, 115]. For populations of stem cells or cancer cells, for example, several techniques have been developed to achieve single-cell micropatterning to investigate cellular heterogeneity.

Microcontact printing (μCP) was one of the first cell-micropatterning techniques [120]; to promote or inhibit cell adhesion, typical μCP involved chemical modification of the substrate surface [148, 159]. More recently developed single-cell-micropatterning techniques involve: atomic force microscopy (AFM) [204], dielectrophoresis (DEP) [57, 185], microfluidic devices [100, 226, 234], and laser-assisted systems [134, 156].

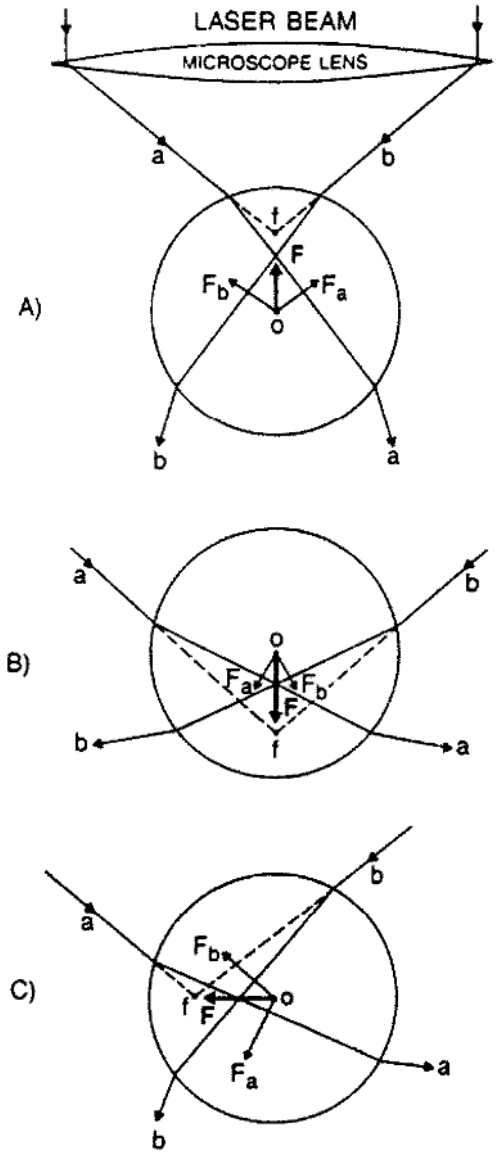

Figure 4.2: Free body diagram of the ray-optics for the stability of a tweezer trap. Displacement of the sphere away from the focus, f, axially (a) or (b), or transversely (c), results in a net restoring force. Reproduced figure from IEEE [5], Copyright 2000.

Microcontact printing and AFM allow the experimenter to tightly control the two-dimensional surface properties of the substrate by creating intricate designs of immobilized proteins for controlling cell adhesion and growth. However, substrate modification alone does not allow for precise, statistically reproducible, cell-micropatterning. DEP and microfluidics utilize fluid flow to move cell-suspensions through microchannels to pattern single-cells. To achieve single-cell micropatterning, microwells or auxiliary microstructures must be incorporated into the system to immobilize microfluidics-delivered cells at each micropatterning site [50, 67, 199]. This enables high-throughput cell-micropatterning, but places limits on substrate geometries and spatiotemporal resolution. Laser cell-micropatterning systems utilize optical forces to trap or guide cells in solution and place them at a specific site on the cell-micropatterning substrate with high spatial (sub-micron) and temporal (seconds) resolution. In conventional laser cell-micropatterning systems, cell-suspensions are typically placed in the micropatterning chamber by nonspecific cell-solution delivery [12, 83, 163] or by an external hollow fiber attached to a micropump [133, 165]. Problems with these methods include low cell throughput, nonspecific patterning areas, air bubbles, and cell aggregation; each can contribute to lower laser cell-micropatterning efficiency.

To address these problems and enhance performance, a novel microfluidics-based, on-chip cell-delivery system was designed as a removable component for the laser cell-micropatterning system. When this system (previously developed by our group [133]) is coupled with the microfluidics-based cell-delivery biochip, it provides unique features: 1) the capacity to simultaneously pattern two or more cell types. Thus, in contrast to the microcontact-printing technique, multiple treatments of the target surface specific to each cell type are not necessary; 2) the capacity to produce specific cell-

micropatterning arrays and geometries with high spatial resolution that can easily be achieved in real time by precisely moving the microscope stages during cell deposition; and 3) the capacity to create three-dimensional cell-pattern constructs by layering various cell types.

4.2 System design and features

The laser cell-micropatterning system was designed around a stationary laser beam. The laser source was a Spectra-Physics 3900S CW Tunable Ti:Sapphire laser pumped by a Millennia Vs and tuned to produce an 800 nm single mode beam with a Gaussian intensity profile. An optical shutter was placed in front of the outlet laser to control the laser state as being “on” or “off.” The beam was coupled into an optical fiber (NKT LMA-15) using a 10x objective lens (Olympus Plan Achromat, 0.25 NA, 10.6 mm WD). The other end of the optical fiber was mounted to fiber collimator (ThorLabs, 0.25 NA, f = 36.01 mm). The exiting beam was reflected off of two mirrors and projected onto a dichroic mirror (Semrock) mounted at a 45° angle. The reflected light then passed into the back aperture of a 50x long working distance objective (Mitutoyo, 0.55 NA, 13 mm WD). The illumination source was a blue or green collimated LED light (Nikon Eclipse) that was directed upward through the laser cell-micropatterning chamber and imaging objective. The light was reflected off of the dichroic mirror and projected through an IR filter and onto a CMOS camera (Photonfocus).

The microscope stage consisted of three motorized stages (Aerotech FA90-25-25-25) mounted together resulting in three-dimensional movement (XYZ). Each stage was controlled by an Aerotech N-drive controller that connected to a computer using an IEEE1394 connection. The submicron resolution of each stage and total travel of 25 mm

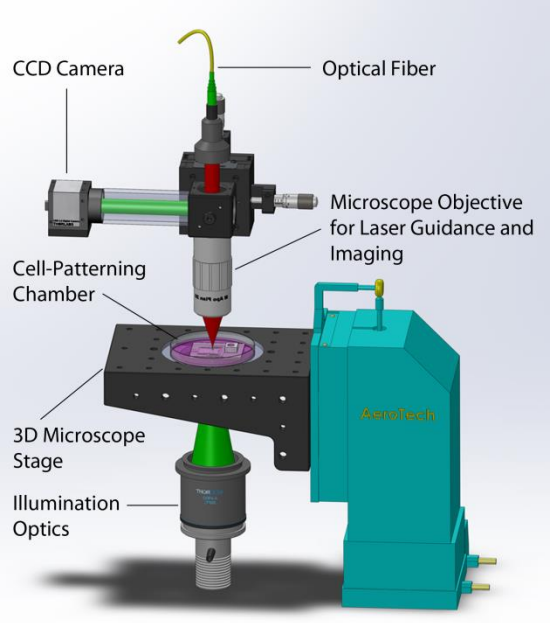

Figure 4.3: Diagram of the microfluidics-based laser cell-micropatterning system.

provided a platform for precise and accurate movement. A custom microscope slide holder was fabricated out of acrylic and mounted to the Z-axis stage to secure specimens. This holder was designed to accommodate standard 25 mm x 75 mm microscope slides as well as 50 mm x 75 mm microscope slides. A complete diagram of the laser cell-micropatterning microscope is depicted in Figure 4.3.

To maintain sterility during laser cell-micropatterning experiments a custom cell-micropatterning chamber was constructed. The cell-micropatterning chamber was a petri dish (60 mm) modified with a 40 mm machine-cut hole in the center. A circular # 1 glass coverslip (50 mm, Fisher Scientific) was mounted on the bottom of the modified petri dish to seal it. The coverslip can be used as a viewing window or directly as the cell-culture substrate. To enclose the cell-patterning chamber, a petri dish lid was modified with a 40 mm machine-cut hole in the center and a circular 50 mm # 1 glass cover slip

was mounted on top of it. The cell-micropatterning chamber was mounted on to the custom microscope slide holder that is attached to three-axis stage. Movement of individual cells from the outlet ports of the microfluidics-based cell-delivery biochip (Section 4.3) to the target site was accomplished by movement of the three-axis stage relative to the stationary laser beam. The cell was trapped in the center of the beam and simultaneously positioned to the desired location on a cell-culture substrate. Navigation of cell manipulation was user-controlled with a standard wired Xbox-360 controller (Microsoft) and a custom designed user interface.

The user interface for controlling the laser cell-micropatterning microscope is designed around an Xbox controller and a custom software program (Rapid Algorithm Computing Environment, RACE). The Xbox controller (Figure 4.4) provides an intuitive platform for controlling radial movements (XY) with one analog joystick and axial movements (Z) with another. There are two different speed modes designed to increase the efficiency of laser the cell-micropatterning microscope: one is a fine movement mode (maximum speeds < 250 μm/s in the XY-plane and < 50 μm/s in the Z-direction) and the other is a coarse movement mode (maximum speed between 1000-2000 μm/s in the XY-plane and between 200-500 μm/s in the Z-direction). When the laser is inactivated (shutter closed), the coarse speed movements are the default mode, but when the laser is activated the fine speed movements override. This is to automatically give the user greater control over the movements of the microscope stage without manually making a switch. Speed is based on joystick displacement from the center, where full displacement results in movement set at the maximum speed. Activation of the laser is controlled by an optical shutter connected to the computer via an RS232 port. A trigger on the Xbox controller (LT) is responsible for opening and closing the shutter to turn the

laser “on” or “off.” The arrow pad enables the speed to be adjusted on the fly; right (increase, +) and left (decrease, -) in the XY-plane, and up (increase, +) and down (decrease, -) in the Z-direction. When the laser is activated, adjustments to the speed in any direction occur in 5 μm/s increments. Storage of a three-dimensional location was capable by marking a specific position encoded by the three stages. This was done by simultaneously holding down the position initializer (RB) and pressing one of the four memory positions (A, B, X, or Y). A memory position recall system was incorporated to create a semi-automated patterning system. By pressing the recall initializer button (LB) and the desired memory position at the same time the stage would automatically return to the stored position. This function could be performed with or without the laser being in the “on” position (open shutter). First the XY-vector of movement would be implemented followed by Z-vector movement to reach the recall position. If it was necessary to interrupt the automated memory recall function the select button could be pressed, stopping the movement of the microscope at the exact position when the button was engaged.

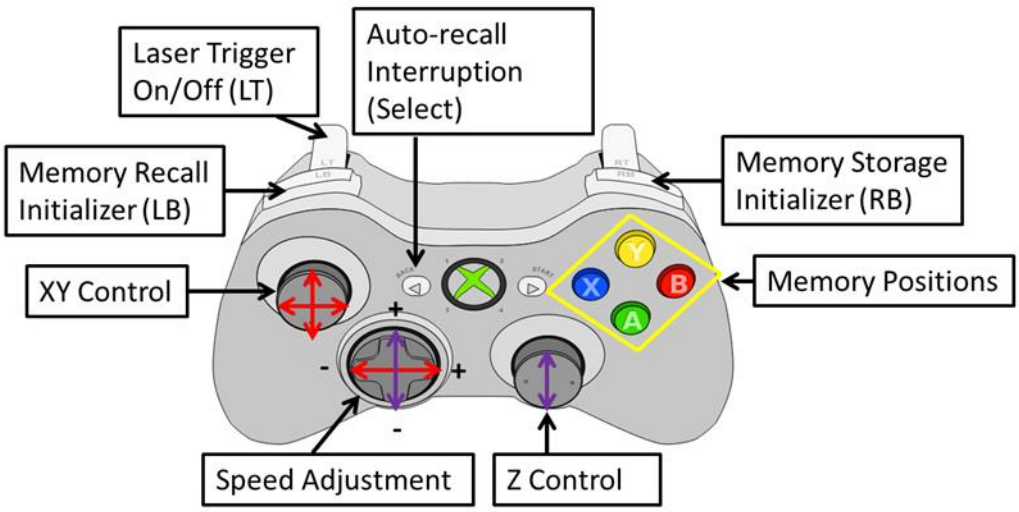

Figure 4.4: Diagram of the Xbox controller used to perform laser cell-micropatterning experiment. Each button is labeled with the function that it performs.

The user interface for RACE is depicted in Figure 4.5. The window on the left is the real time feed to the Photon Focus camera. There are two concentric circles that are part of the main screen. The smaller circle represents the region of interest for a circular cell shape. The diameter of the circle can be adjusted in the display tab of the laser microscope dialog box. This is useful to assist the user in laser cell-micropatterning cells of a certain size. Additionally, in the very center of the concentric circles is where the beam waist can be found. The outer ring provides a reference for the user to know where stored positions are relative to the current position. Corresponding with the color scheme on the Xbox controller, each stored position shows up in the window. There are four components that easily allow the user to identify positions of interest. The position indicator (A, B, X, or Y) appears on the screen with two numbers next to in parentheses. The first number in the parentheses represents the magnitude of the distance the current position is from the stored position in the XY-plane. The second number represents the magnitude of the distance the current position is from the stored position in the Z-

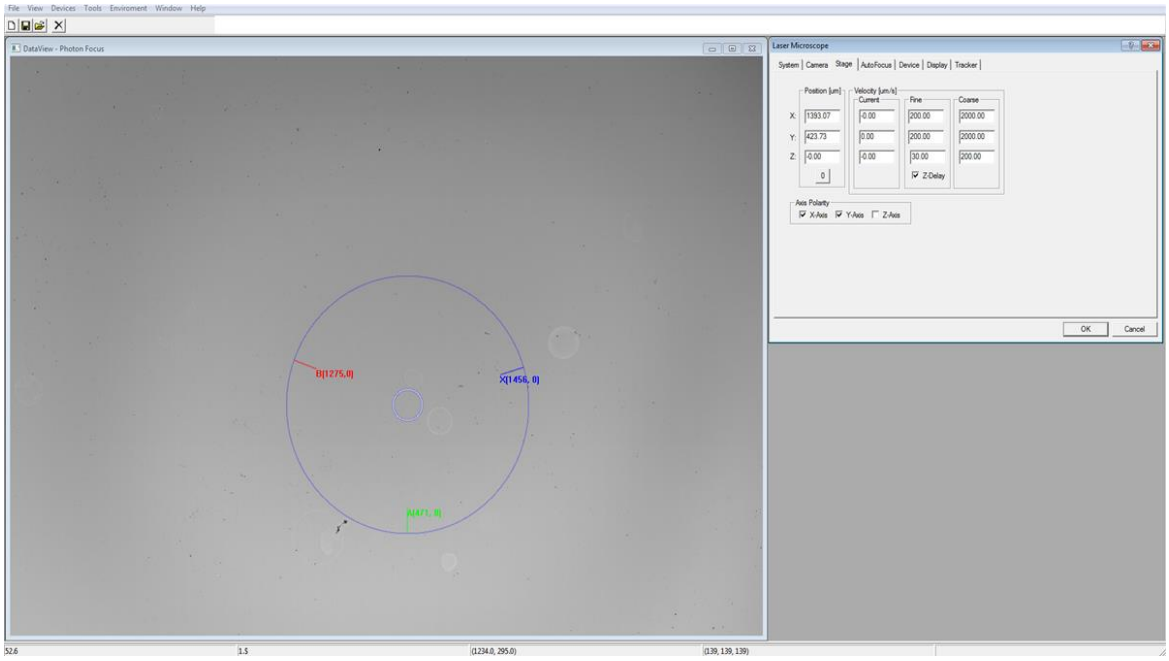

Figure 4.5: Screen-capture image of the RACE user interface.

direction. Finally, there is a small vector that appears on the screen indicating the direction the user must move the stage to reach the stored position. Upon reaching the stored position, the values in the parentheses will read (0,0). Not depicted here but part of the software package is an indicator when the stage is in motion showing the current speed at which the stage is being moved. This is incredibly useful for laser cell-micropatterning in the automatic position recall mode because each cell is slightly different and the overall speed at which they can be patterned varies. Therefore, if the cell falls out of the trap due to the drag force caused by moving at too high of a velocity, the maximum velocity can be adjusted to just below the dropout velocity to pattern in the most efficient manner. The various tabs in the dialog box allow the user to see and adjust the parameters of the microscope. For example, in Figure 4.5 the “stage” tab is highlighted. Here the user can look at the absolute stage position; the velocity of the stage if it is moving; the coarse and fine parameters used for the patterning experiment.

4.3 Microfluidics-based cell-delivery biochip

Microfluidic flow

Microfluidic flow involves the movement of fluid through channels or tubing on the submillimeter scale. This technology is advantageous because the fluid flow is laminar. To predict whether the flow pattern is laminar or turbulent, a dimensionless parameter for the ratio of momentum forces to viscous forces can be calculated. This is known as the Reynolds number (Re). Laminar conditions for fluid flow occur when there are low values of velocity (ν), hydraulic diameter ($\mathrm{D_h}$) of the capillary/tubing or rectangular channel, and the density (ρ) of the liquid; and high values of viscosity (μ) [227]. The Reynolds number is calculated by

$$Re = \frac{\rho \nu D_h}{\mu}. \tag{4.1}$$

Fluids with Re << 2000 typically exhibit laminar flow. Laminar flow in these systems is desirable because fluid flow is smooth and mixing of two streams that flow into a common channel is not turbulent; rather flow in the two adjacent streams mix at their interface by diffusion. These properties enable the characterization of complex microfluidic systems which is useful in biological research [189].

Establishing microfluidic flow

The forces necessary to drive fluid through microchannels can be generated through applied pressure and electrokenetics. In a pressure-driven system, hydrodynamic flow, Q (m^3/s), is given by

$$\mathrm{Q} = \frac{\Delta \mathrm{P}}{R}, \tag{4.2}$$

where $\Delta \mathrm{P}$ is the pressure drop across the channel (Pa), and R is the channel resistance ($Pa \cdot s/m^3$). For a circular channel the resistance is

$$\mathrm{R} = \frac{8\,\mu\mathrm{L}}{\pi \mathrm{r}^4}, \tag{4.3}$$

and for a rectangular channel with a high or low aspect ratio (w << h or h << w);

$$\mathrm{R} = \frac{12\,\mu\mathrm{L}}{wh^3}, \tag{4.4}$$

where μ (Pa·s) is the fluid viscosity, L (m) is the length, r (m) is the radius, h (m) is the height, and w (m) is the width of the channel [198]. If the aspect ratio is near unity (i.e., w ≈ h), the channel resistance is found by [13]

$$R = \frac{12\,\mu\mathrm{L}}{wh^3}\left[1 - \frac{h}{w}\left(\frac{192}{\pi^5}\sum_{n=1,3,5}^{\infty}\frac{1}{n^5}\tanh\left(\frac{n\pi w}{2h}\right)\right)\right]^{-1}. \tag{4.5}$$

The pressure drop can be created by either applying a positive pressure (push) at the inlet with atmospheric pressure at the outlet or by opening the inlet to atmospheric pressure and applying a vacuum (pull) at the outlet. In the work reported here, two different methods of positive pressure application were used to generate microfluidic flow; hydrostatic pressure and the use of a custom built pulsatile pressure application system. The generalized mechanical energy balance in the form of the Bernoulli equation for steady state flow of an incompressible fluid describes the movement of fluid though a system from point 1 (inlet) to point 2 (outlet) [63]

$$\frac{P_1}{\rho} + gZ_1 + \frac{\alpha_1 V_1^2}{2} + \eta W_p = \frac{P_2}{\rho} + gZ_2 + \frac{\alpha_2 V_2^2}{2} + h_{friction}\,, \tag{4.6}$$

where P represents the pressure, ρ is the fluid density, Z is the elevation relative to the reference plane, V is the average fluid velocity, α's are kinetic energy correction terms, W_p is the work done per unit mass of fluid (by a pump), η is the pump efficiency, and $h_{friction}$ is the frictional loss between the two points. For microfluidic flow in the cell-

delivery biochip, hydrostatic pressure based on the height differential between the inlet and outlet is used as the force to move the fluid through the channels. The Bernoulli equation describing the fluid flow is augmented slightly for the changing height of the inlet such that,

$$Z_1 \rightarrow \frac{dZ_1}{dt},$$

which accounts for the change in the inlet height over time. As time elapses the fluid velocity at the outlet is continually reduced until equilibration is reached and the flow stops.

Fabrication of microfluidics-based cell-delivery biochip

The microfluidics-based cell-delivery biochip, shown in Figure 4.6, was comprised of three different layers of polydimethylsiloxane (PDMS). The inlet reservoirs were fabricated by pouring a PDMS solution (10:1 base-curing-agent ratio, Dow Corning) into an empty 35 mm petri dish and baked on a hotplate to obtain a 10 mm thick membrane. The PDMS was cut into two 15-mm square blocks and a 6 mm hole was punched (Harris Uni-Core, Sigma) into the center of the squares to form a reservoir. The top layer was created by pouring PDMS into a 60 mm petri dish and baking on a hotplate to reach a final membrane-thickness of 1 mm. A 25 mm square was cut out of the PDMS membrane and two 4 mm holes were punched (Harris Uni-Core, Sigma) to complete the top layer. The channel layer, with approximately 50 µm deep microchannels, was made using standard photolithography and soft lithography processes previously described in Chapter III. PDMS was poured into a dish containing the master mold on the bottom to produce a layer (approximately 1mm thick) of membrane with a 50 µm deep groove as the channel. Once the PDMS cured the channel layer was peeled off the master mold.

Assembly of the microfluidic biochip started by corona treatment of the both the inlet reservoir blocks and the top layer, followed by baking on a hotplate (140 °C for one hour) to create an irreversible bond. After baking, the channel layer and the underside of the top layer were both corona treated and bonded together, creating a seal to form microfluidic flow channels. To complete the assembly, the entire microfluidic injection biochip was baked on a hotplate (140 °C for one hour). Following sterilization, the chip was ready for use in conjunction with microfabricated cell-culture substrates. The assembly of the cell-micropatterning chamber (top not shown) is illustrated in Figure 4.6.

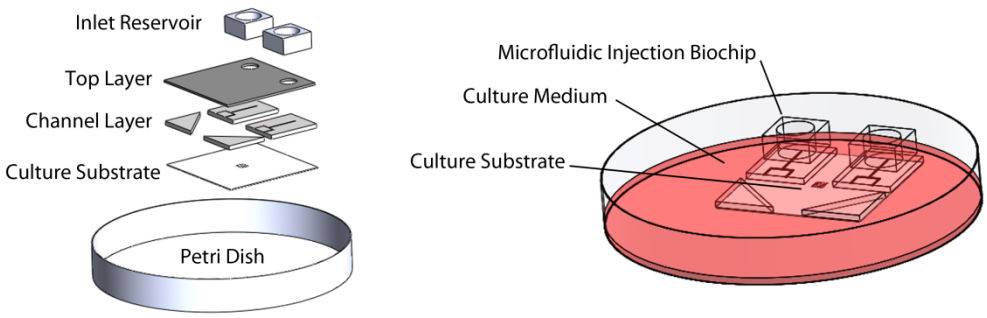

Figure 4.6: An exploded assembly and overall diagram of the microfluidics-based cell-delivery biochip and cell-culture substrate.

4.4 Additional laser cell-micropatterning components

Cell-culture substrates

A CELL-VU® gridded glass coverslip (Millennium Sciences) and a PDMS substrate (described above) were used to validate single-cell placement with the laser cell-micropatterning system to demonstrate it's micron-level accuracy. The surfaces of the coverslips and the PDMS cell-culture substrate were modified to promote cellular adhesion. The gridded glass coverslip was used to precisely define spatial distributions between patterned cells and to demonstrate that removal of the microfluidic cell-delivery

biochip would not disturb the patterned cells. The PDMS substrate was used to highlight the versatility of the microfluidics-based laser cell-micropatterning system in that cell placement in a geometrically-constrained system could easily be accomplished, in order to study cellular development at the single-cell level.

PDMS substrate

A pattern master mold with the desired structures was created via photolithography (detailed in Chapter III). The master mold was silanized with trimethylchlorosilane (TMCS, Supelco) for 30 minutes to assist in PDMS removal. Due to the small structures of the pattern design (e.g., the castle structure in Figure 4.10), 10% v/v xylene (Fisher Scientific) was added to the 10:1 mixture of PDMS solution to decrease viscosity and enhance its deposition into the mold microstructures. Then, the PDMS mixture was spin-coated (500 rpm for 30 s) onto the master mold to generate an approximately 200 µm, uniformly thick membrane. The membrane was baked at 125 °C for 20 minutes to cure the PDMS. The membrane was removed from the mold and baked in a vacuum oven at 125 °C overnight. A three-stage solvent oligomer extraction and a subsequent overnight vacuum drying process were performed to remove any residual solvent. The membrane was cleaned, sterilized, and activated by oxygen plasma before being mounted to the interior of the glass-bottom petri dish. The entire dish was heated at 50 °C for 2 hours to create an irreversible bond between the glass and the PDMS.

Cell-culture substrate surface modification

The surfaces of the cell-micropatterning substrates were modified by physiosorption of a cationic polymer to improve cell attachment. Immediately after a 10 minute oxygen plasma treatment, 1.5 mL of 0.01% w/v poly-l-lysine (PLL) solution

(Sigma) was pipetted into the glass-bottom petri dish. The surfaces of the coverslips and PDMS membranes were allowed to soak in the PLL solution at room temperature for 24 hours. After 24 hours, the PLL solution was removed and the membrane was washed three times with phosphate buffered saline (PBS) solution to remove any unbound PLL.

Cell isolation, fixation, and staining

Primary chick forebrain neurons (CFNs) and chick glial cells were used to demonstrate the utility of the microfluidics-based laser cell-micropatterning system. CFNs were harvested from the cerebral hemispheres of E8 White Leghorn chicks in accordance with the Heidemann protocol [92] (a detailed version of our protocol can be found in Appendix); glial cells were harvested from Embryonic Day 14 White Leghorn chicks in accordance with the Kentroti protocol [113]. Neurons and glia were provided with the same medium used for laser cell-micropatterning: Leibovitz's L-15 medium (Gibco®) without phenol red, supplemented with 1% antibiotic/antimycotic (10,000 units/mL penicillin G sodium, 10,000 µg/mL streptomycin sulfate), 50 µg/mL gentamicin, 2.5 µg/mL amphotericin B (Sigma), 10% fetal bovine serum (FBS) and 2% B27 (Gibco®), to create cell-suspensions of 50 x 10^4 cells/mL. The CFNs were live-stained with Vybrant® DiI cell-labeling solution (Life Technologies). After laser cell-micropatterning, cell-cultures were maintained in 2 mL of laser patterning media for 1 hour at 37 °C and 5% CO_2 in an incubator to promote development and cell attachment to the substrate. Then, all media was removed and cells were fixed in 4% paraformaldehyde (Sigma) for 12 min. The fixation solution was removed, and cells were treated with 0.05% Triton X-100 (Sigma) for 5 min. The Triton X-100 solution was removed; diamidino-2-phenylindole (DAPI) nucleic acid stain (Thermo Scientific) was added, and the cells were left in the dark for 60 min. The DAPI solution was removed, and a mounting agent

(ProLong® Gold Antifade Reagent, Invitrogen) was applied to complete the cell-preservation process.

Cell imaging

Phase-contrast and fluorescent images of laser-patterned CFNs and glial cells (Figure 4.9, 20x magnification) and a single CFN patterned onto a PDMS substrate (Figure 4.10, 40x magnification) were obtained using a Zeiss Axiovert 200 M microscope. The stained nuclei and cell membranes of layered CFNs (Figure 4.11) were imaged with a Nikon Eclipse Ti confocal microscope to illustrate the three-dimensional-patterning ability of the microfluidics-based laser cell-micropatterning system.

4.5 Results

Operation of the microfluidics-based laser cell-micropatterning system

To begin a laser cell-micropatterning experiment, the microfluidic cell-delivery biochip was mounted on top of the cell-culture substrate (Figure 4.6). Laser patterning media was syringe-injected into the cell-delivery biochip inlet reservoirs to prime the microfluidic channels. Once stable gravitational force-induced microfluidic flow was established, cell-suspensions (e.g., 50 x 10^4 cells/mL) were added to the inlet reservoirs. The paths from the inlet reservoirs to the outlet ports were of equal length to ensure cell-suspension was evenly delivered to each port. Figure 4.7(A) schematically represents the microfabricated channel layer. The red highlighted region depicts the 50 µm deep groove that formed the microfluidic channels (one inlet and two output ports). The central microfluidic channels, measured from the center of the inlet reservoirs (6 mm in diameter), were approximately 6 mm long (200 µm wide). After branching, the width of each channel remained approximately 200 µm. At the exit region, each microfluidic

channel fanned out to a final width of 1000 µm at the outlet port to reduce the influence of the total channel length (~17.5 mm) on the flow rate. Figure 4.7(B) shows the actual cross-section of a microfluidic channel. The fabricated channel had slightly distorted dimensions (top width of 210 µm, bottom width of 220 µm, and a channel height of 55 µm) in comparison with the designed rectangular cross-section.

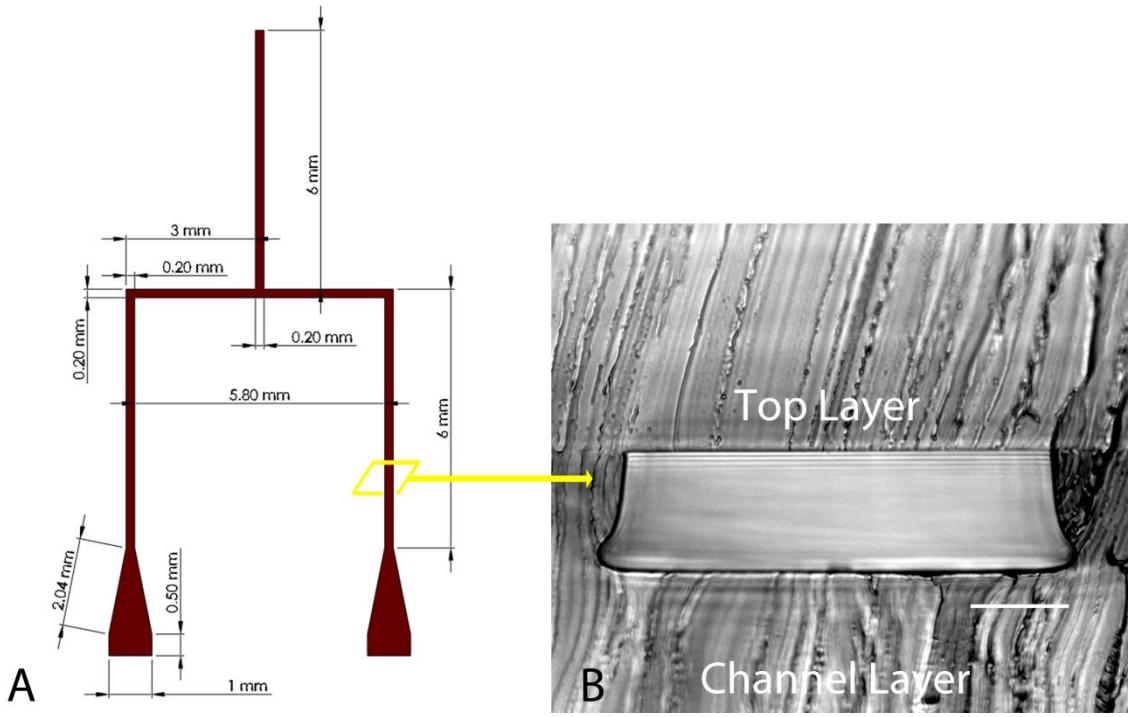

Figure 4.7: A) Two-dimensional schematic of the microfluidic biochip flow-channel layer (depth is 50 µm). B) Phase contrast image (20x) of a microchannel cross-section. Scale bar 50 µm.

A COMSOL multiphysics simulation of the flow rate through the microfluidic channel layer was conducted to determine the exit velocity of cell-suspensions from the microchannels. Figure 4.8 shows the simulation results based on the designed rectangular dimensions. The gravitational force and surface tension created by the amount of fluid in the reservoir (~1.4 mL, 5 mm height, and 6 mm diameter) provided an estimated hydrostatic driving pressure of ~45 Pa. The outlets were connected to a much

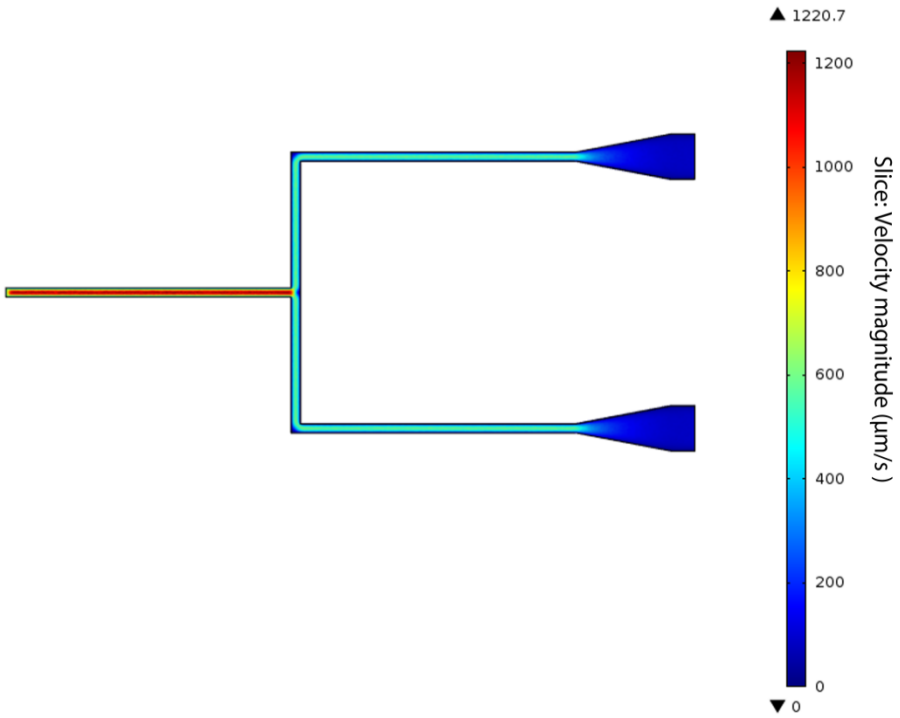

Figure 4.8: COMSOL simulation for the flow rate of cell-suspensions through the microfluidic biochip.

larger reservoir so that the surface tension could be neglected, and the outlet pressure was treated as 0 Pa. Our data demonstrated that, given the simulation parameters, the flow-field velocity for cell-delivery was not sensitive to the minor differences in the channel geometry between the designed and experimental microchannels. The simulation results indicated that the flow rate of cell-suspensions at the outlet ports was approximately 90 µm/s. The simulation results were supported experimentally via a video (data not shown), where cells had been experimentally estimated to leave the outlet ports of the microfluidic biochip at a flow rate between 50-90 µm/s. The flow rates produced were sufficient to keep cells in suspension and slow enough for the laser to trap and guide them from the outlet ports. Movement of the three-axis stage relative to the stationary laser beam allowed cells to be patterned to a predetermined target site on

the cell-culture substrate. A laser power of 150 mW inside the culture chamber allowed cell-manipulation speeds of 200 μm/s radially (XY) and 50 μm/s axially (Z) in the direction of the propagating beam, permitting cells to be patterned to areas on the substrate up to several millimeters (> 5 mm) from an outlet port.

Heterotypic cell-micropatterning

To demonstrate the ability of simultaneous heterotypic cell-micropatterning for the creation of heterotypic cellular arrays, two different homotypic cell-suspensions were added to separate inlet reservoirs of the cell-delivery biochip. Figure 4.9 shows a combined fluorescence and phase-contrast image of a laser-patterned CFN array. Cells originating from the separate inlet reservoirs were simultaneously patterned onto a gridded glass coverslip. One inlet-channel network was used to deliver DiI live-stained cells (red) and the other was used for non-stained cells. The cells were manually placed via laser cell-micropatterning at the edges of a 100 μm x 100 μm square on the gridded glass coverslip. That is, we did not use the computer-controlled positioning algorithms that we reported in 2005 and 2006 to demonstrate submicron accuracy [8, 164]. In this study, we demonstrated with the gridded coverslip that the use of the microfluidic biochip does not adversely affect the resolution of laser cell-micropatterning. Rather, the method reported here eliminated the complications typically associated with placement of multiple cell types by laser cell-micropatterning; improving the performance of the entire system.

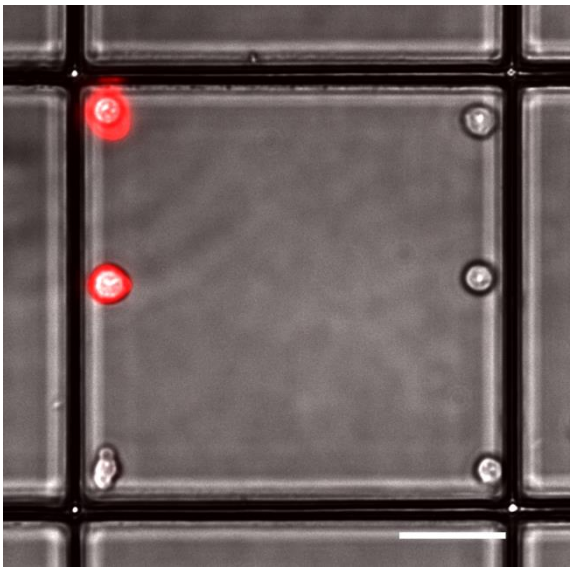

Figure 4.9: Combined fluorescence and phase contrast image (40x) of a laser-patterned CFN array. The two DiI live-stained cells (red) were from one microfluidics-cell-delivery channel, the remainders were from the other channel. Scale bar 25 µm.

Cell-micropatterning onto a PDMS substrate

Fabrication of three-dimensional geometric structures into a cell-culture substrate allows can influence cellular development. As an example, a 20 µm high PDMS castle was microfabricated to confine an individual CFN. The castle had eight radially aligned microchannels (giving the appearance of a circumferentially distributed triangles), which allowed the confined neuron to develop dendrites and an axon that would extend through one of the eight microchannels. Figure 4.10 shows a single CFN that was laser-patterned onto a castle substrate. At 16 hours, the development of the CFN demonstrated the influence that the microchannels have on the axonal projection. Once the growth cone of an extending axon arrives at the end of the microchannel, a choice point is reached that can be used to study regulations of axonal pathfinding (results not shown). In the case of the cells patterned on the gridded glass coverslip (Figure 4.9),

removal of the microfluidic cell-delivery biochip did not disturb the patterned cells and culture continued in an open environment. The patterned cells remained viable, and true single-cell isolation was achieved.

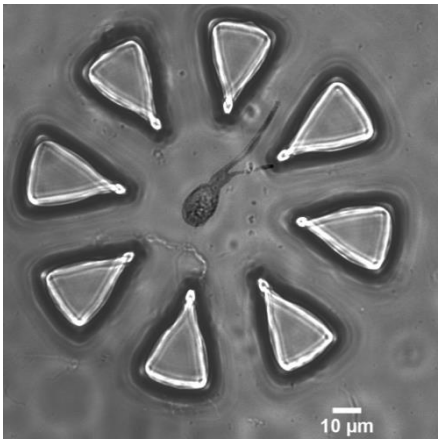

Figure 4.10: A single CFN at 16 hours: It was selected from the microfluidic cell-delivery channel and laser-patterned onto a PDMS-based cell-culture substrate.

Building three-dimensional cellular constructs

Figure 4.11(A) represents a side-view confocal image of laser-patterned cells. Stained nuclei (blue) were identified at three distinct heights indicating three separate cell layers. The bottom layer of cells was patterned from a glial cell-suspension inlet reservoir. The middle and top layers were patterned from a CFN cell-suspension inlet reservoir. CFN membranes were live-stained with DiI (red) to distinguish the various cell layers (Figure 4.11(B)). As can be seen in Figure 4.11(C), only cells from the CFN reservoir were present on the top layer. Despite the 1-hour culture period before the cells were fixed, axonal extension from one neuron to another was observed. These results show that viable three-dimensional cellular constructs can be fabricated using the microfluidics-based laser cell-micropatterning system.

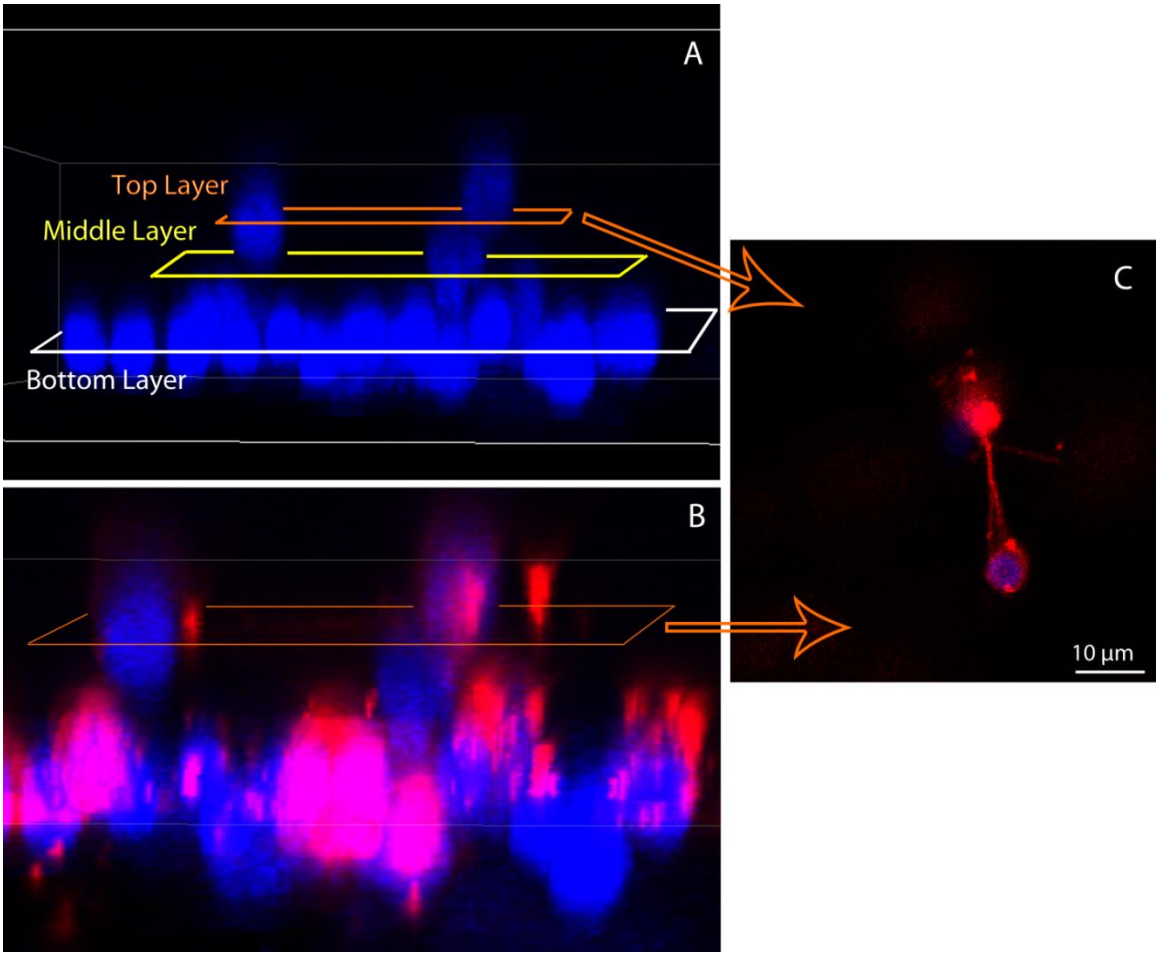

Figure 4.11: Three-dimensional construct of glial cells (Bottom Layer) and CFNs (Middle and Top Layer). (A) DAPI-stained (blue) confocal side-view image showing different heights of cell nuclei. The top layer of cells is highlighted in orange, the middle layer is highlighted in yellow, and the bottom layer is highlighted in white. (B) Side-view confocal image with DAPI-stained (blue) nuclei and DiI-stained (red) CFN membranes. (C) Top-down view of the top layer of patterned CFNs with DAPI-stained (blue) nuclei and DiI-stained (red) cell membranes.

4.6 Discussion

Laser cell-micropatterning and microfluidics

The use of laser optics in cell patterning provides a means to create bottom-up engineered cell constructs and cellular assays. Schiele and colleagues describe the many variations of laser-based direct-write techniques for cell printing [193]. Laser tweezers (described by Ashkin [4]) and laser-guidance systems share many similar characteristics. With an optical-tweezers system, Pine and colleagues reported lifting individual cells plated onto a polyhydroxyethylmethacrylate (polyHEMA) surface and transferring them over a distance of 5 mm at a speed up to 200 μm/s with a laser output power of 100 mW [163]. Similarly, we were able to manipulate cells over a total distance of greater than 5 mm at a speed of 200μm/s in the radial plane and 50 μm/s in the axial direction of the laser beam. Although both systems can be used to achieve comparable two-dimensional cell-patterning results, traditional laser tweezers utilize a high NA (≥ 1.0) microscope objective to generate a strongly focused laser beam (smaller beam waist, also described as spot size), whereas laser guidance employs a lower NA microscope objective to produce a weakly focused laser beam (larger spot size). A highly focused beam creates a very strong trap, but it greatly reduces the effective working distance of the microscope (in Pine's system, it is 100 μm); thus, traditional laser tweezers are not feasible for research in which cells need to be accurately positioned in a three-dimensional construct or onto large structures (>100 μm) of an PDMS cell-culture substrate. For the microfluidics-based laser cell-micropatterning system, the focal length of the 50x long working distance objective is 13 mm with a NA of 0.55. The NA is high enough that a laser tweezer can be achieved for small cells or particles (< 15 μm in diameter), where the axial force component in the direction of the propagating beam is

eliminated and the result is a long working distance laser tweezer system. However, by simply switching the optics to a 20x long working distance microscope objective with NA of 0.42 (working distance of 20 mm), a laser guidance system can be achieved. The versatility of this system allows for individual cell manipulation at functional distances on the order of tens of millimeters; thus it suitable for precise movement of individual cells to a specific location in a three-dimensional culture environment constructed in a petri dish.

The two most common methods used to deliver cells for laser cell-micropatterning exhibit inherent problems that reduce the cell-patterning efficiency. The first method involves non-specific loading (e.g., by pipetting) of cells into the cell-micropatterning chamber prior laser-assisted cell manipulations [12, 83, 163]. This cell-delivery method requires complicated modification of the patterning surface to create areas that both inhibit and promote cell attachment. A cell can be selected from a non-adhesive site and positioned to a desirable location that promotes cell attachment. The second method, performed during laser cell-micropatterning, involves pulsatile injection of small volumes of cell-suspensions into a chamber filled with culture medium [133, 166]. The injection setup consists of costly, mechanically manipulated syringes loaded with a cell-suspension (one per cell type) that is connected to the culture environment by a hollow fiber. Initially, the syringe and hollow fiber must be plumbed to remove air bubbles from the injection line. Periodically throughout cell-micropatterning the position of the fiber must be adjusted to allow for full coverage of the cell-patterning area. Between injection pulses cell clumping and aggregation can result in the fiber clogging. When this occurs, the fiber must be removed from the culture environment, cleared, and reinserted to continue the administration of cells. Each time the system requires adjustment there is a risk of possible culture contamination. To increase the efficiency,

sterility, and specificity of single-cell laser cell-micropatterning, we designed and implemented the microfluidic cell-delivery biochip. The continuous, gravity-driven flow of cell-suspension in the microfluidic channel network provides constant cell-delivery throughout the entirety of cell-micropatterning, which typically lasts between one and two hours.

Two-dimensional heterotypic cellular arrays

Tissues comprise various cell types that are spatially organized to achieve unique function through specific cellular interactions. Precise spatial arrangement of homotypic and heterotypic cells are essential for replicating the cell-cell interactions and functions observed in native tissues. For example, interactions between micropatterned homotypic cell pairs have been shown to influence cell structure, polarity, and proliferation [48, 152]. Numerous heterotypic cell-micropatterning systems have been devised to determine the nature of the interactions between certain cell types [16, 60, 214]. A thorough overview of the use of micropatterning to determine cell morphogenesis and function is provided by Théry [212]. However, many conventional methods to generate homotypic and heterotypic cell interactions focus on the culture or coculture of large numbers of cells that are not spatially regulated into specific cell pairs. Figure 4.9 shows the micropatterning result of the microfluidics-based laser cell-micropatterning system in which individual cells were selected and simultaneously patterned into a 100 μm square to create a heterotypic cellular array. These results demonstrate that the system permits the user to reproducibly control both the isolation of cell pairs and the distance at which they are separated. Advantages of this patterning method (which can be expected to increase single-cell viability) include: the capacity to evaluate the effect individual cells may have on each other without the influence of other

cells; the decrease in overall micropatterning time; and the elimination of possible sources of bacterial contamination. The results of such micropatterning experiments may reveal previously unknown mechanisms related to cellular heterogenesis [2].

Three-dimensional cellular constructs

In vivo, precise spatial and temporal arrangement of different cell types is vital for normal tissue development. A fundamental aspect of recreating the native environment *in vitro* is organizing various types of cells with high spatial and temporal resolution. A number of methods have been used to create three-dimensional constructs *in vitro*. One popular technique involves use of an inkjet printer [20, 231]. Despite this technique's robust ability to create cell layers for tissue constructs, there remains a lack of control over the precise arrangement of cells. Without a spatially defined structure, observing and recording the interaction between cell types or the migration of a cell from one place to another becomes less accurate.

Neuron-glia interactions play an incredibly important role for the proper development of the nervous system. Glial cells function in many ways to support neuronal survival by: 1) maintaining the ionic environment surrounding the neuron, 2) modulating the rate of nerve signal propagation, 3) augmenting synaptic action by regulating neurotransmitter metabolism, 4) providing a scaffold for neuron migration or development, 5) secreting extracellular signaling molecules for axonal guidance, and 6) aiding in the recovery of nerve cells due to injury or disease [150]. In the developing telencephalon, transient midline glial structures support the reciprocal growth of cortical axons to form the corpus callosum [197]. These cells serve as intermediate targets, also known as "guidepost cells," where molecular signaling molecules are secreted to influence axonal pathfinding [211]. While glia monolayers serve as excellent growth

substrates for axons, it has been shown that the beneficial growth properties for axons are dependent on spatial orientation and time [58]. Therefore, in this work we used neuronal-glial co-micropatterning as a realistic example to show our system's ability to create three-dimensional spatiotemporal arrangements of heterogenic cell types.

We demonstrated the ability to create a three-dimensional pyramidal-like structure of patterned glial cells and CFN neurons. Figure 4.11(A) shows the laser cell-micropatterning system's capacity to create multiple layers (three in this case) of cells in a specific manner, resulting in a three-dimensional construct. It can be seen that the pyramid-like structure lost cells from the second and third layers in the time between patterning and imaging. To preserve the structure of three-dimensional-patterned cell constructs, each layer should include extracellular matrix-promoting cells to ensure proper adhesion of the cells of interest. Despite the loss of some of the structure, cells were visible at three distinct levels providing evidence that patterned biological three-dimensional constructs are possible using this method.

Summary

Improvements to our existing laser cell-micropatterning microscope were made to increase the efficiency and throughput. Careful engineering of the optical components resulted in the creation of a long working distance laser tweezer system where cells could be manipulated at speeds in excess of 200 μm/s radially and 50 μm/s axially when incorporated with the microfluidic cell-delivery biochip. The complete system allowed for easy placement of cells into the structures of a PDMS substrate, simultaneous laser cell-micropatterning of multiple cell types, and the construction of small three-dimensional cellular arrays.

CHAPTER V
SINGLE-CELL CULTURE ON PDMS SUBSTRATES

5.1 Introduction

As discussed in the previous chapters, axonal pathfinding involves the recognition of extracellular information in many different forms, including physical (e.g., geometrical and topological) and chemical (e.g., immobilized or diffusible) cues. During development these cues provide directions for guiding axonal growth cones on the specific pathways leading to their desired target. The fidelity for which axonal pathfinding occurs *in vivo* is remarkable given the billions of cells that make up the nervous system. To reproduce the exact set of events that takes place and uncover the multitude of mechanisms involved is virtually impossible. Therefore, it is necessary to simplify the environment in which axonal pathfinding occurs in order to understand the mechanisms by which the nervous system develops.

Various techniques have been developed *in vitro* to reduce the complexities involved in axonal pathfinding. At the heart of this has been the use of microfabrication technologies that can create precise chemical compositions of a substrate surface [66, 120, 205]; three-dimensional micro-topographies [45, 154]; surface patterns of neural adhesion molecules that restrict axonal pathfinding only to those regions where a specific molecule is present [159]; and physical barriers that regulate axonal guidance and extension by constraining the paths in which axons extend [64, 136, 166].

Utilizing many of the principles of the previously mentioned techniques, we explored the effects that physical barriers of a three-dimensional microenvironment can have on axonal pathfinding of individual-neurons. To do this we used the biochip design outlined in Chapter III and the laser cell-micropatterning system described in Chapter IV. We used individual-neuron-cell bodies deposited in the cell-confinement microwells and

the subsequent axonal pathfinding/extension through and beyond a geometric guidance microchannel as a model to study the developmental characteristics of pioneer-neurons. Understanding how individual axonal development is influenced in response to the surrounding three-dimensional microenvironment will provide important information that should be considered when designing future biomedical applications; whether it is for tissue engineering, regenerative medicine, or toxicity screening.

5.2 Single-cell culture

A fundamental principle to any good cell biology experiment is keeping cells healthy and viable. Culturing cells on a PDMS substrate, laser cell manipulation, and extended durations outside of a controlled environment (temperature, relative humidity, and carbon dioxide level) pose a number of hurdles to overcome to ensure a successful result. On top of that, we were concerned with investigating the development of individual-neurons isolated from any physical interaction with other cells. The explicit methods for isolating and culturing individual chick forebrain neurons (CFNs) on PDMS substrates are be described in the Appendix.

Single-cell culture

Dissociation of neurons from the embryonic (E8) chick telencephalon results in a heterogeneous cell-type suspension consisting mainly of two morphologically distinct neuronal cells. The first type is a slender bipolar cell that could be categorized as a Cajal-Retzius cell [143], however, strictly speaking, Cajal-Retzius cells are neurons specific to the human embryonic marginal zone. The second cell type is pyramidal neurons. These cells have a somewhat triangular-shaped cell body, extend a single axon, and present both apical and basal dendritic arborization. *In vitro*, dendritic

arborization of pyramidal cells from the chick forebrain does not typically occur; most cells only reach stage 3 of development [53, 92]. In the avian brain, based upon the position of the cell in the pallium (a dorsal structure of the telencephalon homologous to the mammalian neocortex) there may be a difference in size and appearance of pyramidal neurons. The non-mammalian pallium does not have the characteristic laminar structure that is unique to mammals, however, this nuclear structure is used for cognitive and behavioral functions similar in fashion to their mammalian counterparts (Figure 5.1) [105, 206]. Figure 5.2 represents individual bipolar and pyramidal CFNs at various time points *in vitro*.

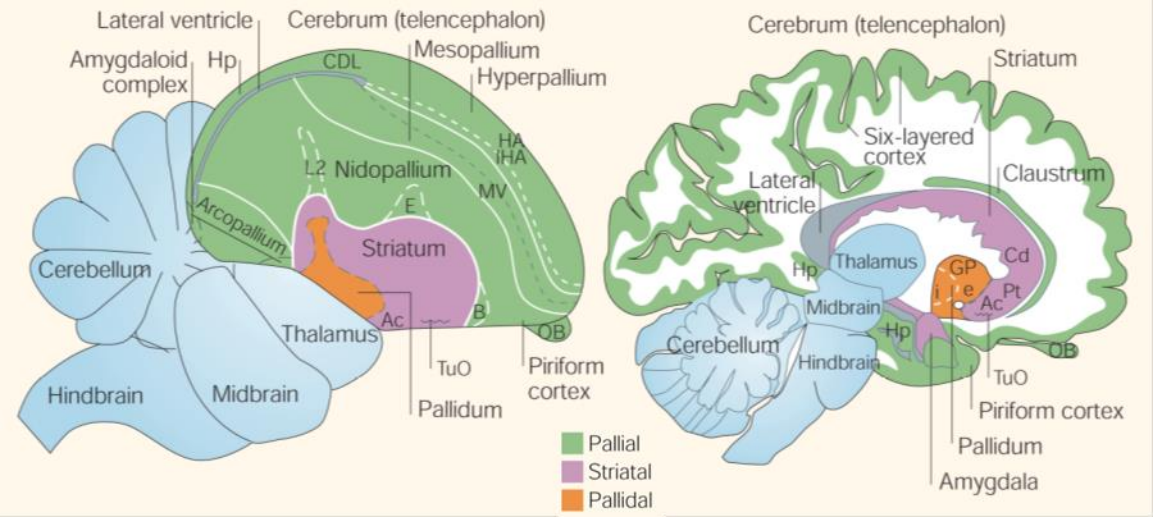

Figure 5.1: Saggital diagrams of the different brain regions for the (left) avian (songbird) and (right) mammalian (human) brains. Solid white lines are lamina (cell-sparse zones separating brain subdivisions). Large white areas in the human cerebrum are axon pathways called white matter. Dashed grey lines divide regions that differ by cell density or cell size; dashed white lines separate primary sensory neuron populations from adjacent regions. Abbreviations: Ac, accumbens; Cd, caudate nucleus; CDL, dorsal lateral corticoid area; E, entopallium; B, basorostralis; HA, hyperpallium apicale; Hp, hippocampus; IHA, interstitial hyperpallium apicale; MV, mesopallium ventrale GP, globus pallidus (i, internal segment; e, external segment); V, hyperstriatum ventrale; L2, field L2; LPO, lobus parolfactorius; OB, olfactory bulb; Pt, putamen; TuO, olfactory tubercle. Adapted by permission from Macmillan Publishers Ltd: Nature Reviews Neuroscience [105], Copyright 2005.

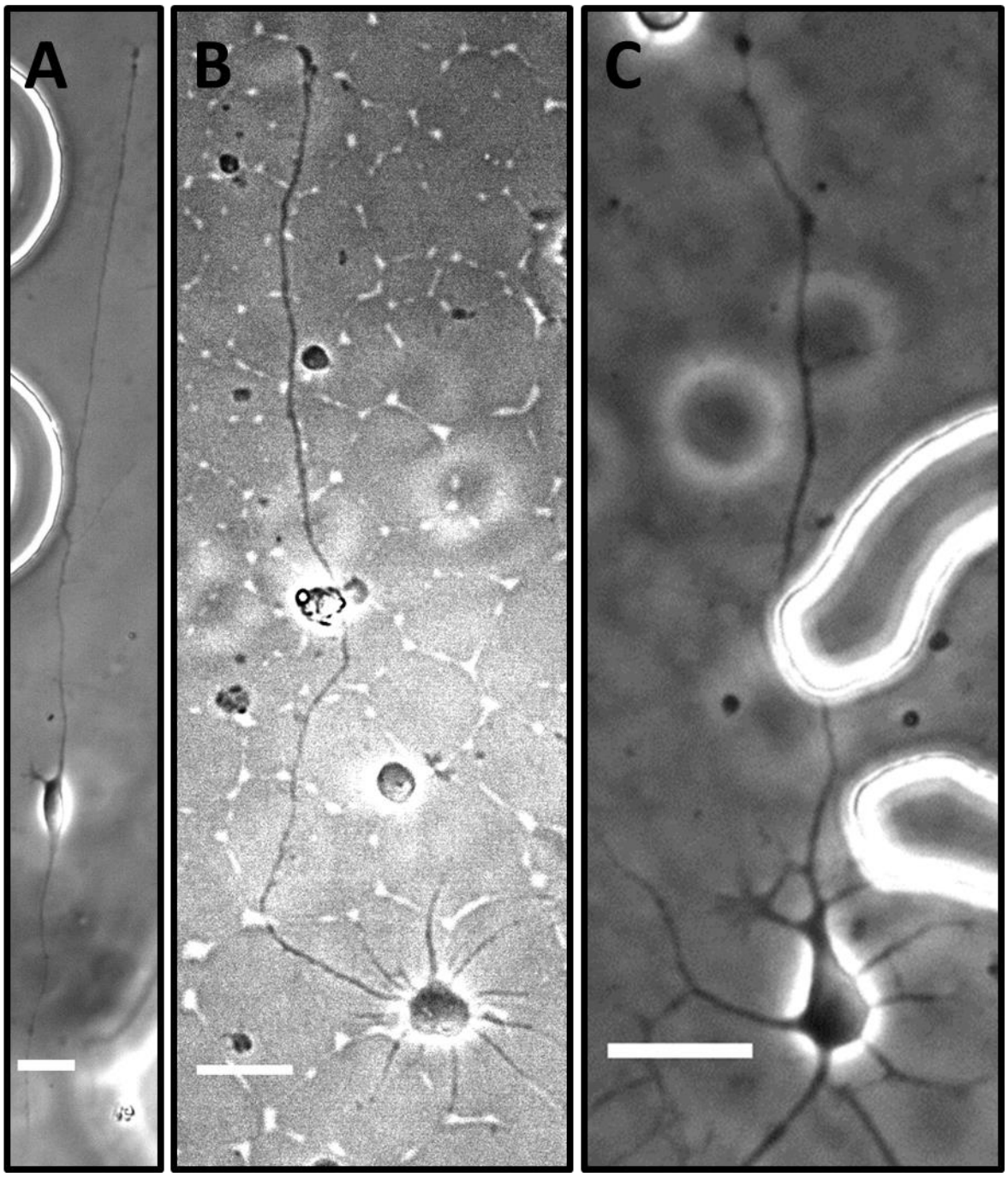

Figure 5.2: Morphology of different cell types from chick cerebral hemispheres cultured on PDMS substrates. A) A bi-polar Cajal-Retzius-like cell 1 DIV. B) Pyramidal neuron with round soma 3 DIV. C) Pyramidal neuron with elongated soma 4 DIV. All scale bars 25 µm.

Using the laser cell-micropatterning system described in Chapter IV, individual chick forebrain neurons (CFNs) were placed into the microwell structures with the design represented in Figure 3.5. Although we did not use the laser cell-micropatterning system to specifically identify cell types, placement of individual cells in exact locations enables developmental observations to be made in response to the geometric environment alone. Thus, based on morphological characteristics of the cell, they can be classified into groups of similarly developing cells. Developmentally, this allows for systematic identification and observations to be made regarding the response of particular cell types to engineered geometric microenvironments.

For neurons to survive in culture they must attach to the substrate surface. In the developing neocortex, extracellular matrix molecules play a vital role in organizing the cellular arrangements. These molecules consist of laminins, proteoglycans (Lecticans), and glycoproteins (Reelin and Tenascins) which form the basal lamina (BL) that surround the brain and blood vessels in the central nervous system [65, 187]. Unfortunately, substrate materials lack the biologically active molecules that allow neurons to readily attach; therefore, culture surface modification must be performed to enhance cellular adhesion. Extracellular matrix proteins as well as cell adhesion molecules promote cell attachment by receptor-mediated binding [114]. Other methods for improving cell attachment involve the use of biologically inactive or synthetic adhesion promoters, such as positively charged polyaminoacids (e.g. polylysine, PLL) that utilize beneficial electrostatic interactions with the negatively charged phospholipids of the cell membrane. Using PDMS as our substrate of choice, we examined the effects that different molecular coatings have on cellular development and the promotion of axonal extension from the geometric constraints. Table 5.1 shows the different

conditions that were tested to promote individual axonal extension. These different molecules and the concentrations they were applied at were chosen based upon their extensive use in similar low density cell-culture studies [32, 64, 91, 153, 166, 225].

Table 5.1: Surface modification conditions tested to assess the ability to promote single-neuron axonal extension. Substrate coating molecules: poly-l-lysine (PLL), polyethylenimine (PEI), and neural cell adhesion molecule L1 (NCAM-L1).

Substrate Coating Molecule	Concentration (µg/mL)
PLL	10
PEI	10
PLL + NCAM-L1	10, 25
PEI + NCAM-L1	10, 25
PLL + Laminin	10, 25
PEI + Laminin	10, 25

5.3 Results

Single-cell development in response to various molecular coatings

The surface treatments that yielded the best results in terms of neurite/axonal extension were obtained by coating a homogeneous layer of PLL (10 µg/mL) followed by the addition of homogeneous layer of neural cell adhesion molecule (NCAM) L1 (25 µg/mL). This determination was made based on observations comparing the correlation of the different substrate coatings to the number of cells that developed to stage 3 in a four day culture period. Similar membrane treatment substituting PLL with PEI generated comparable results. However, since the PLL was a commercially available product that objectively seemed to produce the best results, all future experiments were conducted

following the same surface modification procedure. Treatments using laminin resulted in cell clumping and cellular attachment only at the soma and growth cone, and proved to not be suitable in promoting single-neuron axonal extension. Substrate coatings with only PLL or PEI yielded neurons that attached to the surface but failed to promote axonal extension of individual laser patterned neurons. Instead, expansion of the neurite network in the immediate vicinity of the cell body was observed.

Viability of laser cell-micropatterning

Once the most favorable experimental substrate coating had been decided, single-cell viability of individual laser-patterned neurons was analyzed. The 24 hour cell viability results were analyzed for all cells that were laser-patterned, regardless of the sub-cell type, from 10 different dissections and subsequent laser cell-patterning experimental sessions. Figure 5.3 summarizes these results. Cell viability was evaluated using phase contrast microscopy, where the presence of neurites extending from the soma and absence of circular vacuoles (which indicate programmed cell death) represented a healthy cell. It can be seen that the survival rate of individual laser-patterned CFNs after 24 hours is 62.4% (s = 18.8%). This is consistent with the results obtained by Chada and Heidemann where roughly 60-70% of cells introduced to a culture dish environment attach and remain viable [32, 91]. Thus, laser cell-micropatterning into the structures of a PDMS substrate does not seem to induce any adverse effects on the 24 hour cell viability of individual-neurons. These results are also in congruence with previous laser cell-micropatterning studies with CFNs [166, 184].

Single-neuron axonal extension and pathfinding

Individual CFNs were laser-patterned onto microfabricated PDMS substrates and allowed to culture for 4 days. Chada reported that by four days in culture 10-20% of CFNs seeded at 1,500-2,000 cells/cm^2 developed axons (stage 3) when grown on PLL-coated tissue culture plastic [32, 53]. Under similar culture conditions Heidemann enhanced axonal development by adding additional growth supplements to the culture media, such that 70-80% of CFNs remaining after 4 days in culture developed to stage 3 [91, 92]. In the work reported here we found that individual-neurons patterned into the microstructures of the PDMS biochip at comparable cell densities (~2,000-5,000 cells/cm^2) could undergo the same developmental progression. The main difference

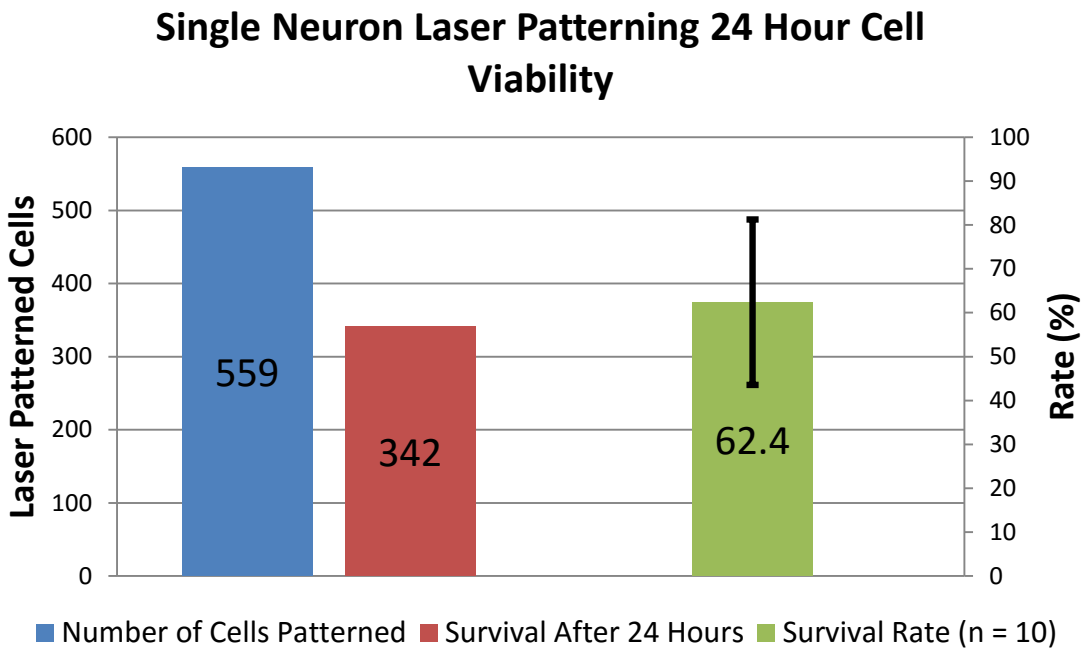

Figure 5.3: Cell viability results for individually laser-patterned chick forebrain neurons. 559 total neurons were laser-patterned over the course of 10 different dissections and subsequent laser cell-micropatterning experiments.

between this study and previous ones is the additional substrate coating of with NCAM L1. Using this as our primary cell attachment molecule we did not have to formulate a complicated growth media like Heidemann [91] in order to get individual cells to extend an axon at low culture densities (shown in Figure 5.4).

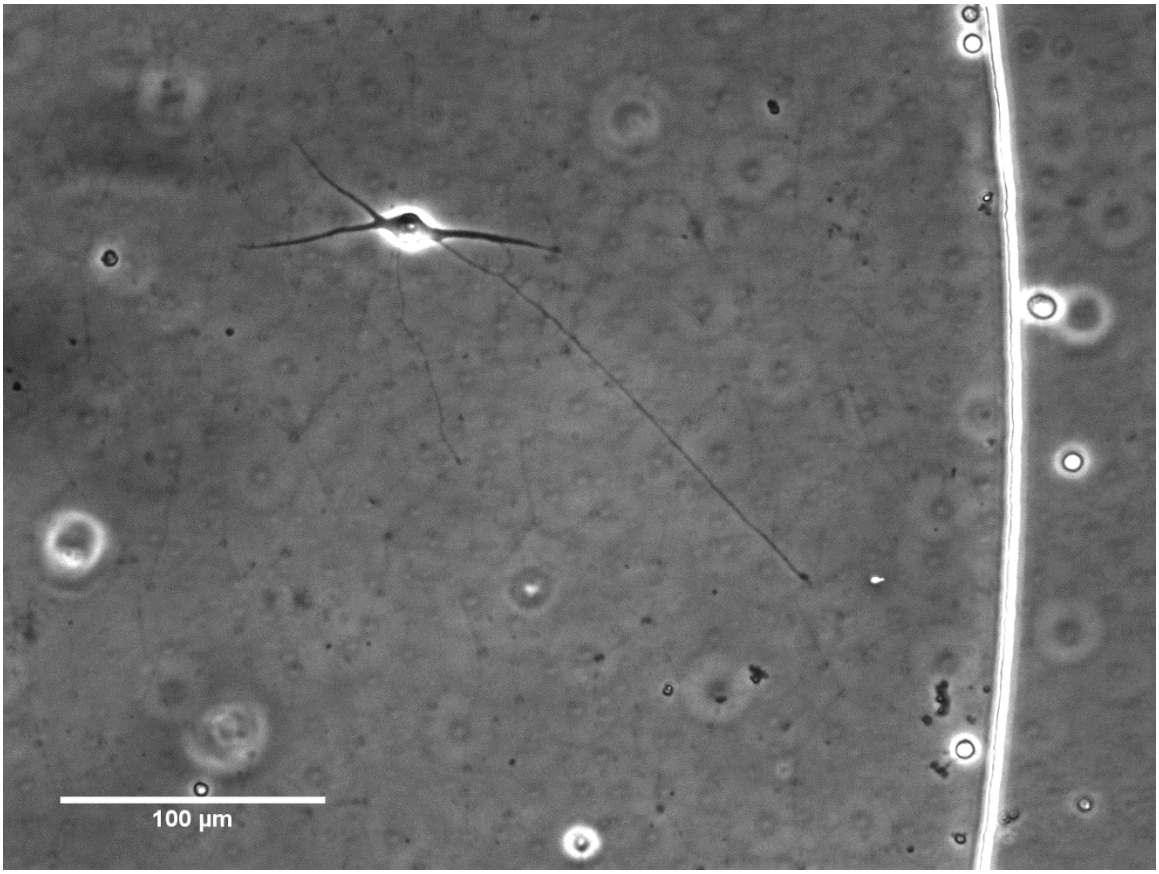

Figure 5.4: Image of a random chick forebrain neuron extending an axon in a low cell density environment.

Using the geometric constraints of the microwell, axonal extension can be restricted to proceed in only one permissible direction. Figure 5.5 represents a typical pyramidal neuron at stage 3 extending through and beyond the confines of the cell body isolation microwell. For the purpose of cellular consistency, only cells expressing morphology similar to that of a pyramidal cell (Figure 1.2 B, Figure 5.2 B, and Figure 5.2

C) were scored for our assessment. As a whole, the success rate for individual laser-patterned CFN to extend through and at least 20 µm beyond the end of the geometric guidance microchannel confinement was 10.3 ± 5.7%. Of the cells that did extend beyond this threshold, the angle at which they crossed the 20 µm barrier was observed. Figure 5.6 represents the distribution of angular extension for 67 axons.

Figure 5.5: Phase contrast image depicting an axon extending through and beyond the confinements of the three-dimensional microstructure. Scale bar 20 µm.

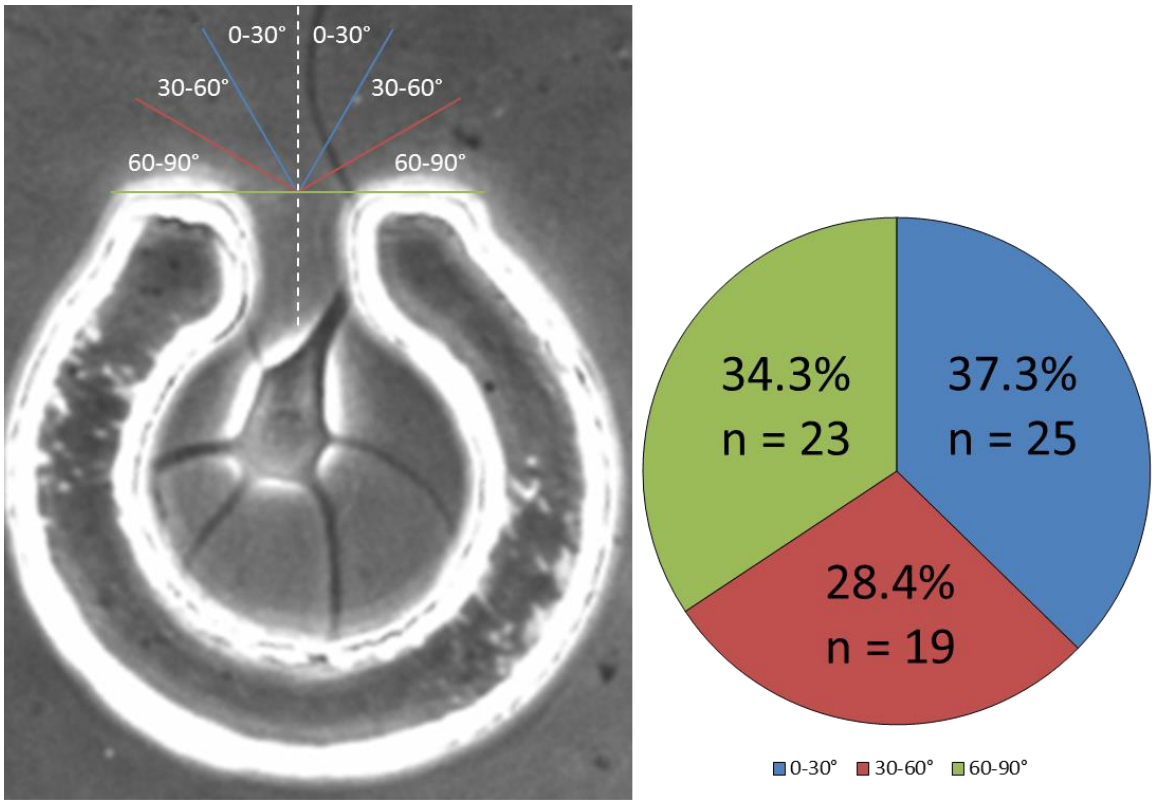

Figure 5.6: Left) Diagram of angular group classifications for individual axonal extension directions 20 µm beyond the end of the geometric guidance microchannel connected to the cell body isolation microwell. Right) Pie chart showing the angular distribution of axons that extended at least 20 µm beyond the end of the geometric guidance microchannel (n_{total} = 67).

5.4 Discussion

Single-neuron axonal pathfinding in response to geometric microstructures

The results indicate that innate pathfinding beyond the end of the geometric guidance microchannel shows no preference for a particular angular direction of axonal extension. Interestingly, all the cells analyzed contacted at least one edge of the geometric guidance microchannel at some point during their pathfinding through and beyond. Of these 67 cells, 10 crossed the 20 µm extension threshold at an angle of 90°,

thus staying in contact with the wall of the geometric microstructure. Mahoney reported that 86% of the total neurites that extended from PC12 cells that made contact with a wall remained in contact with the wall and did not withdraw [136]. Evaluation of the other neurites that extend from the soma and interact with the circular wall was not conducted; however, the difference in observations between the two sets of results is noteworthy. One likely explanation for this phenomenon involves the abrupt change in direction the axon must go through to follow the edge of the wall. Li and Folch investigated axon turning in response to topography and found that when a straight path was not permitted, an axon will turn in the direction that minimizes the turning angle [153]. Thus, because there are possible chemical guidance cues from randomly disturbed cell debris and there is an unobstructed path and for the axon to extend, we would expect it to extend at an angle less than 90°. Many non-dominant guidance factors, including physical-contact guidance, caused the final angular direction of axonal pathfinding to be evenly distributed throughout a 180° range.

The percentage of individual laser-patterned neurons that extend an axon through and beyond the geometric guidance microchannels is relatively low (~10%). While the viability of individually laser-patterned neurons is consistent with other works involving low density cell-culture [32, 91, 166, 184], formation and extension of an axon seemed to be inhibited to some degree when individual cells are placed into the microwells of a three-dimensional PDMS substrates. Francisco et al. theorized that when growth cones interact with geometric constraints a decrease in surface area occurs, likely due to mechanoreception events that result in partial collapse of the growth cone; which is a hallmark of molecular guidance cues that repel growth cones [64]. Although they report that a correlation between axon-advance rates and changes in growth cone

surface area do not seem to exist, they suggest that a decrease in axon formation in enclosed chambers is reflective of nascent growth cones interacting with walls and resulting in retraction of an axon back into the cell body. Given that the current geometric design described here has only one path for an axon to extend, it stands to reason that the design itself may be contributing to the inhibition of axonal extension from individual-neurons. Depending upon the application, this could be beneficial in the sense that the cells that do extend out of the geometric confinements are going to be exploratory in nature and will provide a model in which statistically reproducible pioneer-neuron axonal pathfinding events can be observed.

Summary

We demonstrated here that individual CFNs can be laser-patterned into the structures of a three-dimensional substrate and develop to stage 3 in a low cell density culture environment. Geometric confinement of a cell in all directions except one permissible path results in the extension of an axon that can serve as a model to observe pioneer-neuron axonal pathfinding events in a statistically reproducible manner. Thus, simple or complex geometrical environments can be used to regulate the growth direction, complexity of neurite networks, and formation of an axon for an individual-neuron. After confinement by the geometric guidance microchannel, no dominant guidance factors could solely control axonal pathfinding directionality and thus, the final angular direction of axonal pathfinding was evenly distributed throughout a range of 180°.

CHAPTER VI
SINGLE-NEURON AXONAL PATHFINDING WITH GEOMETRIC GUIDANCE MICROCHANNELS AND CHEMICAL SIGNALING FROM A LOCALIZED MICROFLUIDIC SOURCE

6.1 Introduction

Many *in vivo* developmental and regenerative events utilize the recognition of chemical signaling events. Migration of myogenic skeletal muscle cells [18], neutrophil recruitment to the site of an inflammatory response induced by cancer [223], and central nervous system axonal pathfinding [35] represent a small number of chemotactic biological processes. Recreating the native *in vivo* environment *in vitro* is an arduous task that has yet to be realized; however, many *in vitro* models have been used to mimic certain biological events to elucidate the mechanisms associated with cell-soluble factor interactions. To study cell-soluble factor interactions various gradient-generation devices have been developed. The Boyden chamber assay was originally designed for the analysis of leukocyte chemotaxis and is based on a chamber of two medium-filled compartments separated by a microporous membrane. Cells are placed in an upper compartment and are allowed to migrate through the pores of the membrane into the lower compartment, in which chemotactic agents are present [21, 36]. The Zigmond [242] and Dunn [241] chambers utilize the separation of two filling wells by a small glass bridge to create somewhat defined chemical gradients for cell chemotaxis studies. Pulsatile injection of chemokines using glass micropipettes has been used to create localized chemical gradients, typically for influencing axonal guidance [86, 130]. Simple and elaborate microfluidic systems have been devised to create well defined spatiotemporal chemical gradients for controlling various cellular behaviors [39, 117]. The goal of all these techniques is to create reproducible spatial and temporal biological signaling events to statistically determine the effect a chemotactic agent may have.

Analysis of single-cell behavior to the local microenvironment is important for understanding the higher-level organization of tissues and organisms. Dynamic interactions between transient spatiotemporal biochemical signals and the cells that they target are essential for normal organism development and function. Using microfluidics, several single-cell isolation methods have been developed to address various aspects of environmental control on individual cells [49, 78, 232]. Cellular arrays are useful for measuring single-cell responses for applications in drug testing, toxicology, and basic cell biology [104, 179, 225]. Using strategically placed micropipettes filled with chemoattractant solutions, localized point source concentration gradients can be used to influence the growth cone of an individual cell [130, 170, 201, 238] based on the frequency and magnitude of applied pressure pulses.

Despite the widespread use of these techniques to influence single-neuron axonal guidance in a local environment, simultaneous signaling of multiple cells in a spatially defined manner has yet to be investigated. This is mainly due to the space limitations associated with the number of micropipettes required and the inability to precisely control of the spatial arrangement of cells on a substrate. In the work described here, we present a biochip system capable of providing geometric and chemical guidance for developing axons; mimicking a choice point event of a pioneer-neuron axon by using a physical barrier to geometrically orient the initial axonal pathfinding direction in relation to a localized chemical gradient generated from a microfluidic source within a standard cell-culture environment. To create such a system we must 1) design and fabricate multi-layer PDMS biochips; 2) theoretically and experimentally verify chemical gradient generation; and 3) evaluate the ability of the system to influence axonal pathfinding of an individual-neuron. The biochip design was inspired by the work done

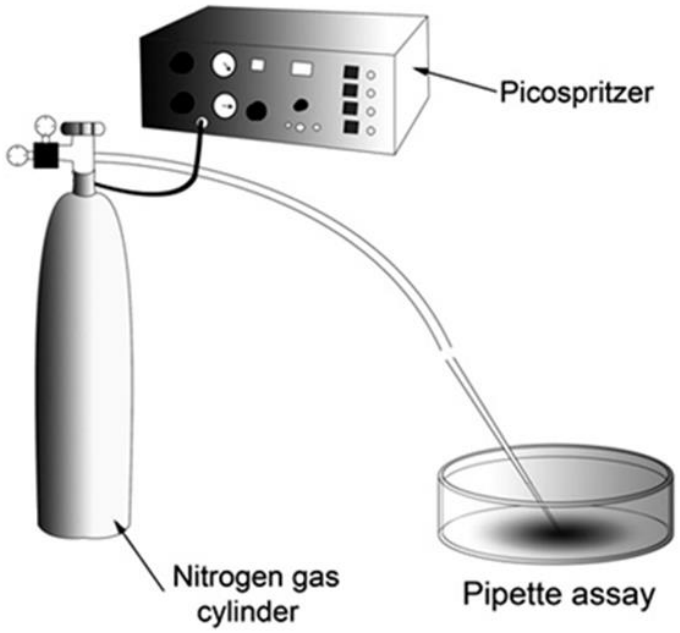

Figure 6.1: Diagram setup of the micropipette experiment where a chemotactic agent is released from a micropipette in the vicinity of cells growing in a Petri dish. Reproduced with permission from Bentham Science Publishers Ltd: Combinatorial Chemistry and High Throughput Screening [171], Copyright 2009.

by Peterman et al. [161, 162] where fluid flow through an aperture connected to a subterranean microfluidic chemical guidance channel allows for small volumes of chemicals to be locally administered into the culture area above. The design of the system essentially inverts the micropipette experiment (Figure 6.1) using a microfluidic chemical guidance channel to create a localized chemoattractant gradient. Two modes for driving fluid through the chemical guidance channel and subsequent gradient generation were devised. One mode of gradient generation was based on pressure pulses to drive fluid through the subterranean chemical guidance channel (similar in fashion to the micropipette assay) and the other involved constant hydrostatic pressure

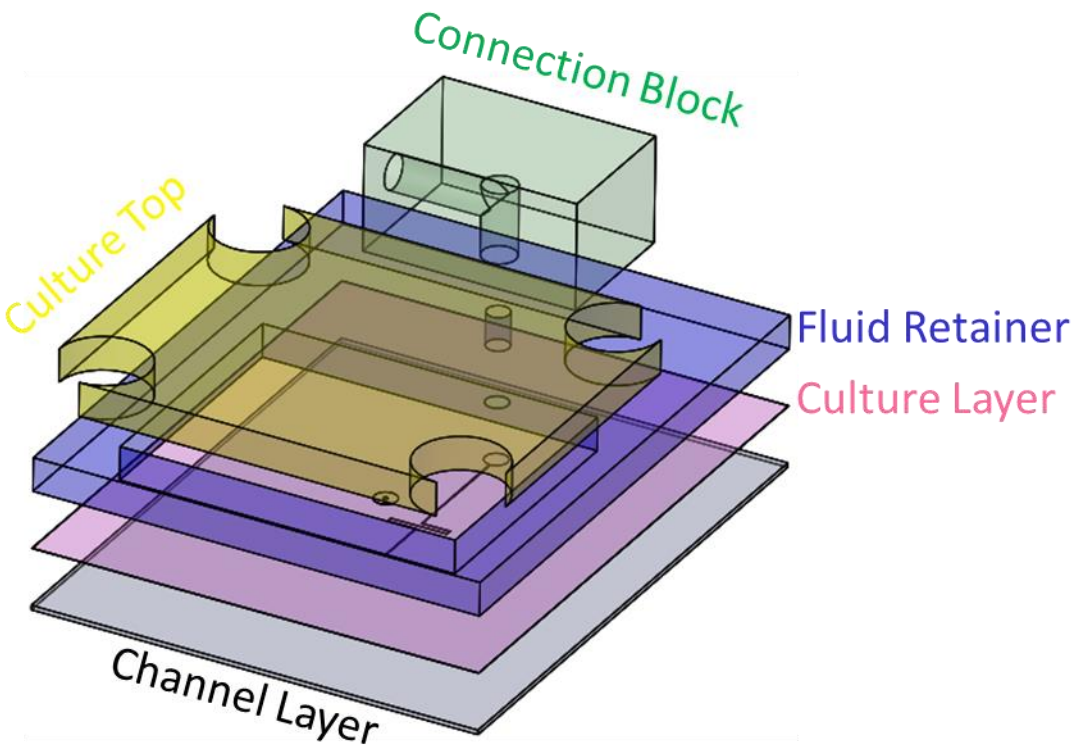

Figure 6.2: Exploded animated design of the complete biochip system.

derived from horizontally oriented microfluidic reservoirs. Both methods proved useful for injecting small volumes of axonal guidance molecules into a localized substrate environment; however, because each neuron will develop at a different rate when isolated *in vitro*, we focused our work on using the continual passive pumping method so that temporal signaling would not be restricted to arbitrary predetermined time points. Using this biochip in conjunction with our laser cell-micropatterning system [56], multiple cells can be placed into microwells (Figure 3.5) at defined distances from a chemical source and subjected to a localized chemical gradient of soluble-molecules; providing a method to study individual axonal responses from a choice point, when there is a transition from geometric to diffusible chemical guidance.

6.2 Biochip Design

The design of the biochip used to generate a localized chemical gradient incorporated the geometric cell isolation structures of the PDMS biochip described in Chapters III and V. Five different layers of PDMS were combined together to create the overall biochip structure (Figure 6.2). The bottom layer is the described as the “channel layer.” The channel layer consists of a 20 µm deep groove in a PDMS membrane of 200 µm thickness. The groove begins with a 2 mm diameter circle connected to a 6 mm long by 100 µm wide channel. This channel rapidly tapers to a width of 50 µm and continues for 21 mm until it terminates. The channel layer dimensions are shown in Figure 6.3. The layer immediately above the channel layer is the “culture layer.” This is a PDMS layer of approximately 40 µm in thickness with two distinct structural attributes. The first attribute is a circular array of 10 cell confinement structures with a wall height of approximately 20 µm. The second attribute is a pair of thru-holes in the culture layer membrane. One thru-hole is 2.5 mm in diameter and the other is 25 µm in diameter and concentric with the cell confinement structures. The 2.5 mm thru-hole is aligned to be concentric with the 2 mm diameter circular groove of the channel layer while the 25 µm diameter thru-hole aligns with the center of the terminal portion of the channel layer. The angle of the geometric guidance microchannel in relation to the thru-hole source (25 µm

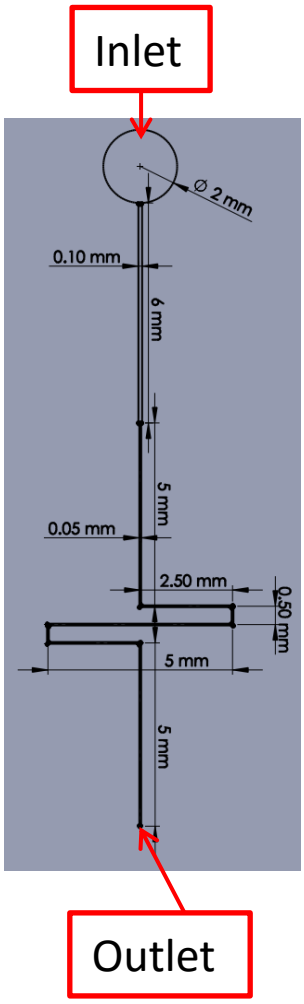

Figure 6.3: Complete dimensional breakdown of the channel layer.

diameter hole) was fabricated to be 0° (directly in line with the geometric guidance microchannel of confinement structure) or 45°. The thru-hole connects the culture layer to the channel layer underneath. When the two layers are permanently bound together, the bottom side of the culture layer creates a seal with the groove of the channel layer to form the microfluidic chemical guidance channel. The next layer is a 50 mm wide x 50 mm long x 3 mm thick slab of PDMS that will serve as a cell-culture fluid retainer. A 3 mm diameter hole is punched in this layer to continue a path in which fluid can be delivered to the channel layer. The reservoir is created by cutting a rectangular hole 40 mm wide by 20 mm long. The final PDMS layer is a connection block that is molded in an acrylic form. The block is 25 mm long x 12 mm wide x 10 mm high and 1/8" stainless steel dowel pins are used to create a cylindrical elbow. The horizontal portion of the elbow allows fluid to remain at a constant height when passive hydrostatic flow is used to drive fluid through the chemical guidance channel layer [240]. To finish the assembly a removable "culture top" layer of 3 mm thick PDMS was placed on top to maintain an exact height differential.

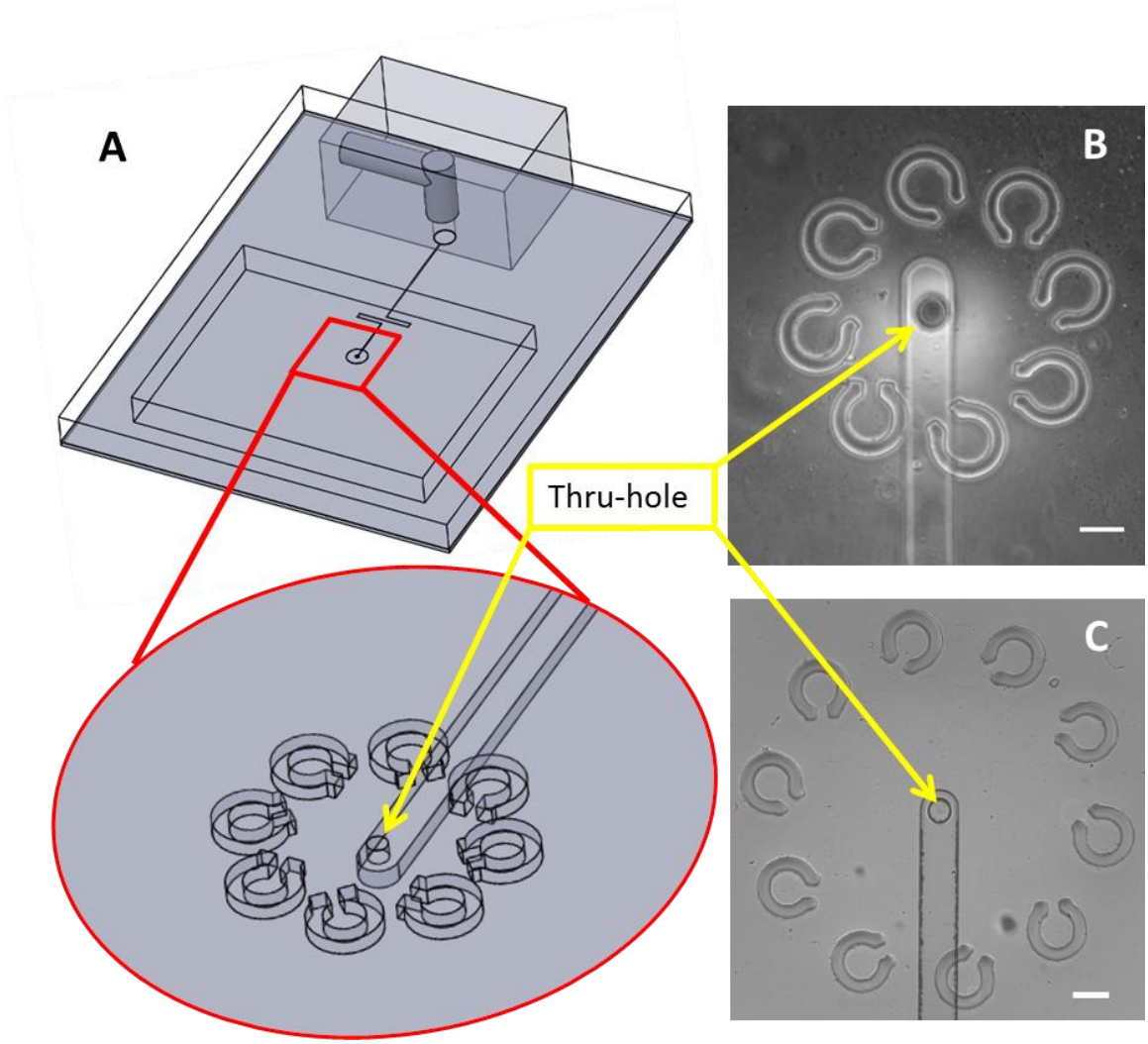

Figure 6.4: A) Diagram of the complete biochip system (culture top not shown) highlighting in red the cell confinement structures in relation to the thru-hole source. Bright field images of completed biochips where the outlets (end of the geometric guidance microchannel) of cell confinement structures are oriented at a 45° angle and 100 µm (B) or 200 µm (C) away from the thru-hole source. Scale bars = 50 µm.

6.3 Theoretical and experimental gradient generation

Generation of a localized gradient of soluble-molecules was established by flowing fluid through the microchannels of the chemical guidance channel layer and out the thru-hole aperture. Fluid was first loaded into the elbow reservoir of the connection block; however, flow does not immediately occur due to the resistance of the microchannel network. To initiate flow in the chemical guidance channel layer network, external pressure was applied at the connection block with a syringe. Once the fluid traversed the microchannel network and exited into the culture area via a thru-hole aperture, a continuum is created so that the hydrostatic pressure generated from the height differential of the connection block relative to the top of the fluid retainer layer is sufficient to continue driving fluid flow. Under these conditions, a steady flow rate and subsequent concentration gradient is generated in the cell-culture environment. We also devised an alternative method for generating a localized gradient. This involved use of a pressure application system consisting of an electrically gated pneumatic valve (CKD, FAB41-8-3-12-CB-4) that was programmed using an Arduino Uno microcontroller to apply pressure pulses (~1 psi) to the connection block at different frequencies and time durations. This enabled the user to change the gradient profile in real time by adjusting any combination of the applied pressure, pulse duration, or frequency of pulses. However, as previously mentioned, this method was not employed for cell-culture studies due to added complexity of the system and differences in the rates of development between individual-neurons placed into the PDMS substrate microstructures.

An initial approximation to the channel volumetric flow rate, Q (m^3/s), can be found by:

$$Q = \frac{\Delta P}{R}, \tag{4.2}$$

where ΔP (Pa) is the pressure drop across the channel and R (Pa·s/m^3) is the total channel resistance. The channel resistance for the rectangular channel was estimated by:

$$R = \frac{12\,\mu L}{wh^3}, \tag{4.4}$$

where μ (Pa·s) is the fluid viscosity, L (m) is the length, h (m) is the height, and w (m) is the width of the channel [198]. The flow velocity was set by using a 7 mm height differential resulting in a driving pressure of 68.7 Pa. Under these conditions the theoretical volumetric flow rate in the channel, using Equations 4.2 and 4.4, is estimated to be ~65 pL/s. Using ~1 µm diameter tracer particles, the maximum channel velocity near the outlet aperture was experimentally evaluated by tracking particle positional displacement in a series of image frames. Taking measurements of continual flow after various durations of time, the maximum steady flow velocity (U_{max}) in the channel was determined to be ~55 µm/s. The average flow velocity, $< u >$, throughout the entire channel can be estimated by [240]:

$$< u > = \frac{2}{3} U_{max}, \tag{6.1}$$

which results in an average experimental channel flow rate of ~37 pL/s. Using the constant pressure drop across the channel, finite element analysis of the fluid flow velocity in the channel and culture area was modeled by solving the Navier-Stokes equation:

$$\rho\left[\frac{\partial \mathrm{v}}{\partial t} + (\mathrm{v}\nabla)\mathrm{v}\right] = -\nabla \mathrm{p} + \mu\nabla^2\mathrm{v} + \mathrm{F}, \tag{6.2}$$

with the condition that $\nabla \mathrm{v} = 0$. Where ρ is the density, v is the flow velocity, p is the pressure, μ is the viscosity, and F is the boundary stress. The conditions for this model

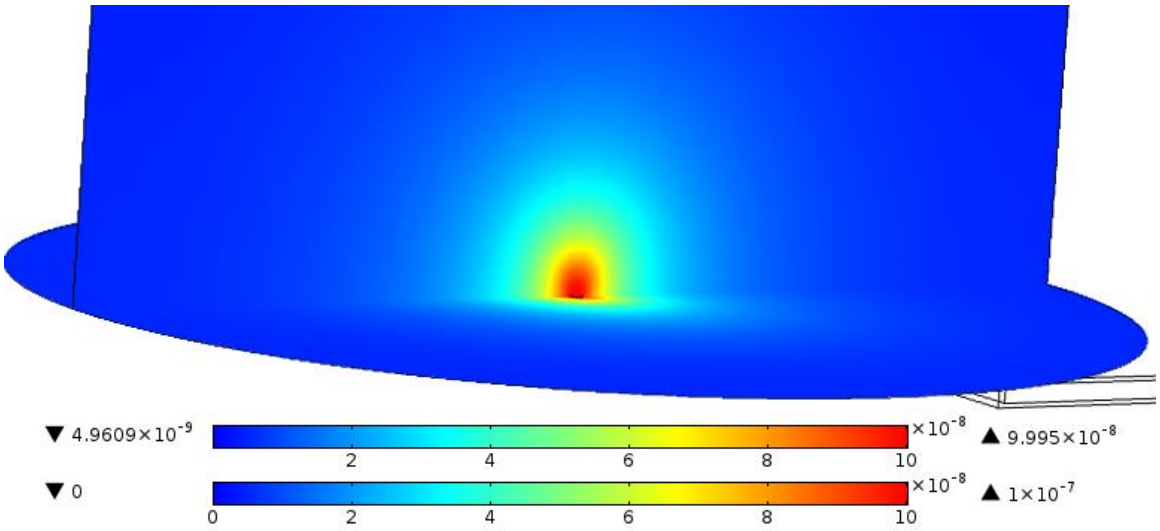

Figure 6.5: COMSOL simulation for the concentration distribution in the culture reservoir after 1 hour of continual flow. The source concentration has a maximum value of 100 nM (1x10^{-7}).

were that the bulk material was set to be water (which has similar properties to the culture media), and interactions between PDMS and the culture media (in this case water) were neglected resulting in a "no slip" boundary condition. Using the flow velocity field (v) obtained from the numerical solution of the Navier-Stokes equation, the concentration of a molecular species (C) in the biochip system can be obtained by solving the diffusion-convection equation:

$$\frac{\partial \mathrm{C}}{\partial t} - D\nabla^2\mathrm{C} + (\mathrm{v}\nabla)\mathrm{C} = 0, \qquad (6.3)$$

where D (m^2/s) is the diffusion coefficient of the specific species. The diffusion-convection equation was solved for a fluid voxel centered on the thru-hole aperture with a 3 mm radius and height of 3 mm with the assumption that initially there is no solute present in the culture area. The simulation results from the biochip system for a one-hour duration of continual fluid flow with a diffusion coefficient of 9.3 x 10^{-11} m^2/s (FITC-BSA) depicted in Figure 6.5. For this scenario we find that at distances of 100 µm and

200 μm from the center of the source, the apparent concentration is about 50% and 25% of the concentration supplied by the chemical guidance channel, respectively. Experimentally, to visualize the chemical gradient, fluorescein isothiocyanate-labeled bovine serum albumin (FITC-BSA) was suspended in phosphate buffered saline (pH = 7.4) to a concentration of 1μM. This solution was added to the connection block of the biochip and pressure was applied with a syringe to initiate flow of the solution through the chemical guidance channel network and out the outlet thru-hole. Once a continuum was created with the outlet and culture reservoir, the external pressure source was removed and gravity-driven flow remained. The culture reservoir was filled with 2 mL of the same PBS to eliminate the possibility of creating an artificial current due to variable solution densities. To eliminate meniscal formation within the culture reservoir area, a PDMS slab with holes cut in the corners was placed on top to keep the liquid height constant while allowing for sufficient gas exchange with the surrounding environment. FITC-BSA was chosen for imaging the gradient because it serves as a model protein-fluorophore conjugate that has a molecular weight of 66 kDa, which is similar in size to many known biological signaling molecules, such as netrin-1 (75 kDa) [74].

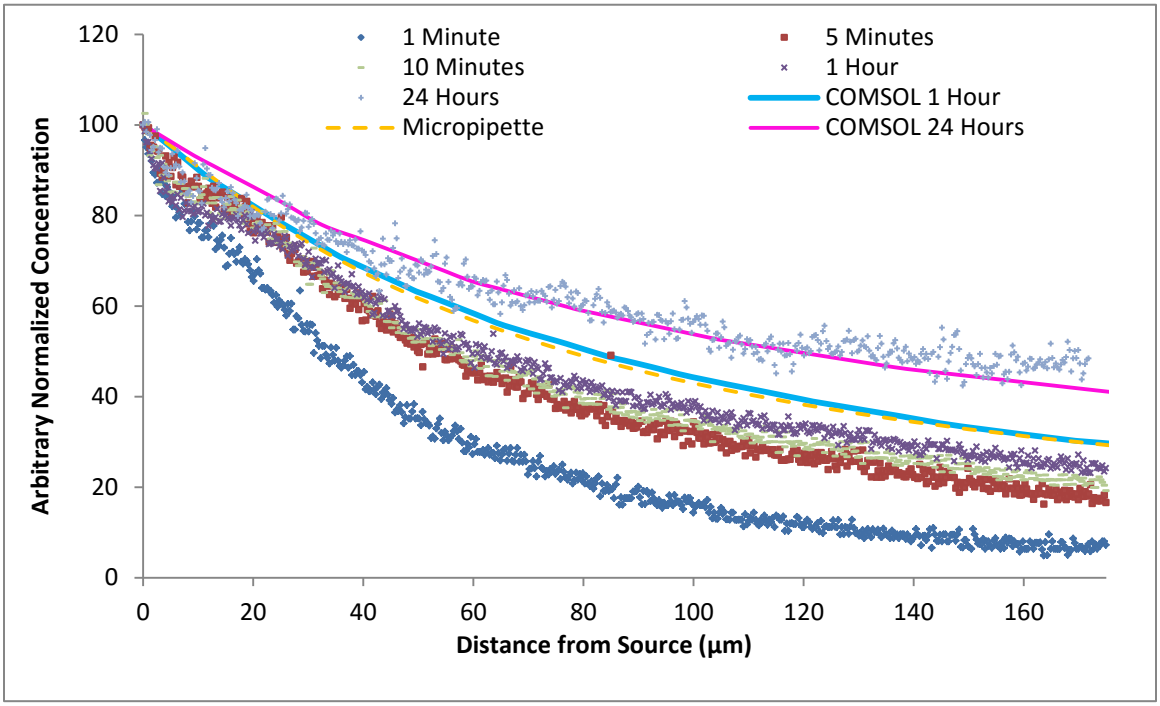

Figure 6.6: Theoretical and experimental molecular gradients at various times and distances from the microfluidic source using 1µM FITC-BSA solution and a hydrostatic applied pressure of 68.7 Pa.

Imaging of the gradient profile was conducted using regular epifluorescence on a Zeiss Axiovert 200 M microscope. Subtracting the background intensity of the image before flow is established, profile intensity measurements were made starting at the edge of the thru-hole. Normalization of the intensity at different time points for the experimental concentration gradient and the model gradient 1 µm above the culture surface are depicted in Figure 6.6.

It can be seen from the experimental profiles that a relatively constant concentration profile is achieved after approximately 5 minutes. Growth cone detection of a diffusible chemical gradient is estimated to be on the order of minutes [76], thus, our system has the ability to rapidly establish a pseudo-stable localized signaling environment for long periods of time. Comparing the experimental 60 minute profile to that predicted by the finite element analysis model there is good congruency between

the two. The finite element model slightly overestimates the experimental values beginning at ~30 µm away from the source. However, looking at the percent change across a 10 µm span (typical size of the growth cone) at 100 µm away from the source we see that the model predicts ~7% change and the experimental value is ~7.5%. Both these values lie well within the accepted minimum range of a 1-10% concentration change across the growth cone that is necessary for detection and eliciting a turning response [74-76, 170]. At 24 hours the finite element model predicts a ~4.25% change and the experimental data demonstrates a ~4% change for a 10 µm span 100 µm away from the edge of the source. The slight decrease in the steepness of the gradient is to be expected because the convection element of solute flow into the culture reservoir is slightly greater than the diffusion. Because the culture reservoir does not serve as an infinite sink there is some accumulation of the solute. For the case of a 1 µM source concentration and an average volumetric flow rate of 37 pL/s, the background concentration after 24 hours would be approximately 1.6 nM; resulting in almost a thousand fold lower concentration than the source. Therefore, bath accumulation and growth cone desensitization over a 24 hour continual flow period at biologically relevant concentration levels (0.1-10 nM) should be negligible.

Based on the flow parameters obtained for the system, the initial concentration of a chemical guidance solution can be determined. It is theorized that the minimum detectable gradient steepness across the growth cone is the smallest when the change in concentration is equal to the dissociation constant, K_D [76, 170]. For most growth cone guidance molecules the dissociation constant is approximately 1 nM, thus adjusting the chemical guidance channel source concentration accordingly we can tune the system to

satisfy this requirement for distances of 100 µm and 200 µm away from the source (depicted in Figure 6.4 (B) and (C)).

The inspiration of the design for the biochip system was to create a microfluidic version of the classical micropipette assay (Figure 6.1). For the micropipette experiments the small diameter of the outlet (~1-2 µm) allows the system to be modeled using convection and diffusion from a point source. Postma and Haastert rigorously analyzed the mathematics of experimentally generated gradients from a micropipette [169]. They assumed that the micropipette behaves as a point source and that the solute will diffuse from the pipette in a half-sphere, with the opening of the pipette being the center of the sphere. Using the boundary condition that the bath is large enough so that at a distance where $x = R$ from the source, the concentration (C) at the boundary $C(R)$ of the bath is constant and remains zero; the convection-diffusion equation out of the micropipette can be described by:

$$\frac{\partial C(x,t)}{\partial t} = D\frac{1}{x^2}\frac{\partial}{\partial x}x^2\frac{\partial}{\partial x}C(x,t) - \frac{F}{2\pi x^2}\frac{\partial}{\partial x}C(x,t), \tag{6.4}$$

where the average liquid flow rate out of the pipette due to repetitive applied pressure pules is represented by F (µm^3/s). At equilibrium, the steady-state concentration profile for a large bath is:

$$C(x) = C_S\frac{1-e^{-\frac{F}{2\pi Dx}}}{1-e^{-\frac{F}{2\pi Dr_0}}}, \tag{6.5}$$

with r_0 being the radius of the opening of the micropipette and C_S is the concentration of the solute at the micropipette tip. Given that C_S and F increase linearly with the applied pressure (P), the absolute concentration is a function of P^2. Neglecting any radial convection, the time constant to reach equilibrium is given by, $T_D = (x\text{-}r_0)^2/D$. For FITC-BSA with D = 9.3x10^{-11} m^2/s at a distance of x = 100 µm from the source with an opening

radius r_0 = 12.5 µm, T_D ≈ 90 s. At *x* = 200 µm away from the source T_D ≈ 380 s (6.3 minutes). Thus, as a first order approximation the equilibrium time constant closely follows the experimental data. Using a volumetric flow rate of 37 pL/s, the point source equilibrium concentration profile (labeled Micropipette) was plotted along with the experimental data shown in Figure 6.6. We find that the finite element model and the point source model closely follow each other at the one hour time point, however, deviate at the 24 hour mark. This most likely is attributed to the assumption that the concentration at the edge of bath remains constant and zero over time (infinite sink). Also, the finite element model looks at a voxel with a 3 mm radius. Given the time period of 24 hours by diffusion alone the distance an FITC-BSA molecule would travel is approximately 2.8 mm. Thus, because the contribution of solute movement due to convection is slightly larger than that of diffusion in proximity to the source, the model predicts some localized accumulation to in the system. Taken altogether, we were able to show that we could create a pseudo-stable chemical gradient over long periods of time using a passive pumping mechanism. We were able to maintain the steepness of the gradient across the span of the growth cone (10 µm) within an appropriate range (~1-10%) for up to 24 hours. This will allow for continual signaling of neurons as they develop *in vitro* to ensure that they will be presented with nearly identical conditions as they begin pathfinding beyond the confines of a geometric guidance microchannel. Additionally, the system can be modeled as a point source for time durations on the order of a few hours.

Chemical guidance media

The guidance media that was used was a complete media (Media 199, 10% Fetal Bovine Serum, 2% B27, and 100 ng/mL NGF 7S) that was “conditioned” with

neuronal and glial factors from cells harvested from E10 chick forebrains. Observations made throughout experimentation showed that isolated cells in proximity (< 500 μm) to established higher density neural networks tended to extend an axon in the direction of the network. This was assumed to be due to chemotactic paracrine signaling associated with the activity of the higher cell density networks. Thus, in an active culture environment there most likely exist a large number of secreted molecules that can influence axonal pathfinding. This broad molecule based approach provided a way to test our biochip without having to identify a specific soluble factor; therefore increasing the likelihood that some form of influence on axonal pathfinding and extension could be observed.

6.4 Results

Axonal pathfinding in response to geometric and chemical guidance

Axonal pathfinding in response to geometric and chemical guidance was observed by laser cell-micropatterning individual-neurons from the E8 chick forebrain into the cell confinement microwells of the biochip designed in Chapter III and used in Chapter V. Before cells were laser-patterned, the chemical guidance channel network was filled with chemical guidance media to provide signaling information to the developing neurons. Due to the passive pumping mechanism of the biochip, cells could be exposed to a continual chemical gradient from the onset of the experiment. After laser cell-micropatterning, the cells were allowed to culture for one day in complete media to promote cell survival. At the end of one day in culture, all the media was removed and replaced with a base media (Media 199 with 2% B27). Each day thereafter all the media was replaced with fresh base media for the duration of the experiment. The

results of individual axonal pathfinding in response to the different geometric and chemical guidance conditions are shown in Figure 6.7. Axonal pathfinding directions at 20 μm beyond the end of the geometric guidance microchannel were categorized into three different angular groups, 0-30°, 30-60°, and 60-90°, as described in Chapter V. It was assumed that it was equally likely that the axonal extension angle would fall into any one of the angular groups as demonstrated in Chapter V; therefore, the percentage of axons for each angular group were statistically compared using a Pearson's chi-square (χ^2) test. When there was no chemical guidance (only geometric guidance), the angular distributions were not statistically different than the assumed distributions. For the biochip where the chemical source was placed at a 0° angle from the end of the geometric guidance microchannel, the percentage of axons extending in the direction of 0-30° and 60-90° was significantly different ($p < 0.05$) from the assumed distribution. Figure 6.8 represents experimental results of axonal pathfinding in response to the chemical gradient.

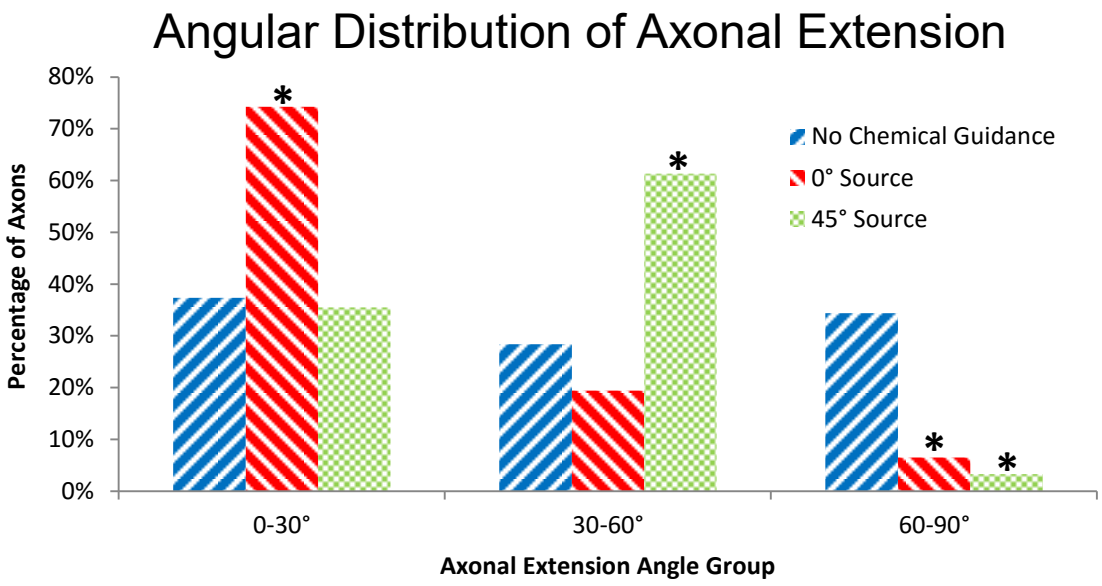

Figure 6.7: Breakdown of the axonal pathfinding directions in relation to the position of the chemical guidance source 20 µm beyond the end of the orientation microchannel. No chemical guidance (n=67), 0° Source (n=31), and 45° Source (n=31). * indicates statistical significance with $p < 0.05$.

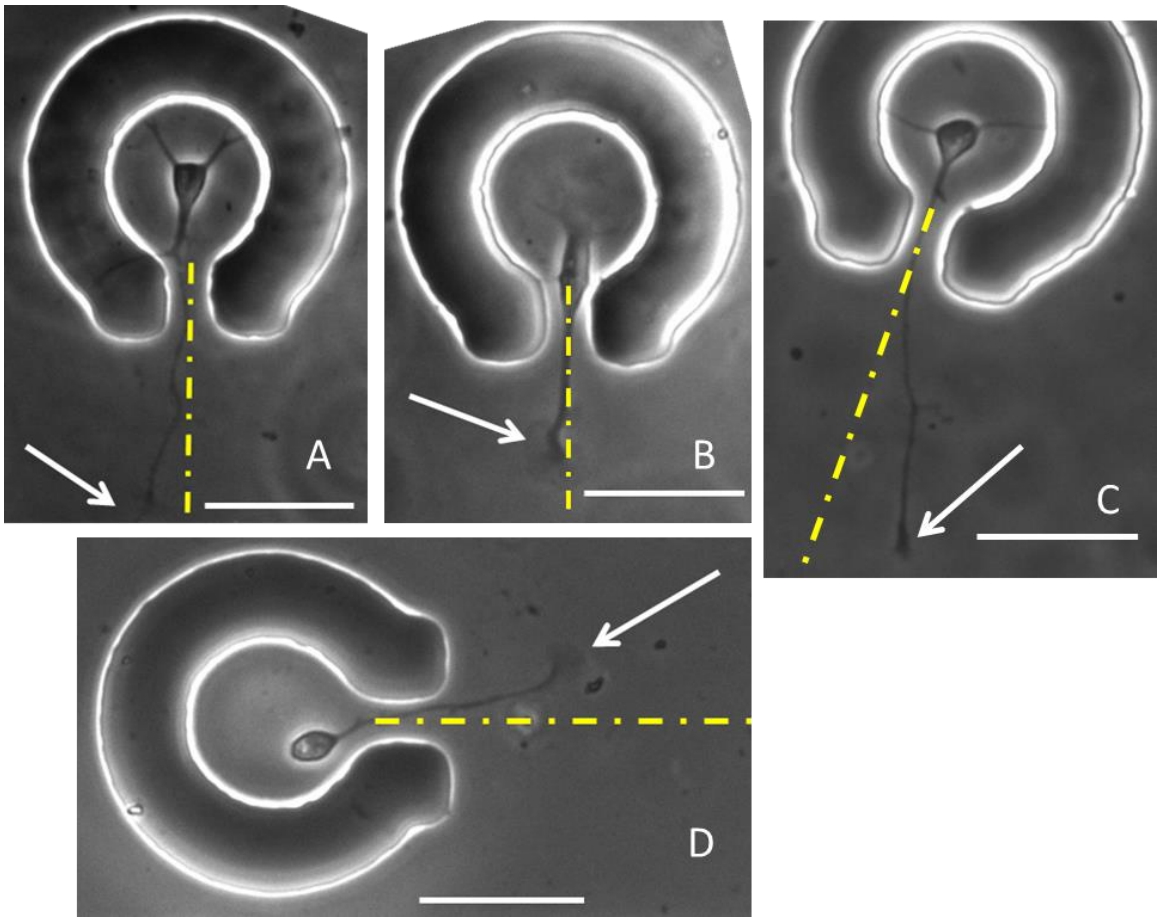

Figure 6.8: Initial axonal pathfinding of individual neurons through and beyond a geometric microchannel constraint in response to a localized chemical signaling gradient. Images A-D represent different CFNs from four different biochips after exposure to the chemical gradient for 1 DIV. Dashed yellow lines indicate the direction of the microfluidic source. White arrows point to the growth cone of the neurons. Scale bar = 50 µm.

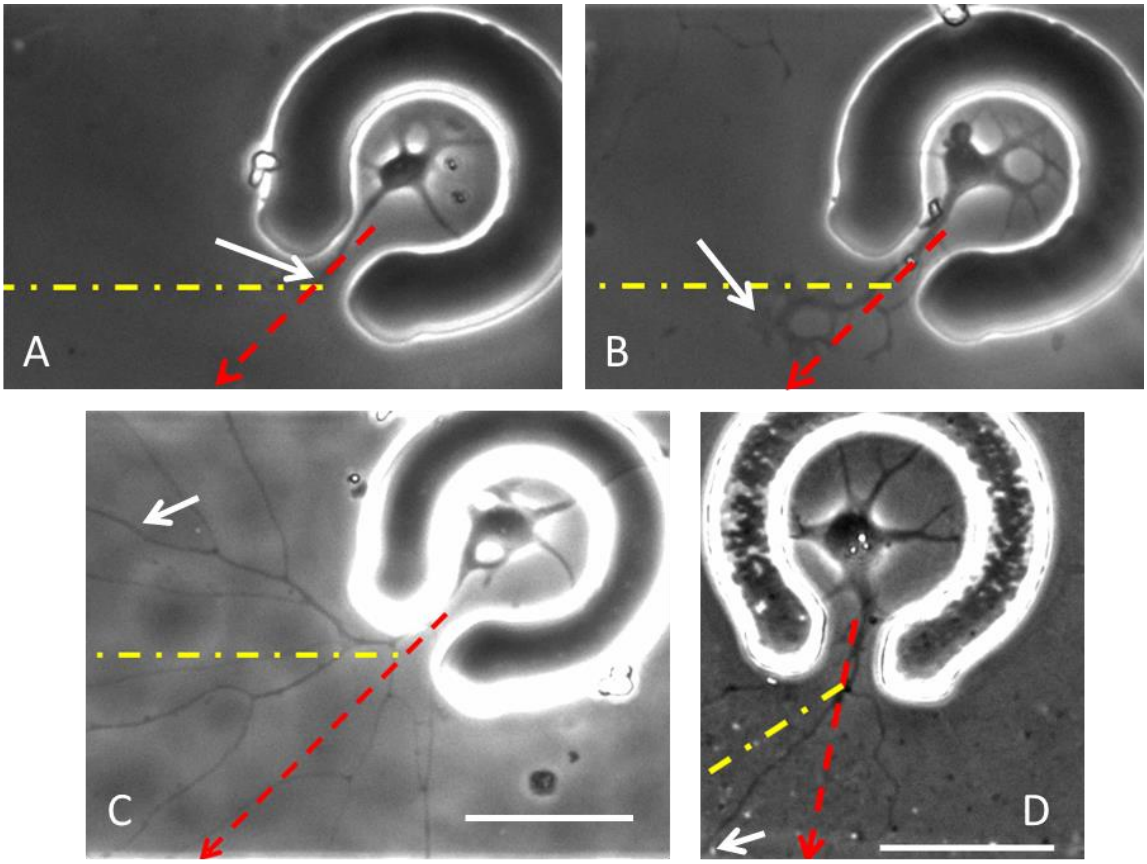

Figure 6.9: Initial axonal pathfinding of individual neurons through and beyond a geometric microchannel constraint in response to a localized chemical signaling gradient placed at a 45° angle from the end of the microchannel. Images A and B represent the same neuron at 1 DIV (A) and 2 DIV (B), respectively. Images C and D represent the development of individual neurons after exposure to the chemical gradient for 3 DIV. Dashed yellow lines indicate the direction of the microfluidic source. Dashed red arrows represent a continuation of the channel orientation trajectory. White arrows point to the growth cone or longest neurite projection. Scale bar = 50 µm

There exist a larger percentage of axons (74.2%) that fall within the 0-30° group and a smaller percentage (6.5%) in the group for 60-90°. The percentage of axons (19.3%) that fall in the 30-60° group is not significantly different from the assumed distribution, which is also the case when there is no chemical guidance (28.4%). The average

extension angle at 20 μm beyond the end of the geometric guidance microchannel was 21.2 ± 18.1° (n = 31).

The biochip with the source placed at a 45° angle from the end of the geometric guidance microchannel also had significant differences in the percentage of axons extending in the 30-60° and 60-90° groups compared to the assumed distribution. Figure 6.9 displays different experimental turning responses for neurons extending an axon beyond the end of the geometric guidance microchannel at a 45° degree angle from the source. Figure 6.10 represents the developmental progression of an individual-neuron over the course of 4 days in culture. Figures 6.11 and 6.12 display the different experimental turning responses for axonal pathfinding when the chemical source placed at an angle of 45° from the end of the geometric guidance microchannel. Of the 39 axons monitored, 31 extended off the 0° orientation line in the direction of the source with an average angle of extension of 34.7 ± 16.5°. The 8 axons that extended away from the gradient had an average angle of extension of 17.8 ± 13.8°.

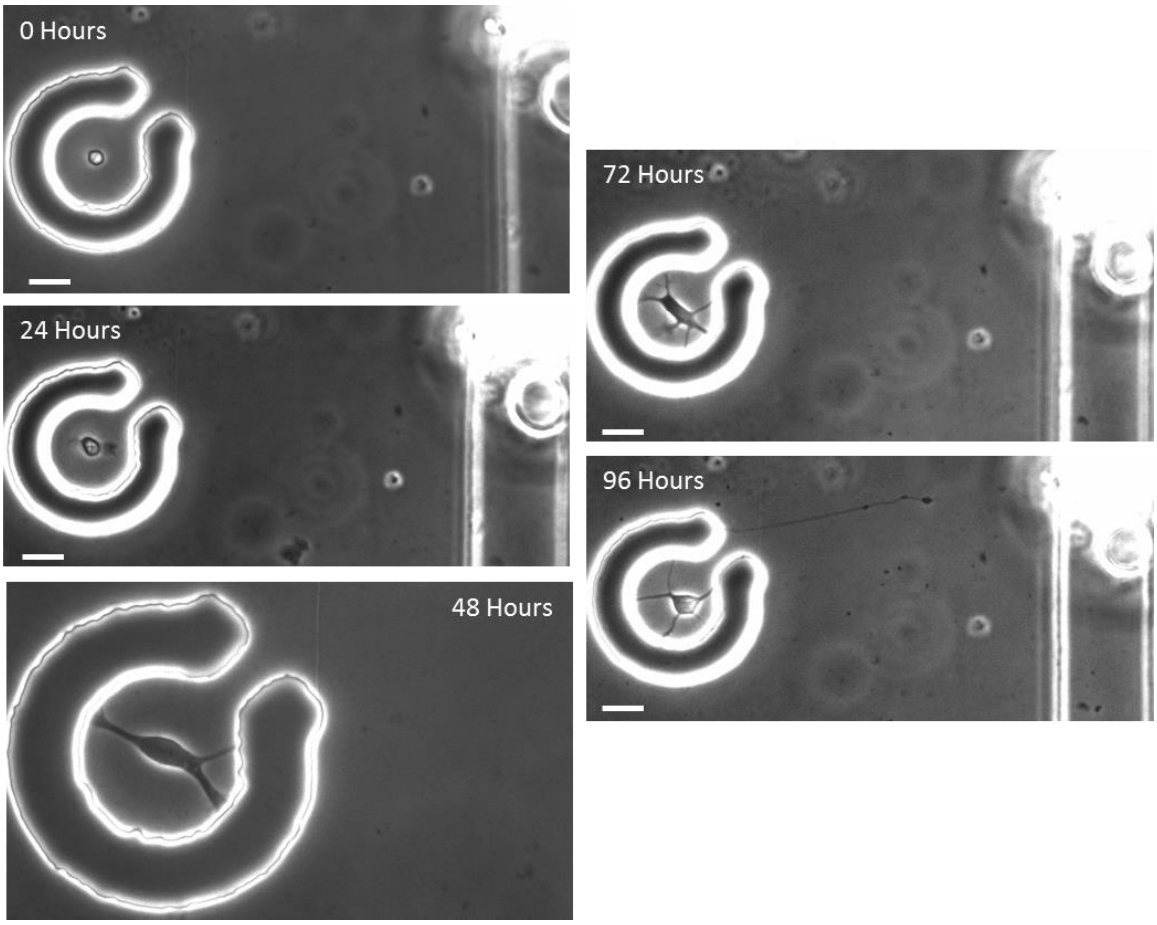

Figure 6.10: Developmental progression of an individual CFN laser cell-micropatterned into the structures of a biochip with the chemical source placed at a 45° angle from the outlet of the geometric guidance microchannel. Exposure to the chemical gradient lasted for a duration of 96 hours. Scale bars = 25 µm.

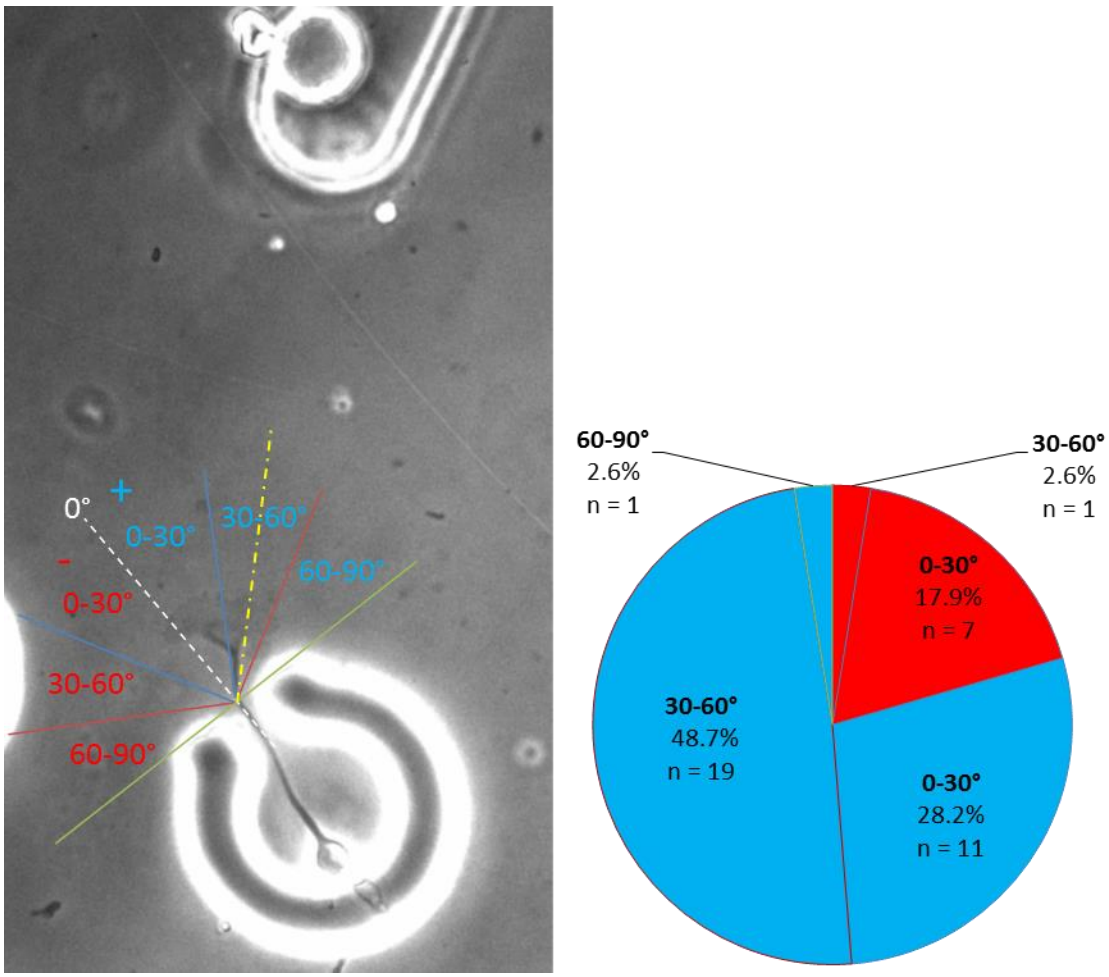

Figure 6.11: Left) Scoring paradigm for axonal pathfinding angular distributions for a biochip with the source placed at a 45° angle from the end of the geometric guidance microchannel. Growth cone turning towards the source (blue) is represented as a positive (+) angle. Growth cone turning away from the source (red) is represented as a negative (-) angle. Right) Pie chart representing the axonal pathfinding distributions for the different angular groups. Blue represents axonal turning towards the source and red represents axonal turning away from the source.

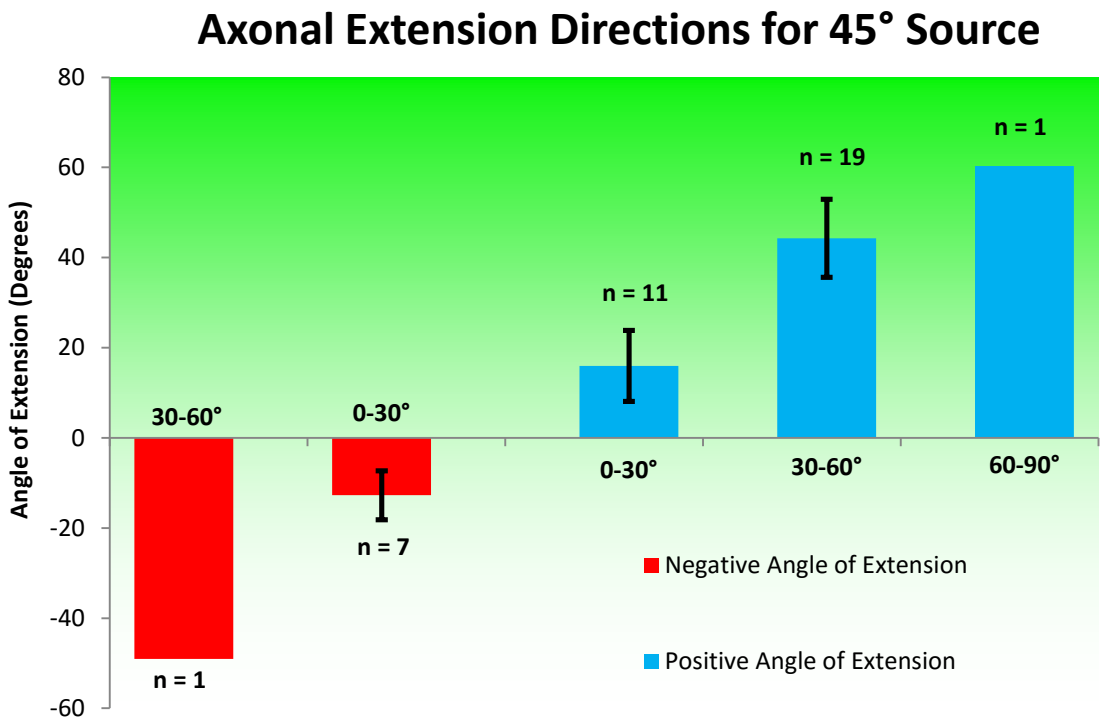

Figure 6.12: Angular extension directions beyond the end of the orientation microchannel for the 45° source. The bars in red represent axons extended in a direction away (negative) from the chemical guidance source while the bars in blue represent axons that extended towards (positive) the source.

6.5 Discussion

Effect of chemical gradient

The results for combined geometric and chemical guidance of axons indicate that the presence of a diffusible chemical gradient of conditioned media entices axonal pathfinding beyond the confines of the geometric guidance microchannel. We found that with the addition of a chemical guidance component (combined 0° source and 45° source) that out 175 pyramidal-like neurons monitored, 39.5 ± 13.8% extended an axon at least 20 µm beyond the end of the geometric guidance microchannel; compared to

10.3 ± 5.7% of neurons in the case of solely geometric guidance. Additionally, for geometric guidance only, 10 of the 67 axons observed stayed in contact with the wall of the microstructure when crossing the 20 µm threshold while 0 of the 70 axons (n = 31 for 0° and n = 39 for 45°) for the chemical guidance system adhered to the wall. This implies that the chemical guidance has a preferential effect for the axon to probe and explore the area away from the wall. Thus, when the chemical guidance source is placed in proximity (< 200 µm) with the geometric guidance microchannel, there appears to be a combinatorial effect that inhibits abrupt changes in axonal extension (such as a 90° turn) within 20 µm immediately beyond the confinement structure.

An axon turning scenario is created when the source is placed at a 45° angle relative to the axis of the geometric guidance microchannel. We found that the axons of 31 out of 39 pyramidal-like neurons extended beyond the end of the geometric guidance microchannel in the direction of the source (denoted as positive turning) — with an average angle of extension of 34.7 ± 16.6°. When compared to other similar growth cone turning assays we see that the average turning angle over a distance of approximately 20 µm yields similar results. Lohof [130] and Zheng [238] used micropipettes filled with chemical guidance solutions to influence the growth cones of embryonic *Xenopus* spinal cord neurons for a signaling period of 2 hours. Lohof using dibutryl cAMP (20 mM) found an average growth cone turning angle towards the source of 29.1 ± 4.9° with an extension rate for the signaling period of 19.1 ± 2.2 µm. Similarly, Zheng observed that the neurotransmitter acetylcholine (100 mM) would elicit an average turning angle towards the source of 21.0 ± 3.8° with an average extension of 25.2 ± 2.9 µm. In response to a netrin-1 gradient for one hour, de la Torre observed that 12 of 15 growth cones of *Xenopus* retinal ganglion cells grew towards the source with an average turning

angle of 18.6 ± 6.7° and an extension rate of 19.2 ± 3.4 μm/hr. Upon repositioning the micropipette, they found that the growth cone would continue turning towards the source indicating that the receptor mechanisms in the growth cone are able to detect dynamic changes in the extracellular environment.

We observed what can be interpreted as chemical guidance beyond the end of the geometric guidance microchannel; however, the strength of the effect remains unknown. For the 45° orientation biochip we observed that the largest proportion of axons fall into 30-60° angular extension range, as was expected if there was a chemical guidance effect. Although our guidance solution consisted of conditioned media with unknown molecular components, we can be reasonably assured that the concentrations at which they are present should be biologically relevant, thus potentially eliminating the possibility of saturating the growth cone receptors to guidance molecules, both attractive and repulsive. Despite not knowing which neurons are being targeted by what molecules, we can observe the effects of the guidance solution on particular morphological cell types. The experimental results presented here are only for pyramidal-like neurons; however, any cell type that is laser-patterned can be studied. This allows us to categorize specific cell types that respond to the chemical gradient and monitor their behavior.

A possible explanation for why the axons of the 45° chemical guidance system, on average did not completely turn 45°, is that the walls of the confinement microwell and geometric guidance microchannel perturb the distribution of the chemical guidance solution. This could initially disrupt the spatial chemical gradient within a certain distance from end of the geometric guidance microchannel (<10 μm), preventing any initial guidance effects. It may also be the case that there is chemical signaling that is being

recognized; however, the typical expansion of the growth cone to detect the spatial gradient may be inhibited by the walls of the microchannel. This latter scenario was studied by Francisco et al., where they observed that when growth cones interact with geometric constraints, such as a microchannel wall, a decrease in surface area occurs [64].This would effectually prevent any growth cone reorientation until a sufficient distance has been achieved where expansion is no longer inhibited and the localized environment can more appropriately be probed. In both Figures 6.8 and 6.9 it can be seen that there is an expansion of the growth cone in response to the chemical gradient for cells of different morphology. It can be seen that this expansion occurs at a sufficient distance beyond the end of the geometric guidance microchannel, while there is no significant expansion within the microchannel. Therefore, the reduction in growth cone area in proximity to the geometric guidance microchannel wall may be responsible for initial desensitization to the chemical gradient.

Summary

In this work we were able to construct a biochip capable of recreating a pioneer-neuron axonal pathfinding event *in* vitro using geometric and chemical guidance to influence the growth cone of an extending axon. Using this system we were able to show that the initial pathfinding trajectory of an individual-neuron's axon beyond the confines of a geometric guidance microchannel can be influenced by a localized chemical gradient. Because of the developmental heterogeneity of individual-neurons placed into the cell confinement microwell, axonal development will proceed at different rates. The ability to passively generate a spatial chemical gradient allows for long term (up to 1 day) continual signaling of isolated individual-neurons which will ensure the presence of chemical influence upon axonal extension beyond the end of a geometric guidance

microchannel. Daily removal and replenishment of the surrounding culture media allows for reestablishment of the gradient without reaching saturation. We observed that substrate geometry for individual compartmentalized neurons plays an important role in the *in vitro* development of an exploratory axon. Taken altogether, the system described herein has the potential to be used as a tool to systematically evaluate various chemical guidance molecules with high repeatability. In addition, we have created a platform for which we can test the developmental neurotoxicity to individual-neurons that various chemicals may have with regards to interruption of diffusible molecule signaling.

CHAPTER VII
CONCLUSIONS AND RECOMMENDATIONS

The ideas and work presented in Chapters I-VI describes the value and implementation of an *in vitro* model for pioneer-neuron axonal pathfinding with combined geometric and chemical guidance. Understanding how axonal pathfinding responds to a change in the local physical and chemical environment has the potential to enable the use of this fundamental biological event of the nervous system for the development of an effective tool for evaluating the developmental neurotoxicity of chemical agents. To achieve single-neuron resolution, we developed a model to be used in conjunction with a laser cell-micropatterning system [56]; determined what we believe to the optimal conditions for promotion of axonal extension from an isolated individual-neuron cultured on a PDMS substrate with a particular geometry; and created a complete system that provides chemical signaling in the form of a continuous gradient to influence axonal pathfinding beyond the confinements of an orientating geometric guidance microchannel.

To increase the efficiency of laser cell-micropatterning, we created a removable biochip system that can be placed directly on top of a cell-culture substrate. Cells are continually introduced to the culture environment at sufficient distances (>1 mm) from a target area on the culture substrate in a manner that allows for rapid identification and placement at a desired location. Multiple cell types can be simultaneously positioned with micron-level accuracy to create two-dimensional and three-dimensional co-cultures. To address the limitation in the application of laser cell-micropatterning stemming from the use of a single Gaussian beam, current work has shown the potential of using spatial light modulators in splitting a single beam into multiple beams with defined spatial

orientation and geometric patterns for positioning multiple cells simultaneously. This would substantially increase the efficiency of laser cell-micropatterning, allowing more cells to be strategically placed in a shorter period of time.

A common experiment that is performed involves placing neuron cell explants or high density neuronal cell suspensions (cell body compartment) in proximity to a microchannel system that is connected to an adjacent compartment (axon compartment) [103, 196, 209]. Chemical signaling in the axon compartment is often employed via diffusible or substrate-bound molecular gradients to influence axonal pathfinding. These systems are great tools to study axon elongation and growth cone turning; however, they cannot be used to monitor single-cell responses. With the laser cell-micropatterning system and cell-delivery biochip that we have developed, individual-neurons can be placed at any distance from the microchannels connecting both compartments and thus the fidelity of individual axonal pathfinding can be observed. Models following this paradigm have the potential to be used for testing neurotoxic effects of chemicals at extremely low doses (~10 nM) isolated to either the axon or cell body compartments, as well as, investigating certain neuroregenerative effects of biological and synthesized chemicals.

The chemical signaling system employed in this work allows for the passive continuous release of chemokines into the cell-culture area. While this greatly reduces the complexity of the system, it also limits its capabilities. We employ a single channel single thru-hole system to influence up to 10 neurons simultaneously. Given that approximately 60% of neurons placed into the confinements of the PDMS substrate will survive for the duration of the experiment, we quickly find that scaling up the number of cells laser-patterned is necessary. Therefore, we must design a more sophisticated

system that allows for multiple (up to 100x) signaling configurations to generate larger data sets. To do this, each signaling unit should be equipped with a microvalve to limit the amount of chemical guidance molecule locally administered. This would be in a fashion similar to that of the micropipette experiment except that there would be minimal dilution of the guidance chemical administered due to physical separation that diffusive mixing. There are currently many different microfluidic systems that employ pneumatic microvalves to limit microfluidic flow [157]. To accomplish this, the complexity of the system must be drastically increased to accommodate applied pressures and timing of pulses to prevent overlap of localized chemical gradients. With added complexity there come increased complications for cell-culture and imaging.

Moving forward, it is my opinion that chemical signaling of axonal growth cones due to gradients will be dominated by defined microfluidic systems involving a chemical source and sink [17]. Because mixing in a microchannel occurs via diffusion, stable defined chemical gradients can be generated. The shapes of the gradients can be artfully designed to evoke a range of growth cone responses [222]. Recently, a passive gradient generator was devised that could influence the axons extending through microchannels from a cell body compartment to an axonal compartment where they were subjected to a chemical gradient [209]. In this work they were able to show that they could minimize the effects of fluid stress on the axons caused by flow, and thus, elicit a pure growth cone turning response due to the chemical gradient. Again, however, these systems still lack the ability to isolate the response of an individual-neuron's axon without interactions with any other cells. It is my belief that using the cell micropatterning system in conjunction with a similar system as just described, large volumes of

information can be obtained for the growth cone response of different neuronal species and cell types.

Another area of ambiguity for *in vitro* neurotoxicity testing models involves the use of multiple species and cell types. The use of primary cell-cultures is beneficial in that they are derived directly from the native tissue. Unfortunately, there still often exists heterogeneity of the cell-culture by cell type, morphology, electrophysiology, and by the type of neurotransmitter produced. The use of primary chick forebrain neurons in our current system suffers immensely from this lack of cellular control. Selecting a healthy viable cell from a heterogeneous cell suspension is rather difficult and is typically limited to the general size and shape as determined by the experimenter. To improve upon our current design, development of a label-free pre-sorting system should be incorporated to provide a selective screen [79]. Microfluidic cell sorting devices have shown the potential to separate cells from a suspension based on size [173]. Immortalized cell lines provide a uniform cell type; however, the mutations that make them immortal, whether natural or intentional, result in a cell type that may not be best suited for testing sensitivity to hazardous chemicals. The use of stem cells and neuroblasts is the logical direction that both *in vitro* and *in vivo* experiments are headed. The ideal cell type for study will be of human origin with the ability to differentiate into a specific cell type for study. This would allow for reduction in the use of animal models while improving the understanding of the effects chemical toxicants may have on specific developmental processes, such as pioneer-neuron axonal pathfinding.

Using the tools and techniques described in the work, we have the potential to create defined neural circuitry. Geometric and chemical guidance of axons to a common target can allow for the interconnection of multiple cell types to create sophisticated

neural networks. If we couple this with the ability to record electrical activity of individual cells, this would add another dimension to which neuronal activities could be monitored. Specific cause and response relationships could be observed for electrical stimulation of one neuron on the rest of the network. Repeated patterns of electrical stimuli could result in “conditioning” of the network in a way that elicits a predictable response. Using this, it is possible to then undergo neurotoxicity testing on the functioning of the defined neural circuit.

Looking to the future, it is clear that there is a need for more tools to be added to a systematically agreed upon approach for more robust assessment of chemical-induced developmental neurotoxicity. We chose to investigate the pathfinding activity of an individual-neuron in response to a “choice point” where physical geometric guidance was replaced by chemical means. There still remains much to be understood about the effects that geometric environment has on the development on an individual-neuron, as well as, understanding the growth cone response to various chemical guidance molecules when in conjunction with different geometries. Further knowledge will enable this system to be used as a tool to evaluate subtle behavioral responses that could result in abnormal development.

APPENDIX
CELL-CULTURE TECHNIQUES

Cell-culture media

Multiple media formulations were employed throughout this work to provide nutrients and growth factors in order to maintain cell viability at the single-cell level. Altogether, there were three main concoctions devised to increase the chances of survival for a single-neuron on PDMS substrate environments: laser patterning media, neuron culture media, and conditioned media. Laser patterning media consisted of a Leibovitz's L-15 medium without phenol red as the base with it being supplemented with:

- 10,000 units/mL penicillin G sodium
- 10,000 µg/mL streptomycin sulfate
- 10% v/v fetal bovine serum (FBS)
- 2% v/v B-27®

L-15 medium was chosen as the base due to the pH buffering system. Unlike many other media which use sodium bicarbonate to regulate pH, L-15 is buffered by phosphates and free base amino acids and does not require regulated CO_2 environments. This was advantageous because laser patterning experiments require dissociated neuronal suspensions to be outside of an incubated environment for periods of up to 4 hours. Also, by using a media without phenol red, we were able to reduce the amount of laser light (800 nm) absorbed; this lead to a decrease in thermal fluctuations and an increase in laser patterning efficiency.

Neuron culture media consisted of Medium 199 with glutamine and phenol red and was supplemented with:

- 10,000 units/mL penicillin G sodium
- 10,000 µg/mL streptomycin sulfate
- 10% v/v fetal bovine serum (FBS)
- 2% v/v B-27®
- 100 ng/mL NGF 7S

Medium 199 was originally developed for nutritional studies of chick embryo fibroblasts, which is why it was used as the base for chick forebrain neuron cell-culture. It should be noted here that special attention must be paid to the buffering mechanisms employed for different media formulations. Media utilizing Earle's salts are buffered with bicarbonate/carbonic acid systems and must be maintained in a CO_2 incubator to maintain proper pH; otherwise, in atmospheric conditions the media will see a rise in pH. Solutions buffered with Hank's salts are designed for atmospheric conditions and should not be used in a CO_2 incubator. Use of a Hank's salts media in an incubator will result in a rapid drop in pH, which will cause harm to the cell-culture. Finally, if extended periods of cell-culture are required outside of an incubator environment, (4-(2-hydroxyethyl)-1-piperazineethanesulfonic acid) HEPES can be added to media to provide an extra buffering capacity between a pH of 7.2 through 7.6. When using HEPES care must be taken to limit exposure to ambient light because there is evidence of phototoxicity from the production of hydrogen peroxide [129].

In the CNS, conditioned media has been shown to increase the survival of cells over non-conditioned media and promote long axonal extensions of hippocampal and cortical neurons [233]. In the peripheral nervous system, conditioned media was able to

support chick sympathetic and rat dorsal root ganglia (DRG) neurons with the same effectiveness as media supplemented with mouse submaxillary NGF [218]. In addition to use as a primary cell source for biological experiments, co-culture of neuron and glial cells from E10 chick forebrain hemispheres were used to condition media. Conditioned media is media that has been used to support a culture environment where secreted trophic factors and signaling molecules, as well as, waste products accumulate. Because we are working with isolated individual-neurons, we were interested in testing the efficacy of conditioned medium with regards to single-cell signaling (discussed in detail in Chapter 6).Conditioned media was generated by plating 1 million neurons in 35 mm petri dishes treated with 100 µg/mL PLL and adding 2.5 mL of regular culture media. Media was completely changed daily disposed of until 3 DIV. Subsequent media changes involved saving and filtering the used media up to 7DIV. Once all conditioned media was collected it was mixed together and used in chemical signaling experiments.

Primary cell isolation: Chick forebrain neurons

Primary CFNs were harvested from the frontal lobes of day 8 embryonic white leghorn chicks. Fertilized eggs were obtained from the Charles Lee Morgan Poultry Center in the morning and placed directly into a Styrofoam HovaBator™ equipped with an automatic egg rotator and air circulation fan. The incubation environment was maintained at 37°C and 100 mL of deionized water was added to the bottom bi-daily to maintain a humidified atmosphere. On day 8, the eggs were removed and liberally sprayed with 70% ethanol and placed into a sterile dissection hood. After the ethanol had evaporated, the top of the egg was cracked with the blunt end of large forceps and the embryo was removed. The embryo was placed in to a 35 mm dish containing a ~2 mL of Hank's Balanced Salt Solution (HBSS) without calcium, magnesium, and phenol

red. The embryo was decapitated near the trunk and the head was placed into another 35 mm dish containing a similar volume of HBSS. Using Dumont #5 forceps, the head was rotated to position the beak facing down with the midbrain and forebrain facing up. Carefully, the #5 forceps were used to cut/pinch the overlying membrane around the perimeter of the forebrain; from the midline rostral position traveling laterally and caudally along the edge of the eye, then moving medially to the posterior position of the left-to-right brain fissure separating the two forebrain hemispheres form the midbrain. This process is repeated around the other lobe until both hemispheres can be removed intact. Using a scooping motion, the lobes are transferred to another 35 mm dish for separation and removal of the meninges. Under a dissection microscope, the meninges are easily removed by grabbing onto a portion of the lateral edge and gently shaking the lobes until it pulls away, usually intact. After removal of the meninges, the forebrain tissue is transported to a 15 mL tube containing ~2 mL of the HBSS solution.

Upon transportation of the forebrain to a biological hood, the HBSS is removed and 1.5 mL of 0.25% Trypsin (Gibco®) is added to the tube. The contents are gently swirled to ensure all surfaces of the tissue have come in contact with the solution and then placed into an incubator (37°C, 95% RH, 5% CO_2) for 10 minutes. After 10 minutes, the Trypsin solution is carefully removed; paying close attention to not remove any tissue fragments, and 1 mL of laser patterning media with 10% serum was added to neutralize any remaining trypsin enzyme. The tissue was then triturated 5 to 6 times with a 1 mL plastic pipette tip, being careful not to introduce any air bubbles into the solution. The cell suspension was then centrifuged at 1000 RPM for 4 minutes. The supernatant was removed to eliminate cellular debris and 1 mL of fresh laser patterning media was added and the cells were re-suspended. This process was repeated again noting that the

second and third times the cells were triturated only 2 to 3 times to re-suspend in solution. Finally, the 20 µL of the cell suspension was removed and mixed with Trypan blue die then placed into a hemocytometer to be counted. At this point, the cells were ready to be plated or laser-patterned.

Primary cell isolation: Glial cells

According to Tsai, glial cells do not develop in the chick forebrain until day 10; therefore isolation of glial cells for certain experiments closely followed the protocol outlined by Kentroti [113, 213]. Glial cells were obtained from day 10 embryonic chick cerebral hemispheres. As previously described, eggs were wiped with 70% ethanol and placed into a dissection hood. The top of the egg was removed and the embryo was extracted and placed into a 60 mm dish containing HBSS without calcium, magnesium, and phenol red. The embryo was decapitated with the aid of scissors. The head was then placed into a new 60 mm dish. To isolate the cerebral hemispheres, first the inchoate skull plate has to be removed. After that, the cerebral hemispheres were removed in a similar fashion as that for the day 8 forebrain and placed into a 15 mL tube containing HBSS. The HBSS was removed and 2 mL of 0.25% Trypsin was added and then incubated (37°C, 95% RH, 5% CO_2) for 10 minutes. After incubation, 2 mL of glial media was added and the cells were suspended via trituration. Due to the size and integrity of the cerebral hemispheres at this stage, the tissue was further mechanically dissociated by sieving through a nylon mesh (70 µm pore diameter) into a 50 mL centrifuge tube. The cell suspension was centrifuged one time at 1000 RPM for 4 minutes, followed by removal of the supernatant re-suspension in glial media. The cell suspension (~10 mL) was counted plated into a T75 culture flask and allowed to culture at standard incubation conditions (37°C, 95% RH, 5% CO_2).

After 24 hours, only a small percentage of cells attached to the plastic culture flask. Until the cells reach confluence, the media was changed with 10 mL of fresh glial media (Medium 199 with 10% v/v FBS) being added every 3 days. Typically, by 7 days the culture had reached confluence and the cells were passaged. To passage the cells, first the glial media was removed and the cells were washed with PBS. The PBS was removed and then 5 mL of 0.25% Trypsin EDTA was added for 5 minutes to aid in the detachment of the cells from the culture flask. The Trypsin was neutralized with 5 mL of glial media and the suspension was transferred to a 50 mL tube were it was centrifuged at 1000 RPM for 4 minutes. The supernatant was removed and the cells were re-suspended in 10 mL of glial media. A small volume of cell suspension was removed and diluted for use in experiments while the remaining cells were re-plated in T50 culture flasks. The re-plated cells were used up until the fourth passage, by which the viability and activity begins to decline [210].

REFERENCES

1 Alom Ruiz S and Chen C S 2007 Microcontact printing: A tool to pattern *Soft Matter* **3** 168-77

2 Altschuler S J and Wu L F 2010 Cellular heterogeneity: Do differences make a difference? *Cell* **141** 559-63

3 Ashkin A 1970 Acceleration and trapping of particles by radiation pressure *Phys Rev Lett* **24** 156-59

4 Ashkin A 1997 Optical trapping and manipulation of neutral particles using lasers *PNAS* **94** 4853-60

5 Ashkin A 2000 History of optical trapping and manipulation of small-neutral particle, atoms, and molecules *Selected Topics in Quantum Electronics, IEEE Journal of* **6** 841-56

6 Ashkin A *et al* 1986 Observation of a single-beam gradient force optical trap for dielectric particles *Opt. Lett.* **11** 288-90

7 Baio J, Prevalence of autism spectrum disorder among children aged 8 years -- autism and developmental disabilities monitoring network, 11 sites, united states, 2010, Morbidity and Mortality Weekly Report Surveillance Summaries, Center for Disease Control and Prevention, 2014

8 Bakken D E *et al* 2005 Laser micropatterning of polylactide microspheres into neuronal-glial coculture for the study of axonal regeneration *Macromol. Symp.* **227** 335-44

9 Bal-Price A K *et al* 2010 In vitro developmental neurotoxicity (dnt) testing: Relevant models and endpoints *NeuroToxicology* **31** 545-54

10 Banker G and Goslin K 1998 Culturing nerve cells

11 Banker G A and Cowan W M 1977 Rat hippocampal neurons in dispersed cell culture *Brain Research* **126** 397

12 Barron J A *et al* 2005 Laser printing of single cells: Statistical analysis, cell viability, and stress *Ann. Biomed. Eng.* **33** 121-30

13 Beebe D J *et al* 2002 Physics and applications of microfluidics in biology *Annual review of biomedical engineering* **4** 261-86

14 Bellinger D *et al* 1987 Longitudinal analyses of prenatal and postnatal lead exposure and early cognitive development *N Engl J Med* **316** 1037-43

15 Bernard S *et al* 2001 Autism: A novel form of mercury poisoning *Med Hypotheses* **56** 462-71

16 Bhatia S N *et al* 1997 Controlling cell interactions by micropatterning in co-cultures: Hepatocytes and 3t3 fibroblasts *J. Biomed. Mater. Res.* **34** 189-99

17 Bhattacharjee N *et al* 2010 A neuron-benign microfluidic gradient generator for studying the response of mammalian neurons towards axon guidance factors *Integrative Biology* **2** 669-79

18 Bischoff R 1997 Chemotaxis of skeletal muscle satellite cells *Developmental dynamics* **208** 505-15

19 Bodas D and Khan-Malek C 2006 Formation of more stable hydrophilic surfaces of pdms by plasma and chemical treatments *Microelectron Eng* **83** 1277-79

20 Boland T *et al* 2006 Application of inkjet printing to tissue engineering *Biotechnol. J.*, Vol. **1** 910-17

21 Boyden S 1962 The chemotactic effect of mixtures of antibody and antigen on polymorphonuclear leucocytes *J Exp Med* **115** 453-66

22 Boyes W K *et al* 1998 Epa's neurotoxicity risk assessment guidelines *Fundam Appl Toxicol* **40** 175-84

23 Breier J M *et al* 2010 Neural progenitor cells as models for high-throughput screens of developmental neurotoxicity: State of the science *Neurotoxicology and Teratology* **32** 4-15

24 Breier J M *et al* 2008 Development of a high-throughput screening assay for chemical effects on proliferation and viability of immortalized human neural progenitor cells *Toxicological Sciences* **105** 119-33

25 Bressler J *et al* 1999 Molecular mechanisms of lead neurotoxicity *Neurochem. Res.* **24** 595-600

26 Brewer G J and Cotman C W 1989 Survival and growth of hippocampal neurons in defined medium at low density: Advantages of a sandwich culture technique or low oxygen *Brain Research* **494** 65-74

27 Bull R J *et al* 1983 The effects of lead on the developing central nervous system of the rat *NeuroToxicology* **4** 1-17

28 Burden-Gulley S M *et al* 1997 The role of cell adhesion molecule l1 in axonal extension, growth cone motility, and signal transduction *Cell Tissue Res* **290** 415-22

29 Burke K *et al* 2006 Methylmercury elicits rapid inhibition of cell proliferation in the developing brain and decreases cell cycle regulator, cyclin e *NeuroToxicology* **27** 970-81

30 Canfield R *et al* 2003 Intellectual impairment in children with blood lead concentrations below 10 µg per deciliter *N Engl J Med* **348** 1517-26

31 Cannon J R and Timothy Greenamyre J 2011 The role of environmental exposures in neurodegeneration and neurodegenerative diseases *Toxicological Sciences*

32 Chada S *et al* 1997 Cytomechanics of neurite outgrowth from chick brain neurons *J. Cell. Sci.* **110** 1179-86

33 Charach A *et al* 2011 Attention deficit hyperactivity disorder

34 Chedotal A *et al* 1998 Semaphorins iii and iv repel hippocampal axons via two distinct receptors *Development (Cambridge, England)* **125** 4313-23

35 Chédotal A and Richards L J 2010 Wiring the brain: The biology of neuronal guidance *Cold Spring Harb Perspect Biol* **2**

36 Chen H-C 2005 Boyden chamber assay *Cell migration* 15-22

37 Chilton J K 2006 Molecular mechanisms of axon guidance *Dev Biol* **292** 13-24

38 Chu S *et al* 1986 Experimental observation of optically trapped atoms *Phys Rev Lett* **57** 314

39 Chung B G and Choo J 2010 Microfluidic gradient platforms for controlling cellular behavior *Electrophoresis* **31** 3014-27

40 Coecke S *et al* 2007 Workgroup report: Incorporating in vitro alternative methods for developmental neurotoxicity into international hazard and risk assessment strategies *Environ Health Perspect* **115** 924-31

41 Costa L G *et al* 2004 Developmental neuropathology of environmental agents *Annual Review of Pharmacology and Toxicology* **44** 87-110

42 Costa L G *et al* 2007 An in vitro approach to assess the toxicity of certain food contaminants: Methylmercury and polychlorinated biphenyls *Toxicology* **237** 65-76

43 Craig A M and Banker G 1994 Neuronal polarity *Annu Rev Neurosci* **17** 267-310

44 Crofton K M *et al* 2011 Developmental neurotoxicity testing: Recommendations for developing alternative methods for the screening and prioritization of chemicals *ALTEX* **28** 9-15

45 Curtis A and Wilkinson C 1997 Topographical control of cells *Biomaterials* **18** 1573-83

46 De Silva M N *et al* 2004 Micro-patterning of animal cells on pdms substrates in the presence of serum without use of adhesion inhibitors *Biomed. Microdevices* **6** 219-22

47 De Silva M N *et al* 2006 Two-step cell patterning on planar and complex curved surfaces by precision spraying of polymers *Biotechnol. Bioeng.* **93** 919-27

48 Desai R A *et al* 2009 Cell polarity triggered by cell-cell adhesion via e-cadherin *J. Cell. Sci.* **122** 905-11

49 Di Carlo D *et al* 2006 Single-cell enzyme concentrations, kinetics, and inhibition analysis using high-density hydrodynamic cell isolation arrays *Anal. Chem.* **78** 4925-30

50 Di Carlo D *et al* 2006 Dynamic single cell culture array *Lab on a Chip* **6** 1445-49

51 Disablilites N C o B D a D and Prevention C F D C a, Fetal alcohol syndrome: Guidelines for referral and diagnosis, Department of Health and Human Services, 2004

52 Dorea J G *et al* 2013 Toxicity of ethylmercury (and thimerosal): A comparison with methylmercury *J Appl Toxicol* **33** 700-11

53 Dotti C *et al* 1988 The establishment of polarity by hippocampal neurons in culture *J. Neurosci.* **8** 1454-68

54 Dowell-Mesfin N *et al* 2004 Topographically modified surfaces affect orientation and growth of hippocampal neurons *J Neural Eng* **1** 78

55 Easter S S, Jr. *et al* 1994 Initial tract formation in the vertebrate brain *Prog Brain Res* **102** 79-93

56 Erdman N *et al* 2014 Microfluidics-based laser cell-micropatterning system *Biofabrication* **6** 035025

57 Faenza A *et al* 2013 High yield patterning of single cells from extremely small populations *Anal. Chem.* **85** 3446-53

58 Faissner A 2009 Axon guidance by glia *Encyclopedia of neuroscience* 1063-72

59 Farina M *et al* 2011 Mechanisms of methylmercury-induced neurotoxicity: Evidence from experimental studies *Life Sciences* **89** 555-63

60 Felton E J *et al* 2012 Heterotypic cell pair co-culturing on patterned microarrays *Lab on a Chip* **12** 3117-26

61 Finkelstein Y *et al* 1998 Low-level lead-induced neurotoxicity in children: An update on central nervous system effects *Brain research. Brain research reviews* **27** 168-76

62 Forcelli P A *et al* 2012 Neonatal exposure to antiepileptic drugs disrupts striatal synaptic development *Ann Neurol* **72** 363-72

63 Fournier R L 2011 Basic transport phenomena in biomedical engineering

64 Francisco H *et al* 2007 Regulation of axon guidance and extension by three-dimensional constraints *Biomaterials* **28** 3398-407

65 Franco S J and Müller U 2011 Ecm functions during neuronal migration and lamination in the mammalian central nervous system *Dev Neurobiol* **71** 889-900

66 Fricke R *et al* 2011 Axon guidance of rat cortical neurons by microcontact printed gradients *Biomaterials* **32** 2070-76

67 Frimat J-P *et al* 2011 A microfluidic array with cellular valving for single cell co-culture *Lab on a Chip* **11** 231-37

68 Gallo G and Letourneau P C 1999 Axon guidance: A balance of signals sets axons on the right track *Current biology : CB* **9** R490-2

69 Ganz M L 2007 The lifetime distribution of the incremental societal costs of autism *Archives of Pediatrics & Adolescent Medicine* **161** 343-49

70 Gibson J L 1904 A plea for painted railing and painted walls of rooms as the source of lead poisoning among queensland children *Australasian Medical Gazette* **23** 149-53

71 Giordano G and Costa L G 2012 Developmental neurotoxicity: Some old and new issues *ISRN Toxicology* **2012** 12

72 Goldberg J L 2003 How does an axon grow? *Genes Dev* **17** 941-58

73 Gomez N *et al* 2007 Polarization of hippocampal neurons with competitive surface stimuli: Contact guidance cues are preferred over chemical ligands *J R Soc Interface* **4** 223-33

74 Goodhill G J 1997 Diffusion in axon guidance *European Journal of Neuroscience* **9** 1414-21

75 Goodhill G J 1998 A mathematical model of axon guidance by diffusible factors *Advances in Neural Information Processing Systems* 159-65

76 Goodhill G J and Urbach J S 1999 Theoretical analysis of gradient detection by growth cones *J Neurobiol* **41** 230-41

77 Goodman C S and Shatz C J 1993 Developmental mechanisms that generate precise patterns of neuronal connectivity *Cell* **72 Suppl** 77-98

78 Gossett D *et al* 2011 Sequential array cytometry: Multi-parameter imaging with a single fluorescent channel *Ann. Biomed. Eng.* **39** 1328-34

79 Gossett D R *et al* 2010 Label-free cell separation and sorting in microfluidic systems *Anal Bioanal Chem* **397** 3249-67

80 Grandjean P and Landrigan P J 2006 Developmental neurotoxicity of industrial chemicals *Lancet* **368** 2167-78

81 Grandjean P and Landrigan P J 2014 Neurobehavioural effects of developmental toxicity *The Lancet Neurology* **13** 330-38

82 Grandjean P *et al* 2010 Adverse effects of methylmercury: Environmental health research implications *Environ Health Perspect* **118** 1137-45

83 Guduru S K *et al* 2005 Analysis of neurite outgrowth for a laser patterned neuronal culture *2nd International IEEE EMBS Conference on Neural Engineering* 336-39

84 Guilak F *et al* 2009 Control of stem cell fate by physical interactions with the extracellular matrix *Cell Stem Cell* **5** 17-26

85 Gundersen R W and Barrett J N 1979 Neuronal chemotaxis: Chick dorsal-root axons turn toward high concentrations of nerve growth factor *Science* **206** 1079-80

86 Gundersen R W and Barrett J N 1980 Characterization of the turning response of dorsal root neurites toward nerve growth factor *J Cell Biol* **87** 546-54

87 Hammarback J A *et al* 1988 Growth cone guidance by substrate-bound laminin pathways is correlated with neuron-to-pathway adhesivity *Dev Biol* **126** 29-39

88 Hanson J N *et al* 2008 Textural guidance cues for controlling process outgrowth of mammalian neurons *Lab Chip* **9** 122-31

89 Haubert K *et al* 2006 Pdms bonding by means of a portable, low-cost corona system *Lab on a Chip* **6** 1548-49

90 He W and Bellamkonda R V 2005 Nanoscale neuro-integrative coatings for neural implants *Biomaterials* **26** 2983-90

91 Heidemann S R *et al* 2001 Inhibition of axonal morphogenesis by nonlethal, submicromolar concentrations of methylmercury *Toxicology and Applied Pharmacology* **174** 49-59

92 Heidemann S R *et al* 2003 The culture of chick forebrain neurons *Neurons: Methods and Applications for the Cell Biologist* **71** 51-65

93 Herbert M R 2010 Contributions of the environment and environmentally vulnerable physiology to autism spectrum disorders *Curr Opin Neurol* **23** 103-10

94 Hill E J *et al* 2008 Differentiating human nt2/d1 neurospheres as a versatile in vitro 3d model system for developmental neurotoxicity testing *Toxicology* **249** 243-50

95 Hirata T 2009 Axon outgrowth *Encyclopedia of neuroscience* 311-13

96 Hodgkin A L and Huxley A F 1952 A quantitative description of membrane current and its application to conduction and excitation in nerve *J Physiol* **117** 500-44

97 Högberg H 2009 The Wenner-Gren Institute, Stockholm University

98 Hopker V H *et al* 1999 Growth-cone attraction to netrin-1 is converted to repulsion by laminin-1 *Nature* **401** 69-73

99 Hortsch M 1996 The l1 family of neural cell adhesion molecules: Old proteins performing new tricks *Neuron* **17** 587-93

100 Hsiao A P *et al* 2010 Microfluidic device for capture and isolation of single cells *Proc. Soc. Photo Opt. Instrum. Eng.* **7759** 77590W-90W-9

101 Hu Q *et al* 2011 Low-level lead exposure attenuates the expression of three major isoforms of neural cell adhesion molecule *NeuroToxicology* **32** 255-60

102 Huang F and Schneider J S 2004 Effects of lead exposure on proliferation and differentiation of neural stem cells derived from different regions of embryonic rat brain *NeuroToxicology* **25** 1001-12

103 Huang T *et al* 2015 Development of a compartmentalized biochip for axonal isolation and neuronal-circuit formation at the single-cell level 83-104

104 Ino K *et al* 2008 Cell culture arrays using magnetic force-based cell patterning for dynamic single cell analysis *Lab on a Chip* **8** 134-42

105 Jarvis E D *et al* 2005 Avian brains and a new understanding of vertebrate brain evolution *Nat Rev Neurosci* **6** 151-59

106 Jiayi Zhang S V, Heng Xu, Yoon-Kyu Song, Hyun-Kon Song, G. Tayhas R. Palmore, Justin Fallon, Arto V. Nurmikko 2006 Combined topographical and chemical micropatterns for templating neuronal networks *Biomaterials* **27** 5734

107 Jones K and Smith D 1973 Recognition of the fetal alcohol syndrome in early infancy *The Lancet* **302** 999-1001

108 Jurewicz J *et al* 2013 Chemical exposure early in life and the neurodevelopment of children–an overview of current epidemiological evidence *Annals of agricultural and environmental medicine* **20**

109 Jusko T a *et al* 2008 Blood lead concentrations < 10 microg/dl and child intelligence at 6 years of age *Environ Health Perspect* **116** 243-8

110 Kaech S and Banker G 2007 Culturing hippocampal neurons *Nat Protoc* **1** 2406-15

111 Kam L *et al* 2001 Axonal outgrowth of hippocampal neurons on micro-scale networks of polylysine-conjugated laminin *Biomaterials* **22** 1049-54

112 Kamiguchi H and Lemmon V 1997 Neural cell adhesion molecule l1: Signaling pathways and growth cone motility *J. Neurosci. Res.* **49** 1-8

113 Kentroti S and Vernadakis A 1997 Differential expression in glial cells derived from chick embryo cerebral hemispheres at an advanced stage of development *J. Neurosci. Res.* **47** 322-31

114 Khan S and Newaz G 2010 A comprehensive review of surface modification for neural cell adhesion and patterning *J Biomed Mater Res A* **93** 1209-24

115 Khetani S R and Bhatia S N 2008 Microscale culture of human liver cells for drug development *Nat. Biotechnol.* **26** 120-26

116 Kidd T *et al* Slit is the midline repellent for the robo receptor in drosophila *Cell* **96** 785-94

117 Kim S *et al* 2010 Biological applications of microfluidic gradient devices *Integrative Biology* **2** 584-603

118 Kuehn B M 2010 Increased risk of adhd associated with early exposure to pesticides, pcbs *Jama* **304** 27-28

119 Kulkarni R P *et al* 2007 Differences in protein mobility between pioneer versus follower growth cones *Proc Natl Acad Sci U S A* **104** 1207-12

120 Kumar A and Whitesides G M 1993 Features of gold having micrometer to centimeter dimensions can be formed through a combination of stamping with an elastomeric stamp and an alkanethiol "ink" followed by chemical etching *Appl. Phys. Lett.* **63** 2002-04

121 Landrigan P *et al* 1975 Neuropsychological dysfunction in children with chronic low-level lead absorption *The Lancet* **305** 708-12

122 Landrigan P J 2010 What causes autism? Exploring the environmental contribution *Current opinion in pediatrics* **22** 219-25

123 Landrigan P J *et al* 1976 Increased lead absorption with anemia and slowed nerve conduction in children near a lead smelter *J Pediatr* **89** 904-10

124 Landrigan P J *et al* 2012 A research strategy to discover the environmental causes of autism and neurodevelopmental disabilities *Environ Health Perspect* **120** a258-a60

125 Lanphear B P *et al* 2005 Low-level environmental lead exposure and children's intellectual function: An international pooled analysis *Environ Health Perspect* **113** 894-9

126 Lee J N *et al* 2003 Solvent compatibility of poly (dimethylsiloxane)-based microfluidic devices *Anal. Chem.* **75** 6544-54

127 Lein P *et al* 2005 In vitro and other alternative approaches to developmental neurotoxicity testing (dnt) *Environ Toxicol Pharmacol* **19** 735-44

128 Leonardo E D *et al* 1997 Guidance of developing axons by netrin-1 and its receptors *Cold Spring Harb Symp Quant Biol* **62** 467-78

129 Lepe-Zuniga J L *et al* 1987 Toxicity of light-exposed hepes media *J Immunol Methods* **103** 145

130 Lohof A M *et al* 1992 Asymmetric modulation of cytosolic camp activity induces growth cone turning *J Neurosci* **12** 1253-61

131 Lowery L A and Van Vactor D 2009 The trip of the tip: Understanding the growth cone machinery *Nat Rev Mol Cell Biol* **10** 332-43

132 Luckenbill-Edds L 1997 Laminin and the mechanism of neuronal outgrowth *Brain Res Rev* **23** 1-27

133 Ma Z *et al* 2011 Laser-guidance-based cell deposition microscope for heterotypic single-cell micropatterning *Biofabrication* **3** 034107

134 Ma Z *et al* 2010 Laser guidance-based cell micropatterning *Cell and organ printing* 137-59

135 MacLennan A J *et al* 1997 Immunohistochemical localization of netrin-1 in the embryonic chick nervous system *J. Neurosci.* **17** 5466-79

136 Mahoney M J *et al* 2005 The influence of microchannels on neurite growth and architecture *Biomaterials* **26** 771-78

137 Makris S L *et al* 2009 A retrospective performance assessment of the developmental neurotoxicity study in support of oecd test guideline 426 *Environ Health Perspect* **117** 17-25

138 Mark A E *et al* 2008 Determining the optimal pdms–pdms bonding technique for microfluidic devices *Journal of Micromechanics and Microengineering* **18** 067001

139 May D E and Kratochvil C J 2010 Attention-deficit hyperactivity disorder *Drugs* **70** 15-40

140 Mazia D *et al* 1975 Adhesion of cells to surfaces coated with polylysine. Applications to electron microscopy *J. Cell Biol.* **66** 198-200

141 McDonald J C and Whitesides G M 2002 Poly(dimethylsiloxane) as a material for fabricating microfluidic devices *Accounts of Chemical Research* **35** 491-99

142 Messersmith E K *et al* 1995 Semaphorin iii can function as a selective chemorepellent to pattern sensory projections in the spinal cord *Neuron* **14** 949-59

143 Meyer G *et al* 1999 Feature article: What is a cajal–retzius cell? A reassessment of a classical cell type based on recent observations in the developing neocortex *Cereb Cortex* **9** 765-75

144 Millet L J *et al* 2007 Microfluidic devices for culturing primary mammalian neurons at low densities *Lab on a Chip* **7** 987-94

145 Ming G-l *et al* 2002 Adaptation in the chemotactic guidance of nerve growth cones *Nature* **417** 411-18

146 Miodovnik A 2011 Environmental neurotoxicants and developing brain *Mt Sinai J Med* **78** 58-77

147 Mortimer D and Goodhill G J 2009 Axonal pathfinding *Encyclopedia of neuroscience* 1133-38

148 Mrksich M *et al* 1997 Using microcontact printing to pattern the attachment of mammalian cells to self-assembled monolayers of alkanethiolates on transparent films of gold and silver *Exp. Cell Res.* **235** 305-13

149 Naisberg Y *et al* 1996 Biophysical shunt theory for neuropsychopathology part ii: Neuronal network miswiring *Med Hypotheses* **46** 517-21

150 Nedergaard M *et al* 2003 New roles for astrocytes: Redefining the functional architecture of the brain *Trends Neurosci.* **26** 523-30

151 Needleman H L *et al* 1979 Deficits in psychologic and classroom performance of children with elevated dentine lead levels *New England Journal of Medicine* **300** 689-95

152 Nelson C M *et al* 2004 Vascular endothelial-cadherin regulates cytoskeletal tension, cell spreading, and focal adhesions by stimulating rhoa *Mol. Biol. Cell.* **15** 2943-53

153 Nianzhen Li A F 2005 Integration of topographical and biochemical cues by axons during growth on microfabricated 3-d substrates *Exp. Cell Res.* **311** 307

154 Nikkhah M *et al* 2012 Engineering microscale topographies to control the cell–substrate interface *Biomaterials* **33** 5230-46

155 Oberto A *et al* 1996 Lead (pb+2) promotes apoptosis in newborn rat cerebellar neurons: Pathological implications *J Pharmacol Exp Ther* **279** 435-42

156 Odde D J and Renn M J 2000 Laser-guided direct writing of living cells *Biotechnol. Bioeng.* **67** 312-8

157 Oh K W and Ahn C H 2006 A review of microvalves *Journal of Micromechanics and Microengineering* **16** R13

158 Oka H *et al* 1999 A new planar multielectrode array for extracellular recording: Application to hippocampal acute slice *J Neurosci Meth* **93** 61-67

159 Oliva A A *et al* 2003 Patterning axonal guidance molecules using a novel strategy for microcontact printing *Neurochem. Res.* **28** 1639-48

160 Olney J W 2002 New insights and new issues in developmental neurotoxicology *NeuroToxicology* **23** 659-68

161 Peterman M C *et al* 2004 Localized chemical release from an artificial synapse chip *P Natl Acad Sci USA* **101** 9951-54

162 Peterman M C *et al* 2004 Fluid flow past an aperture in a microfluidic channel *Anal. Chem.* **76** 1850-56

163 Pine J and Chow G 2009 Moving live dissociated neurons with an optical tweezer *IEEE T. Biomed. Eng.* **56** 1184-88

164 Pirlo R K *et al* 2006 Cell deposition system based on laser guidance *Biotechnol. J.*, Vol. **1** 1007-13

165 Pirlo R K *et al* 2011 Laser-guided cell micropatterning system *Rev. Sci. Instrum.* **82** 013708-08-6

166 Pirlo R K *et al* 2011 Biochip/laser cell deposition system to assess polarized axonal growth from single neurons and neuron/glia pairs in microchannels with novel asymmetrical geometries *Biomicrofluidics* **5**

167 Pittman A J *et al* 2008 Pathfinding in a large vertebrate axon tract: Isotypic interactions guide retinotectal axons at multiple choice points *Development* **135** 2865-71

168 Ponce R A *et al* 1994 Effects of methyl mercury on the cell cycle of primary rat cns cells in vitro *Toxicology and Applied Pharmacology* **127** 83-90

169 Postma M and van Haastert P J 2009 Mathematics of experimentally generated chemoattractant gradients *Chemotaxis* 473-88

170 Pujic Z *et al* 2008 Analysis of the growth cone turning assay for studying axon guidance *J Neurosci Meth* **170** 220-8

171 Pujic Z *et al* 2009 Assays for eukaryotic cell chemotaxis *Comb Chem High Throughput Screen* **12** 580-8

172 Purves D *et al* 2012 Neuroscience 5th ed 509-534

173 Qin W *et al* 2013 Laser guidance–based cell detection in a microfluidic biochip *J Biomed Opt* **18** 060502-02

174 Rabin R 1989 Warnings unheeded: A history of child lead poisoning.Pdf *Am J Public Health* **79** 1668-74

175 Radio N M and Mundy W R 2008 Developmental neurotoxicity testing in vitro: Models for assessing chemical effects on neurite outgrowth *NeuroToxicology* **29** 361-76

176 Ramon y Cajal S 1890 A quelle epoque apparaissent les expansions des cellules nerveuses de la moëlle épinière du poulet? *Anat. Anz.* **5 (Nr. 21 and 22)** 609-13, 31-39

177 Raper J and Mason C 2010 Cellular strategies of axonal pathfinding *Cold Spring Harb Perspect Biol* **2** a001933

178 Raper J A 2009 Growth cones *Encyclopedia of neuroscience* 981-85

179 Rettig J R and Folch A 2005 Large-scale single-cell trapping and imaging using microwell arrays *Anal. Chem.* **77** 5628-34

180 Rice D and Barone S, Jr. 2000 Critical periods of vulnerability for the developing nervous system: Evidence from humans and animal models *Environ Health Perspect* **108 Suppl 3** 511-33

181 Robinette B L *et al* 2011 In vitro assessment of developmental neurotoxicity: Use of microelectrode arrays to measure functional changes in neuronal network ontogeny *Frontiers in Neuroengineering* **4**

182 Robinson R 2009 In mammalian muscle, axonal wiring takes surprising paths *PLoS Biol*

183 Rodier P M 1995 Developing brain as a target of toxicity *Environ Health Perspect* **103 Suppl 6** 73-76

184 Rosenbalm T N *et al* 2006 Cell viability test after laser guidance **6084**608418-18-8

185 Rosenthal A and Voldman J 2005 Dielectrophoretic traps for single-particle patterning *Biophys. J.* **88** 2193-205

186 Ruardij T G *et al* 2000 Adhesion and patterning of cortical neurons on polyethylenimine-and fluorocarbon-coated surfaces *Biomedical Engineering, IEEE Transactions on* **47** 1593-99

187 Ruoslahti E 1996 Brain extracellular matrix *Glycobiology* **6** 489-92

188 Rutter M 2005 Incidence of autism spectrum disorders: Changes over time and their meaning *Acta Paediatr* **94** 2-15

189 Sackmann E K *et al* 2014 The present and future role of microfluidics in biomedical research *Nature* **507** 181-89

190 Sagiv S K *et al* 2010 Prenatal organochlorine exposure and behaviors associated with attention deficit hyperactivity disorder in school-aged children *Am J Epidemiol* **171** 593-601

191 Sanford S D *et al* 2008 Growth cone responses to growth and chemotropic factors *Eur J Neurosci* **28** 268-78

192 Schantz S L 1996 Developmental neurotoxicity of pcbs in humans: What do we know and where do we go from here? *Neurotoxicology and Teratology* **18** 217-27

193 Schiele N R *et al* 2010 Laser-based direct-write techniques for cell printing *Biofabrication* **2** 032001

194 Sensenbrenner M *et al* 1978 Neuronal cells from chick embryo cerebral hemispheres cultivated on polylysine-coated surfaces *Dev Neurosci* **1** 90-101

195 Serafini T *et al* 1994 The netrins define a family of axon outgrowth-promoting proteins homologous to c. Elegans unc-6 *Cell* **78** 409-24

196 Shi P *et al* 2010 Combined microfluidics/protein patterning platform for pharmacological interrogation of axon pathfinding *Lab on a Chip* **10** 1005-10

197 Shu T and Richards L J 2001 Cortical axon guidance by the glial wedge during the development of the corpus callosum *J. Neurosci.* **21** 2749-58

198 Sia S K and Whitesides G M 2003 Microfluidic devices fabricated in poly (dimethylsiloxane) for biological studies *Electrophoresis* **24** 3563-76

199 Skelley A M *et al* 2009 Microfluidic control of cell pairing and fusion *Nat. Methods* **6** 147-52

200 Sminova L *et al* 2014 Developmental neurotoxicity: Challenges in the 21st century and in vitro opportunities *Alternatives to Animal Experimentation: ALTEX* **31** 129-56

201 Song H-j *et al* 1997 Camp-induced switching in turning direction of nerve growth cones *Nature* **388** 275-79

202 Song H-j and Poo M-m 2001 The cell biology of neuronal navigation *Nat Cell Biol* **3** E81-E88

203 Sperry R W 1963 Chemoaffinity in the orderly growth of nerve fiber patterns and connections *P Natl Acad Sci USA* **50** 703-10

204 Staii C *et al* 2009 Positioning and guidance of neurons on gold surfaces by directed assembly of proteins using atomic force microscopy *Biomaterials* **30** 3397-404

205 Stevens M M *et al* 2005 Direct patterning of mammalian cells onto porous tissue engineering substrates using agarose stamps *Biomaterials* **26** 7636-41

206 Suzuki I K and Hirata T 2013 Neocortical neurogenesis is not really “neo”: A new evolutionary model derived from a comparative study of chick pallial development *Development, Growth & Differentiation* **55** 173-87

207 Tahirovic S and Bradke F 2009 Neuronal polarity *Cold Spring Harb Perspect Biol* **1**

208 Tang D and Goldberg D J 2000 Bundling of microtubules in the growth cone induced by laminin *Molecular and Cellular Neuroscience* **15** 303-13

209 Taylor A M *et al* 2015 Passive microfluidic chamber for long-term imaging of axon guidance in response to soluble gradients *Lab on a Chip* **15** 2781-89

210 Taylor A R *et al* 2007 Astrocyte and muscle-derived secreted factors differentially regulate motoneuron survival *J. Neurosci.* **27** 634-44

211 Tessier-Lavigne M and Goodman C S 1996 The molecular biology of axon guidance *Science (New York, N Y)* **274** 1123-33

212 Théry M 2010 Micropatterning as a tool to decipher cell morphogenesis and functions *J. Cell. Sci.* **123** 4201-13

213 Tsai H M *et al* 1981 3h-thymidine autoradiographic analysis of telencephalic histogenesis in the chick embryo: I. Neuronal birthdates of telencephalic compartments in situ *J Comp Neurol* **198** 275-92

214 Tsuda Y *et al* 2006 Heterotypic cell interactions on a dually patterned surface *Biochem. Biophys. Res. Commun.* **348** 937-44

215 USEPA 1998 Chemical hazard data availability study: What do we really know about the safety of high production volume chemicals? *Journal* 35

216 USEPA, America's children and the environment, United States Environmental Protection Agency, 2013

217 Vancha A R *et al* 2004 Use of polyethyleneimine polymer in cell culture as attachment factor and lipofection enhancer *BMC biotechnology* **4** 23

218 Varon S *et al* 1981 Trophic activities for dorsal root and sympathetic ganglionic neurons in media conditioned by schwann and other peripheral cells *Developmental Brain Research* **1** 73-87

219 Vickers J A *et al* 2006 Generation of hydrophilic poly(dimethylsiloxane) for high-performance microchip electrophoresis *Anal. Chem.* **78** 7446-52

220 Von Philipsborn A C *et al* 2006 Microcontact printing of axon guidance molecules for generation of graded patterns *Nat Protoc* **1** 1322-28

221 W. Mundy S P, T. Shafer, M. Gilbert, J. Cowden, K. Crofton, D. Herr, K. Jensen, K. Raffaele, N. Radio, and K. Schumacher 2010 Building a database of developmental neurotoxicants: Evidence from human and animal studies *Journal*

222 Wang C J *et al* 2008 A microfluidics-based turning assay reveals complex growth cone responses to integrated gradients of substrate-bound ecm molecules and diffusible guidance cues *Lab Chip* **8** 227-37

223 Waugh D J J and Wilson C 2008 The interleukin-8 pathway in cancer *Clinical Cancer Research* **14** 6735-41

224 Wedeen R P 1984 Poison in the pot: The legacy of lead

225 Wei L *et al* 2014 Single-neuron axonal pathfinding under geometric guidance: Low-dose-methylmercury developmental neurotoxicity test *Lab on a Chip* **14** 3564-71

226 Wheeler A R *et al* 2003 Microfluidic device for single-cell analysis *Anal. Chem.* **75** 3581-86

227 Whitesides G M *et al* 2001 Soft lithography in biology and biochemistry *Annual review of biomedical engineering* **3** 335-73

228 Wiencken-Barger A *et al* 2004 The role of l1 in axon pathfinding and fasciculation *Cereb Cortex* **14** 121-31

229 Wilson Jones M and Thomas Bass W 2003 Fetal alcohol syndrome *Neonatal Network* **22** 63-70

230 Withers G S *et al* 2006 Effects of substrate geometry on growth cone behavior and axon branching *J Neurobiol* **66** 1183-94

231 Xu T *et al* 2005 Inkjet printing of viable mammalian cells *Biomaterials* **26** 93-99

232 Yin H and Marshall D 2012 Microfluidics for single cell analysis *Curr Opin Biotechnol* **23** 110-19

233 Yoshida M *et al* 1995 Neurotrophic effects of conditioned media of astrocytes isolated from different brain regions on hippocampal and cortical neurons *Experientia* **51** 133-36

234 Yun K-S and Yoon E 2005 Micro/nanofluidic device for single-cell-based assay *Biomed. Microdevices* **7** 35-40

235 Zahir F *et al* 2005 Low dose mercury toxicity and human health *Environmental Toxicology and Pharmacology* **20** 351-60

236 Zhang J and Wheeler J J 2010 Mercury and autism: A review *Education and Training in Developmental Disabilities* **45** 107

237 Zhang W Y *et al* 2004 Elastomer-supported cold welding for room temperature wafer-level bonding *Micro Electro Mechanical Systems, 2004. 17th IEEE International Conference on. (MEMS)* 741-44

238 Zheng J Q *et al* 1994 Turning of nerve growth cones induced by neurotransmitters *Nature* **368** 140-4

239 Zhou J *et al* 2010 Recent developments in pdms surface modification for microfluidic devices *Electrophoresis* **31** 2-16

240 Zhu X *et al* 2004 Arrays of horizontally-oriented mini-reservoirs generate steady microfluidic flows for continuous perfusion cell culture and gradient generation *Analyst* **129** 1026-31

241 Zicha D *et al* 1991 A new direct-viewing chemotaxis chamber *J. Cell. Sci.* **99** 769-75

242 Zigmond S H 1977 Ability of polymorphonuclear leukocytes to orient in gradients of chemotactic factors *J. Cell Biol.* **75** 606-16

243 Zimmer B *et al* 2011 Coordinated waves of gene expression during neuronal differentiation of embryonic stem cells as basis for novel approaches to developmental neurotoxicity testing *Cell Death & Differentiation* **18** 383-95

244 Zimmer B *et al* 2012 Evaluation of developmental toxicants and signaling pathways in a functional test based on the migration of human neural crest cells *Environ Health Perspect* **120** 7